

# Using digital traces to build prospective and real-time county-level early warning systems to anticipate COVID-19 outbreaks in the United States

Lucas M. Stoleran,<sup>†1,2,3</sup> Leonardo Clemente,<sup>†1</sup> Canelle Poirier,<sup>1,2</sup> Kris V. Parag,<sup>4</sup> Atreyee Majumder,<sup>5</sup> Serge Masyn,<sup>5</sup> Bernd Resch,<sup>7,8</sup> Mauricio Santillana,<sup>1,2,6\*</sup>

<sup>1</sup>Computational Health Informatics Program, Boston Children's Hospital, Boston, MA, USA

<sup>2</sup>Department of Pediatrics, Harvard Medical School, Boston, MA, USA

<sup>3</sup>Department of Mathematics, Oklahoma State University, Stillwater, OK, USA

<sup>4</sup>NIHR Health Protection Research Unit,

Behavioural Science and Evaluation, University of Bristol, Bristol, UK.

<sup>5</sup>Global Public Health, Janssen R&D

<sup>6</sup>Harvard University, T.H. Chan School of Public Health, Boston, MA, USA

<sup>7</sup>Department of Geoinformatics - Z-GIS, University of Salzburg, Salzburg, Austria.

<sup>8</sup> Center for Geographic Analysis, Harvard University, Cambridge, MA, USA.

<sup>†</sup> These authors contributed equally to this study.

\*To whom correspondence should be addressed; E-mail: msantill@g.harvard.edu.

**The ongoing COVID-19 pandemic continues to affect communities around the world. To date, almost 6 million people have died as a consequence of COVID-19, and more than one-quarter of a billion people are estimated to have been infected worldwide. The design of appropriate and timely mitigation strategies to curb the effects of this and future disease outbreaks requires close monitoring of their spatio-temporal trajectories. We present machine learning methods to anticipate sharp increases in COVID-19 activity in US coun-**

**ties in real-time. Our methods leverage Internet-based digital traces – e.g., disease-related Internet search activity from the general population and clinicians, disease-relevant Twitter micro-blogs, and outbreak trajectories from neighboring locations– to monitor potential changes in population-level health trends. Motivated by the need for finer spatial-resolution epidemiological insights to improve local decision-making, we build upon previous retrospective research efforts originally conceived at the state level and in the early months of the pandemic. Our methods –tested in real-time and in an out-of-sample manner on a subset of 97 counties distributed across the US– frequently anticipated sharp increases in COVID-19 activity 1-6 weeks before the onset of local outbreaks (defined as the time when the effective reproduction number  $R_t$  becomes larger than 1 consistently). Given the continued emergence of COVID-19 variants of concern –such as the most recent one, Omicron– and the fact that multiple countries have not had full access to vaccines, the framework we present, while conceived for the county-level in the US, could be helpful in countries where similar data sources are available.**

## **Introduction**

With more than 6 million deaths worldwide as of March 2022, the COVID-19 pandemic has become a global catastrophic event (1). The United States (US) alone has reported more than 80 million infections, and nearly 1 million deaths (2). While COVID-19 vaccination strategies have been deployed in the US since the early months of 2021, the proportion of fully vaccinated individuals is still low, at around 64%. With the emergence of new variants of SARS-CoV-2 –the virus responsible for infecting people with COVID-19– such as Omicron, the observed waning of immunity conferred by vaccines (3), and the fact that many non-pharmaceutical

interventions (NPIs), such as mask mandates and social distancing have become less frequently practiced, the US is still highly vulnerable to the effects of the COVID-19 outbreaks (4). Thus, our best line of defense against uncontrolled outbreaks remains to be vaccinated and to adjust our social behavior when sharp increases of infections are first detected (5, 6). In the context of designing timely and appropriate public health responses to slow down infections and eventual deaths, robust real-time indicators of COVID-19 activity are of great importance as they guide authorities in their decision-making processes.

Tracking COVID-19 in real-time with reliable data sources remains a challenge despite many initiatives led by hospitals, local health authorities, and the research community (7). For instance, PCR COVID-19 test results are typically delayed by multiple days and reported with days or weeks of delay. Testing availability may significantly impact the recorded number of positive COVID-19 cases, which may suggest that changes in COVID-19 activity reflect testing volumes rather than the underlying proportions of infections in the population (1, 8). Furthermore, the reliability, consistency, and in general the quality of reported COVID-19 data—such as confirmed cases, hospitalization, and deaths—varies highly from country to country (and within countries) frequently due to disparities in economic resources locally allocated to monitor and respond to the pandemic (7).

Statistical models have been proposed to address delays in data collection and ascertainment biases retrospectively and in real-time (9–12). Computational mechanistic (Susceptible-Infected-Recovered, SIR) models, on the other hand, have been used to reconstruct the spatio-temporal patterns of the spread of COVID-19 retrospectively and to forecast likely COVID-19 cases and deaths to occur in the near future (13–19). Many studies characterizing the quality and accuracy of forecasts have emerged from COVID-19 initiatives coordinated by the U.S. Centers for Disease Control and Prevention (CDC) (20). Those models are usually based on mechanistic SIR-like systems (21) and/or Bayesian frameworks (22). Despite their ability to explore

potential “what if” scenarios and their accuracy during periods where the epidemic curves have been monotonically increasing or decreasing, most of these forecasting models have not been very consistent or reliable in anticipating sharp changes in disease activity (23).

Several studies have also shown the potential utility of “digital” (or Internet-based) data sources as a complementary way to track (and/or confirm) changes in disease activity at the population level (24–31). In the past, many approaches explored valuable information from search engines (29, 32–35), Twitter microblogs (36–38), and electronic health records (39–41) for real-time estimates of disease prevalence, and characterized the limitations of those non-traditional data sources in the context of influenza (42, 43). In the past two years, statistical and machine learning approaches have explored how to incorporate disease-related Internet search data to track and forecast COVID-19 activity (44–46), and some of their limitations have been documented as well (47). The logic behind using disease-related “digital data” to monitor disease activity is that user-generated *digital traces* may capture changes in human behavior (human mobility, situational awareness, increases in certain clinical treatments, population-level topic interests, social media trending content) that may have an impact on disease transmission and/or may reflect increases in symptomatic infections (48, 49).

Kogan et al. explored the effectiveness of Google Trends, Twitter microblogs, clinician searches, anonymized human mobility from mobile phones records, and smart thermometers to anticipate increases and decreases in COVID-19 activity at the state level, as reported by healthcare systems (50). By combining multiple data streams, they proposed a Bayesian indicator capable of predicting an impending COVID-19 outbreak with several weeks of anticipation in near-real time. Their methods were successful when tested in a retrospective fashion and during the first half of the year 2020. However, at the time of their study, Kogan and colleagues did not have enough data to perform out of sample validation tests, which is now possible given the higher number of COVID-19 outbreaks. Moreover, Kogan et al. did not explore the feasibility

of using their approaches at finer spatial resolutions, such as the county level, where the signal to noise ratio in aggregated digital data streams may be compromised and where most outbreak control strategies are implemented in the US.

**Our contribution:** Here we present a framework to deploy a prospective real-time machine learning-based early warning system to anticipate or confirm COVID-19 outbreaks at the county level in the United States. Our analysis restricts our choice of counties to those with the infrastructure to conduct vaccine clinical trials or those with more than 1 million inhabitants. Our systems leverage the predictive power of both individual Internet-based data sources and their combined consensus. We quantify their predictive performance in a prospective out-of-sample way from January 2020 to January 2022, including the most recent periods when the highly contagious Omicron variant was detected. By implementing event-detection algorithms on each of these Internet-based time series and employing machine-learning strategies to combine this information, we anticipate the onset of local COVID-19 outbreaks – defined as the time when the local effective reproductive number,  $R_t$ , becomes larger than 1 in a given region (51).

## Results

We analyzed COVID-19 activity in 97 US counties across the US between January 1, 2020, and January 1, 2022. First, we identify weeks when the local reproductive number (commonly denoted by  $R_t$ ) was higher than 1 (with 95% C.I. as described in (52)), suggesting that the local number of secondary COVID-19 infections was larger than 1 per index case. We labeled each first week when the local  $R_t$  transitioned from a value smaller than 1 to one above 1 as *outbreak onset* for each location (see Data and Methods section for details). Interchangeably, we also refer to these outbreak onsets as *events* in this manuscript. We identified 464 outbreak onsets at the county level. From this total, 367 events were used to test our methods out-of-sample, after using the first outbreak onset of each location as initial training data. We replicated this analysis

for the 50 US states, where we identified 252 outbreak onsets at the state level (a total of 202 out-of-sample outbreak onsets).

We obtained COVID-19-related digital streams for the same time period with the goal of identifying, for example, moments in time when (a) COVID-19 related Internet searches, such as fever or anosmia, showed sharp increases – perhaps signaling a population-wide increase of symptomatic infections –, (b) when clinicians were looking for dosage information for specific medications to control fever or other COVID-19 symptoms, or (c) when Twitter users expressed that they or their family/friends may have caught COVID-19, among other signatures. We then explored the ability of our methods to extract information from these data sources (individually and as a consensus) to anticipate outbreak onsets for each geographical scale.

Our results are summarized in Figs 1 and 2 for the county and state levels, respectively. By dynamically training<sup>1</sup> our machine learning methods to recognize temporal patterns that precede increases in COVID-19 activity, we tested their ability to anticipate outbreak onsets. Specifically, we quantified how early they could anticipate unseen outbreaks (referred to as *earliness*), the number of times they anticipated, synchronously identified, or lately confirmed a subsequently observed outbreak (referred to as an *early*, *synchronous* or *late warning*). We also quantified the number of times our methods triggered an alarm, but no outbreak onset was subsequently observed (referred to as a *false alarm*), and the number of *missed outbreaks* when no alarm preceded an outbreak onset.

Specifically, we defined an *early warning* whenever an alarm was triggered up to six weeks before the outbreak onsets. The choice of a six-week window was made to plausibly relate a digital trend change with a potential subsequent infection. For example, if a person uses Google to search for COVID-19 related information due to a likely symptomatic infection, that person's COVID-19 infection may be confirmed in the following week or two, if they are admitted to a

---

<sup>1</sup>By dynamically training, we refer to the use of all available historical information at a given point in time to produce any prospective future-looking prediction.

health care facility or tested by a provider. Alternatively, such person may search for COVID symptoms not in response to their own symptoms but to someone else’s within their close contact network (that may eventually infect them). In that case, the lag between that Internet search and an eventual confirmed infection may be longer, perhaps up to 4-6 weeks. We also defined *synchronous warning* and *late warning* whenever an alarm was triggered on the same date or up to two weeks later than the identified outbreak onset, respectively.

In both Figs 1 and 2, panel (A) serves as a graphical representation of the different outcomes observed in our early warning systems, namely, when the system leads to a successful early, synchronous or late warning; a false alarm, and a missed outbreak. Two other scenarios were characterized: one that explores when the system may have suggested a full outbreak would occur but only a mild increase in COVID-19 activity was subsequently observed, labeled as *warning, increase is observed*, and another labeled as a *soft warning*, that is observed when the system almost triggered an alarm and an increase of COVID-19 activity was subsequently seen –this could signal an improper model calibration, perhaps a consequence of the small number of events to train the models in a given location. For simplicity, the COVID-19 cases reported by Johns Hopkins University (JHU) are shown in gray, and an early warning indicator is shown in light orange. The horizontal dotted black line represents an early warning system’s decision boundary, i.e., a threshold value used to activate an outbreak alarm. Please refer to our Data and Methods Section for a more detailed description of the event definitions, machine learning methods, and our validation criteria.

## **County-level Performance**

Fig 1 (B) displays a summary count of all the outbreak onsets observed at the county level. Each horizontal bar is colored, from orange to purple, depending on the event class previously described. In this work, we developed two different machine learning methods: (i) the *Sin-*

*gle Source* method that explores the predictive power of individual digital sources by detecting increases in the search volume of a given term, and (ii) the *Multiple Source* method that incorporates many different signals, optimizing on their best individual performances, to produce a single output. We refer the reader to our Data and Methods section for more details on the formulation of our methodologies. We compared the predictive performance of our methods against an intuitive baseline, which we refer to as *Naive method*. The Naive method predicts an outbreak will happen whenever there is an increase in the number of confirmed COVID-19 cases, i.e., if the COVID-19 cases increase on week  $t$  compared to week  $t - 1$ , the Naive method triggers an alarm at week  $t$ .

**Early warnings:** The alarms produced by the Naive method resulted in early warnings for 337 out of the 367 total events (92%) and displayed 23 synchronous and one late warning in the remaining 19 events (6%). The best signal in the Single Source method (Google search term “How long does covid last?”) identified 237 early warnings (65%), 25 synchronous (7%), and 30 (8%) late warnings. Here we use the term “best signal” to reference those digital traces with a higher number of early warnings across the 97 counties in our dataset. We obtained a comparable performance for the Google search term “side effects of vaccine”, with 227 early warnings (62%), 19 synchronous (5%), and no late warnings. The Multiple Source method identified 213 early warnings (61%), 23 synchronous (6%), 37 late (10%) warnings. **Soft warnings and missed outbreaks:** The Naive method missed six events (2%) and the Single Source method for the two displayed Google Trends (“How long does covid last?” and “side effects of vaccine”) missed 75 and 106 events (20% and 29%), respectively. For the Multiple Source method, 61 out of the 87 remaining events were soft warnings (17% of the total events) and 26 were missed outbreaks (7% of the total events).

**False alarms:** Fig 1 (C) summarizes the false alarms for the different methods in our analysis. The Naive method registered 617 false alarms (about 1.7 times the number of observed



outbreaks). In comparison, the Single Source method led to 374 false alarms for the term “How long does covid last?” and 479 false alarms for the term “side effects of vaccine” (1 and 1.3 times the number of outbreaks, respectively). The Multiple Source method produced the lowest amount with only 114 false alarms (0.3 times the number of outbreaks). A minimum number of false alarms should be preferred to avoid alarm fatigue. The Multiple Source method performs best in this aspect. The Naive Method also exhibited the highest number of “warnings with an increase” observed (252 registered events), followed by the Single Source method (139 events for “How long does covid last?” and 171 for “side effects of vaccine”) and the Multiple Source method with 36 events.

Fig 1 (D) shows a graphical representation of the probability of resurgence  $P(R_t > 1)$ , i.e., the probability that the effective reproductive number is higher than one given the data<sup>2</sup>, along with the weekly confirmed COVID-19 cases (gray-filled curve in the top), and three representative signals for the Naive, Single, and Multiple Source methods for the county of Marion (FL). We chose to depict this specific county as an example where our methods performed well (but similar visualization for all counties and states can be found in the SI). The outbreak onsets were defined when  $P(R_t > 1) > 0.95$  and marked with red vertical lines that extend across the five horizontal panels in Fig 1 (D) containing the COVID-19 case counts and the three early warning methods. Triggered alarms are displayed as vertical tick marks for each method (Naive, Single, and Multiple Source methods in gray, blue and, yellow, respectively).

**Earliness:** Fig 1 (E) shows the **earliness** (in weeks) for the alarms triggered by each method. The bars represent a count of the number of activated alarms within the out-of-sample time window (between six weeks before and two after the outbreak onset). Triggered alarms that did not precede any increment in the activity of confirmed COVID-19 cases within the six-week observational window were considered false alarms (displayed in red). We observed that most

---

<sup>2</sup>Technically, we compute the conditional probability  $P(R_t > 1 | I_1^t)$  where  $I_1$  denotes the initially infected population. For notational simplicity, we write  $P(R_t > 1)$  throughout the manuscript.

early warning activation counts of the Naive and Single Source methods fell within the 4 and 6 weeks early range (68% Naive, and 61% and 62% for the Single Source). The Multiple Source method's highest count (55 alarms) fell within the six-week early mark (26%). The rest of the activations were spread across the 5 to 1 week-early mark, with a higher number of activations as we reached the sync warning mark.

**Omicron-attributable outbreaks:** A total of 62 outbreak onsets were observed at the county level after December 01, 2021. The Single Source method correctly identified 35 and 43 early warnings (56% and 69%) for the Google Trends terms “How long does covid last?” and “side effects of vaccine”, respectively. The Multiple Source method could anticipate 42 (68%) outbreak onsets.

## State-level performance

Fig 2 summarizes the state-level results. **Early warnings:** The alarms produced by the Naive method preceded COVID-19 outbreak onsets in 178 out of the 202 total events (88%), displayed a synchronous warning in 23 (11%) events and only one late warning. The best signal in the Single Source method (Google Trends “How long does covid last?”) identified 128 early warnings (63%), 13 synchronous (6%), and 18 late warnings (9%). Comparable results were found for the Google Trends term “Chest Pain” with 120 early warnings (59%), 12 synchronous warnings (6%), and 12 late warnings (6%). On the other hand, the Multiple Source method produced 99 early warnings (49%), 22 synchronous warnings (11%), and 24 late warnings (12%). **Soft warnings and missed outbreaks:** The Naive method had no missed events, and the Single Source method for the two displayed Google Trends (“How Long Does Covid Last” and “Chest pain”) missed 43 and 58 events (21% and 29%), respectively. For the Multiple Source method, the remaining 57 events were characterized by 41 soft warnings and 16 missed outbreaks, representing 20% and 8% of the total events.

**False alarms:** The Naive method led to 271 false alarms (Fig 2 (C)), about 1.3 times the number of observed outbreaks. The Single Source method produced 171 false alarms for the Google Trends term “How long does covid Last” and 151 false alarms for the term “chest pain” (about 0.84 and 0.74 times the number of outbreaks, respectively). The Multiple Source method led to 34 false alarms (about 0.24 times the number of outbreaks), the lowest of all methods. For “warnings with an increase observed”, the Naive method exhibited 74 events, followed by the Single Source method 82 and 63 events for the two best signals) and the Multiple Source method with only 20 events.

Fig 2 (D) shows a graphical representation of the probability of resurgence  $P(R_t > 1)$  and weekly confirmed COVID-19 cases in Florida. The top signals for the Single Source method and the output of the Multiple Source method are also shown, with tick marks representing the triggered alarms for each method. In Fig 2 (E), we observe that the Naive method’s highest early warning counts fell within the -6, -3, and -1 week mark (approximately 59% of total early warning rates). The highest counts for the Single Source method fall between the four and six-week early mark (65% and 69% for the best signals, respectively). The majority of early warning activations of the Multiple Source methods fall between the one and three-week early range (60%).

**Omicron-attributable outbreaks:** We observed 19 state-level outbreak onsets occurring after December 1, 2021. The Single Source methodology preceded 13 and 12 (68% and 63%, accordingly) outbreak onsets. The Multiple Source method preceded 17 out of the 19 (89%).

## Geographical County-Level Analysis

Given the lower number of false alarms and the number early warning rates of the Multiple Source method, we investigated this method more extensively. Fig 3 shows a detailed breakdown of the performance for each county in our dataset. We implemented a k-means clustering

approach to group the counties based on their COVID-19 weekly activity. We separated each set of selected locations into three different groups: the set of counties that experienced their first outbreak at the beginning of 2020 (blue), the set of counties that experienced their first outbreak during summer 2020 (yellow), and a set of counties that experienced their first major outbreak after the summer of 2020 (green). Fig 3 (A) shows the geographical location of the selected counties across the United States map, where the colors represent each cluster. The clustering analysis highlights how the COVID-19 outbreak dynamics seem heavily dependent on the geographical location. Counties in Cluster 1 were mainly located in the northeast part of the country, while Counties in Clusters 2 and 3 were scattered throughout the south and north/central regions, respectively.

Fig 3 (B) shows a list of counties under the colored timeseries representing each cluster center. Along with its name and corresponding number, we display a set of tick marks at the bottom representing the out-of-sample outbreak onset (varying from 2 to 7). For each outbreak onset, we trained our method on the previous onsets. For this reason, onset 1 is used for training only and was not included in the analysis. We then show the performance of the Multiple Source method predicting the out-of-sample outbreak onset with different colors. In general, counties in Cluster 1 experienced at most four onset events, while counties in Clusters 2 and 3 experienced up to seven outbreak onsets (we refer to our Data and Method sections for a precise definition of outbreak onsets). The performance of the Multiple Source method was consistent throughout the three groups. In cluster 1, we observed mostly early warnings and soft warnings, while mixed results were obtained for clusters 2 and 3. However, it is worth noting that those clusters contain more than twice the number of group members of cluster 1. The multiple source method successfully improved over time for some counties. That was the case for Shelby (TN, 13) and Tarrant (TX, 14) in Cluster 2, Philadelphia (PA, 2), Lake (IN, 4), Laporte (IN, 5), and Hamilton (OH, 9) in Cluster 3. Counties where our Multiple Source method did not provide

early warnings included Middlesex (MA, 8) and Queens (NY, 11) in Cluster 1, Jackson (MO, 8) and Cook (IL, 17) in Cluster 2, Cumberland (NC, 3), Palm Beach (FL, 20), and Hillsborough (FL, 33) in Cluster 3.

## **Geographical State-Level Analysis**

By extending our analysis to the state level (Fig 4), we observe that the COVID-19 trajectories generated by the clustering analysis remained consistent with their county-level counterpart (early outbreak states in the northeast, summer, and post-summer outbreaks in the south and north, respectively). States where the Multiple Source method successfully predicted most of the outbreak onsets included Ohio (6), Connecticut (12), Indiana (5) in Cluster 1, Nevada (2), Florida (8), Tennessee (16), and North Carolina (19) in Cluster 2. On the other hand, states where our method did not predict most onsets ahead of time included Michigan (8), Maine (9), and Massachusetts (13) in Cluster 1, Arizona (3), South Carolina (9), Virginia (17), Texas (20) in Cluster 2, Missouri (1), Montana (12), and Wyoming (17) in Cluster 3.

## **Feature Importance Analysis**

Our Multiple Source method dynamically selected the most predictive Internet-based data streams, as well as historical epidemiological information –both at the state and county levels–, for each location to produce future-looking early warnings. We analyzed which data streams were most informative in our early warning systems across time, individually, and across locations (see Data and Methods section for more details). Tables 1 and 2 show the top 10 most frequently digital and historical proxies selected by the Multiple Source method, across all locations, to predict each out-of-sample outbreak onset at the county and state levels. In both cases, the number of out-of-sample outbreak onsets varied from 2 to 7. Moreover, many counties experienced at least two onsets, while fewer counties experienced more than six onsets. Hence, we

display six columns with the corresponding number ( $n$ ) of locations for the analysis. **County-level:** For the outbreak onsets 2 and 3, our Multiple Source method predominantly selected the Google Trends terms "covid," "covid-19," and "covid symptoms," along with local confirmed COVID-19 cases as its primary selected data sources. For later outbreak onsets, we observed an increase in the importance of Neighbor Activity (weekly epidemiological reports from geographically close counties) as a top selected source after onsets 4, 5, and 6. Some of the remaining terms in the top 10 list represented general symptoms of respiratory diseases such as "chest pain", "fever", "nasal congestion". **State-level:** We found consistent performances for the Multiple Source Method at the state level, with COVID-19 related Google trends leading the list of most selected streams for onsets 2 and 3. After onset 4, state-level neighbor activity also appeared as a highly selected source. Other relevant terms in the top 10 list included "Acute bronchitis", "cough", and "Asthma".

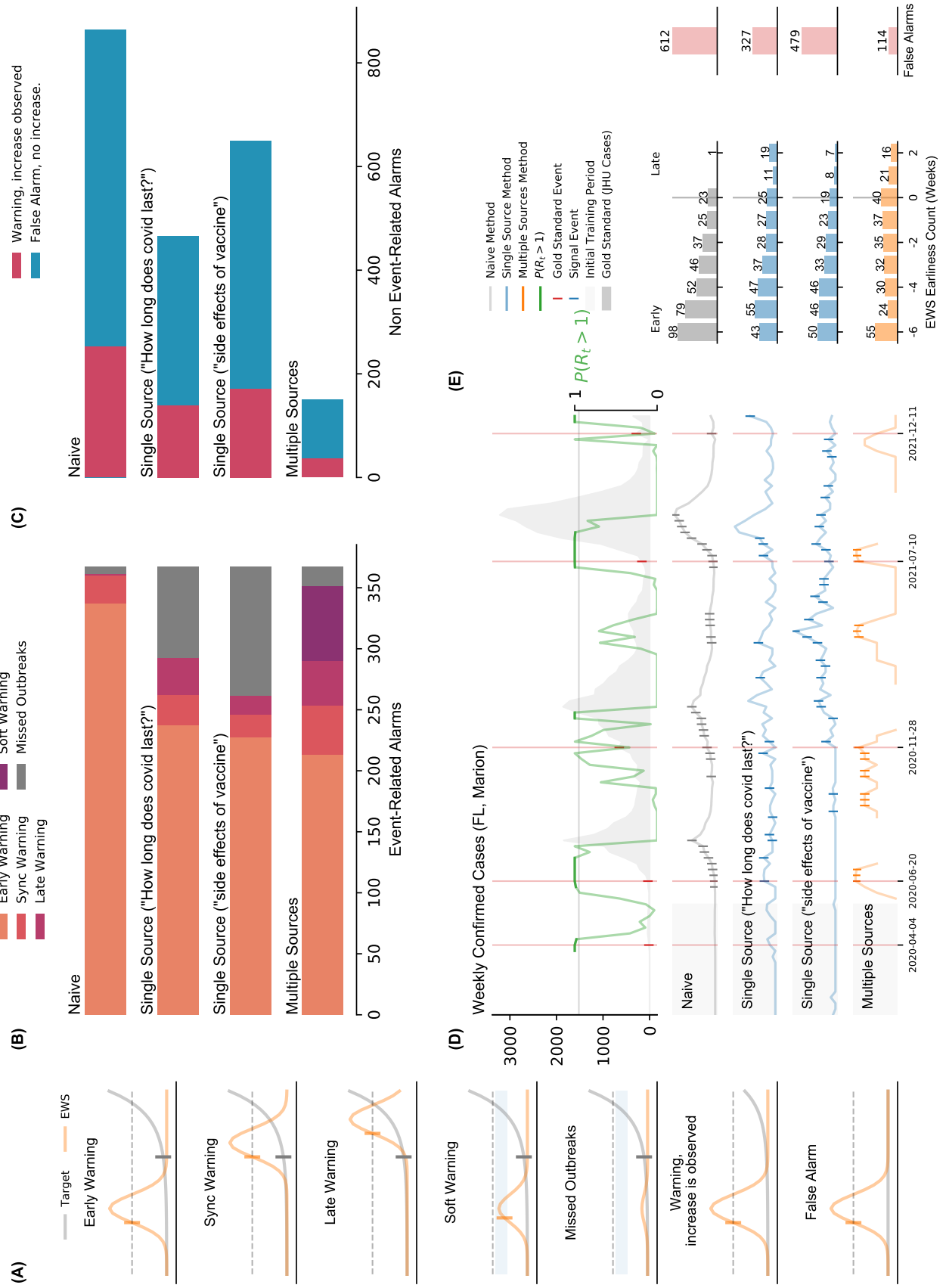


Figure 1: A summary of our results at the county level.

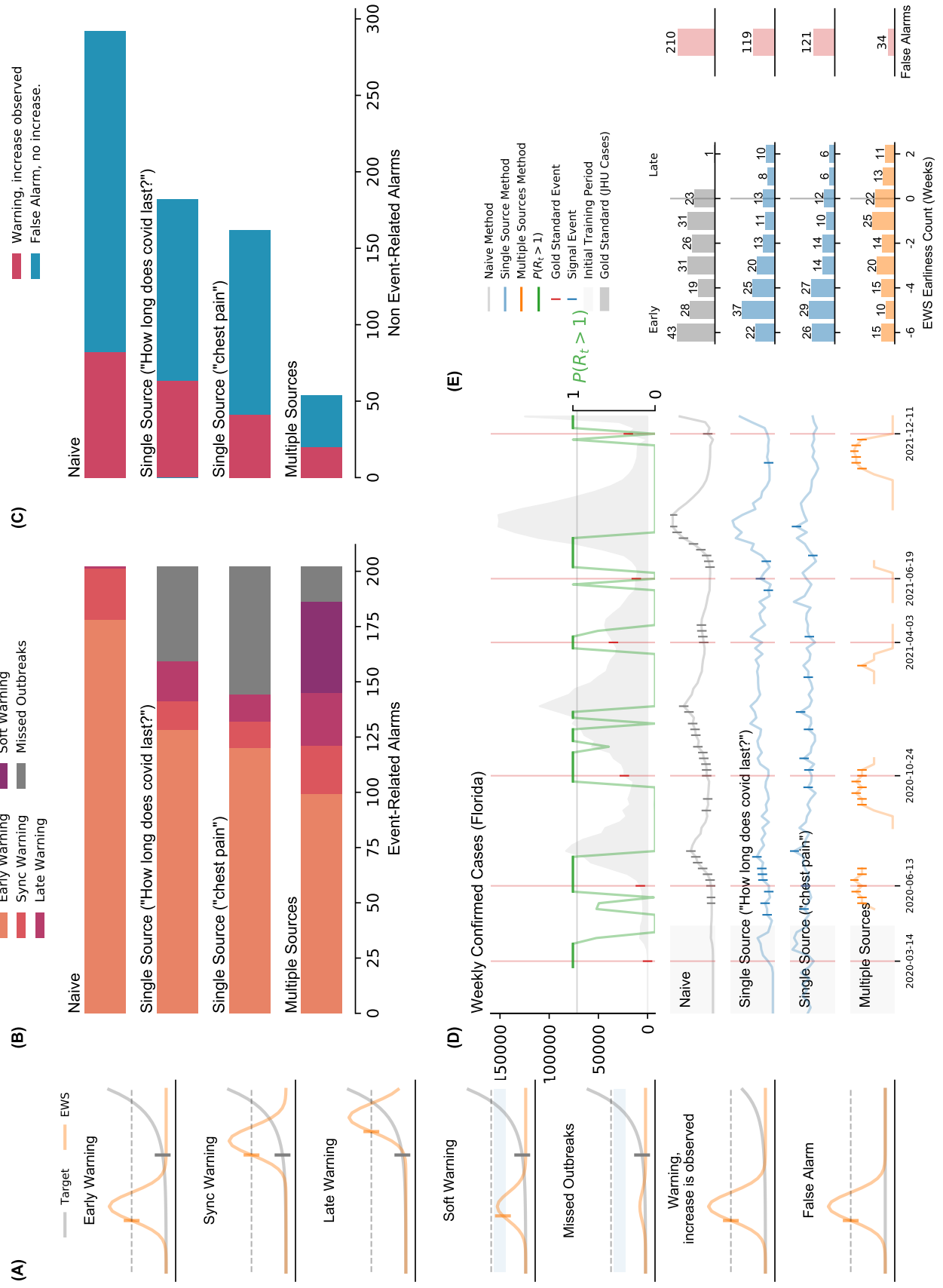
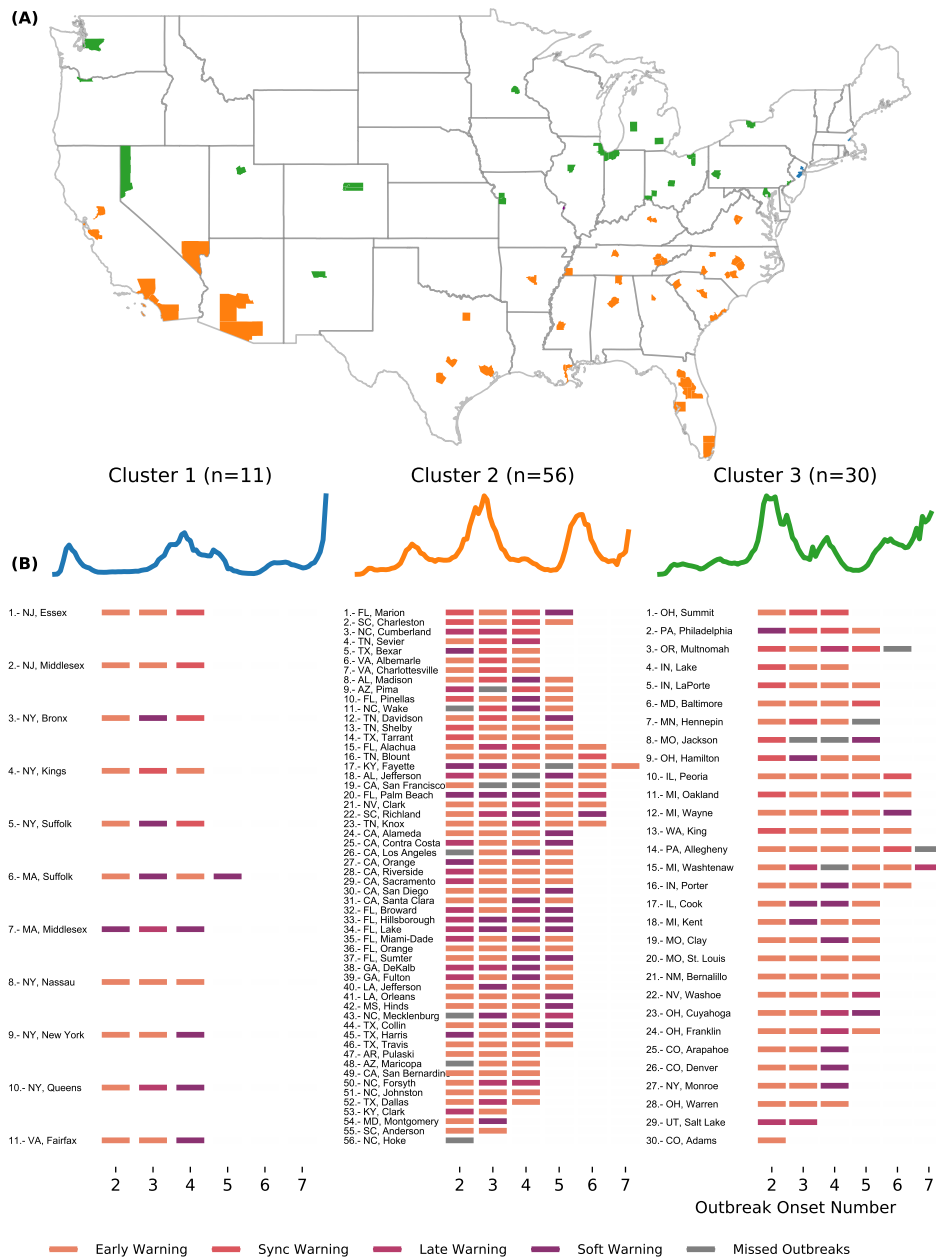
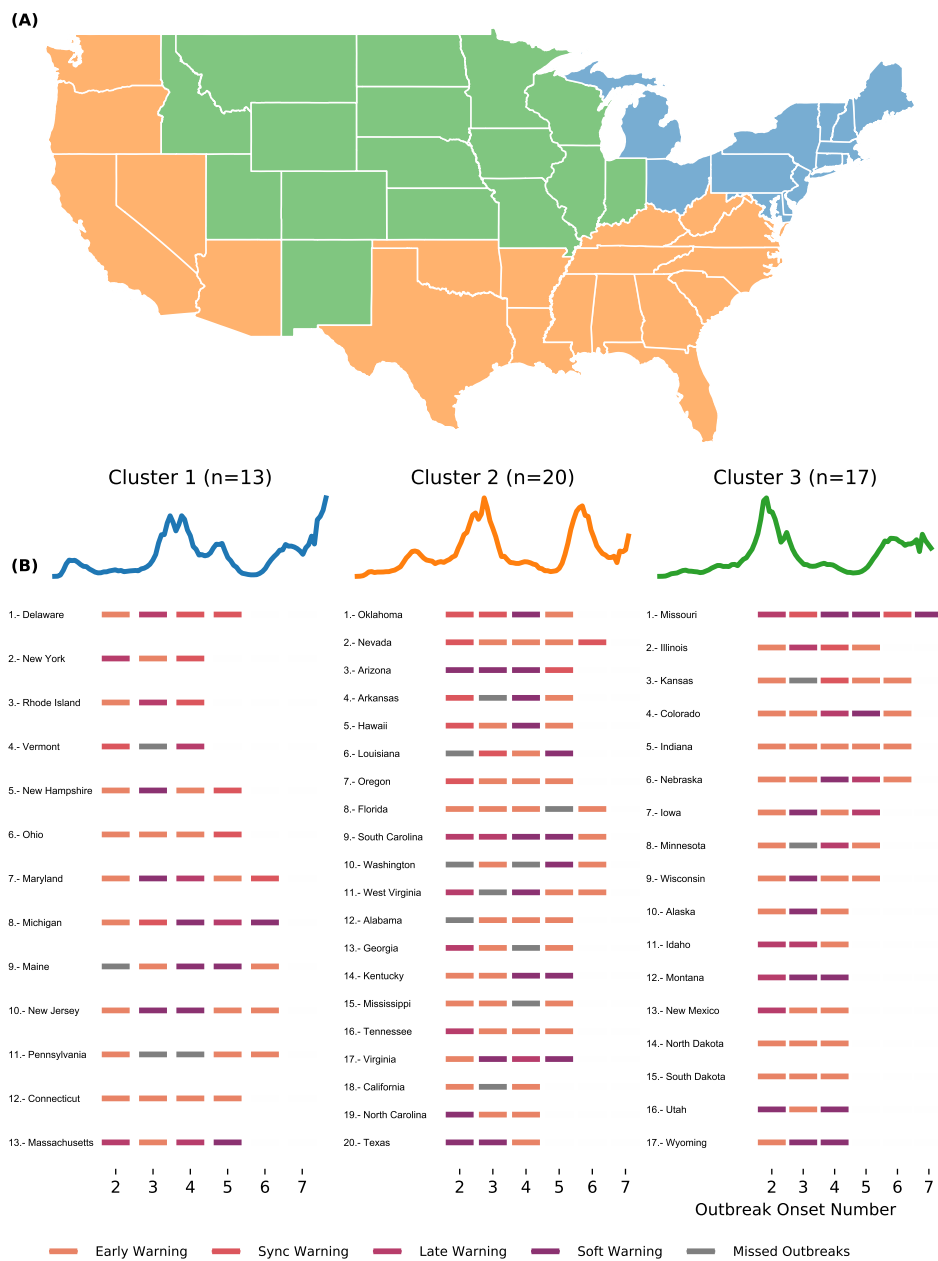


Figure 2: A summary of our results at the state level.





**Figure 3: Clustering analysis at the county level based on confirmed COVID-19 case trajectories.** (A) The geographical map color-codes each location based on their cluster. A total of three clusters described groups of counties that experienced their first outbreak onset early in 2020 (blue), during summer (yellow) and, late in 2020 (green). (B) Orange-to-purple and gray markers correspond to the performance of the Multiple Source Method for each out-of-sample outbreak onset. For example, the first location in cluster 1, Essex (NJ), experienced three out-of-sample events: the first two were early warnings, whereas the second event was a synchronous warning.



**Figure 4: Clustering analysis at the state level based on COVID-19 confirmed cases trajectories.** (A) The geographical map color-codes each location based on their cluster. A total of three clusters describe groups of states that experienced their first outbreak onset early in 2020 (Cluster 1 in blue), during summer (Cluster 2 in yellow) and, late in 2020 (Cluster 3 green). (B) The set of orange-to-purple and gray markers correspond to the performance of the Multiple Source Method for each out-of-sample outbreak onset.

	Onset 2 (n=97)	Onset 3 (n=95)	Onset 4 (n=91)	Onset 5 (n=64)	Onset 6 (n=17)	Onset 7 (n=3)
0	(GT) covid (81)	(GT) covid symptoms (48)	(GT) covid symptoms (34)	Neighbor Activity (28)	Neighbor Activity (8)	Neighbor Activity (3)
1	(GT) covid-19 (80)	(GT) covid-19 (43)	Neighbor Activity (31)	(GT) covid symptoms (19)	(GT) covid-19 (6)	Confirmed Cases (2)
2	(GT) covid symptoms (68)	(GT) covid (41)	(GT) covid (26)	Confirmed Cases (15)	(GT) covid symptoms (4)	(GT) Asthma (1)
3	Confirmed Cases (51)	Confirmed Cases (31)	Confirmed Cases (25)	(GT) covid (14)	(GT) Anosmia (3)	(GT) Actinic keratosis (1)
4	(GT) chest pain (46)	(GT) chest pain (22)	(GT) covid-19 (21)	(GT) Ageusia (14)	(GT) covid (2)	(GT) Fibrillation (1)
5	(GT) quarantine (39)	(GT) Acne (20)	(GT) Anosmia (18)	(GT) Anosmia (12)	(GT) Nasal congestion (2)	(GT) Floater (1)
6	(GT) how long does covid last (29)	(GT) fever (18)	(GT) Ageusia (18)	(GT) covid-19 (11)	(GT) Phlegm (2)	(GT) Panic attack (1)
7	(GT) covid-19 who (24)	(GT) Ageusia (18)	(GT) chest pain (13)	(GT) Night sweats (8)	(GT) fever (2)	(GT) covid symptoms (1)
8	(GT) chest tightness (20)	Neighbor Activity (14)	(GT) Acne (10)	(GT) chest pain (7)	(GT) Laryngitis (2)	(GT) covid-19 (1)
9	(GT) Abdominal obesity (15)	(GT) how long does covid last (12)	(GT) Acute bronchitis (10)	(GT) Autoimmune disease (5)	(GT) Asthma (2)	(GT) Anosmia (1)

**Table 1: Most selected data streams (ordered by frequency from top to bottom) of the Multiple Source method at the county level.** The number of instances a data stream was selected (values within parentheses) reduced over time, given some locations experienced fewer outbreak events than others. GT stands for Google Trends.

19

	Onset 2 (n=50)	Onset 3 (n=50)	Onset 4 (n=50)	Onset 5 (n=36)	Onset 6 (n=15)	Onset 7 (n=1)
0	(GT) covid (42)	(GT) covid symptoms (19)	Neighbor Activity (15)	Neighbor Activity (16)	Neighbor Activity (8)	(GT) Rhinitis (1)
1	(GT) covid-19 (41)	(GT) covid-19 (18)	(GT) covid symptoms (12)	(GT) covid symptoms (13)	(GT) covid symptoms (5)	(GT) Biliary colic (1)
2	(GT) covid symptoms (32)	(GT) covid (16)	(GT) Acute bronchitis (8)	Confirmed Cases (8)	(GT) covid (5)	(GT) Intracranial pressure (1)
3	Confirmed Cases (27)	Confirmed Cases (14)	(GT) Ageusia (7)	(GT) Shivering (7)	(GT) Cough (4)	(GT) Low-grade fever (1)
4	(GT) chest pain (25)	Neighbor Activity (13)	Confirmed Cases (7)	(GT) covid (5)	Confirmed Cases (4)	(GT) Rheum (1)
5	(GT) quarantine (19)	(GT) chest pain (13)	(GT) fever (7)	(GT) Bronchitis (5)	(GT) Fever (3)	(GT) Esophagitis (1)
6	(GT) how long does covid last (16)	(GT) fever (11)	(GT) Asthma (7)	(GT) Nasal congestion (5)	(GT) Chest pain (3)	
7	(GT) Abdominal obesity (14)	(GT) Acute bronchitis (11)	(GT) Anosmia (7)	(GT) Hyperventilation (4)	(GT) Asthma (3)	
8	(GT) fever (12)	(GT) Ageusia (7)	(GT) Bronchitis (5)	(GT) Asthma (4)	(GT) Eye pain (3)	
9	(GT) chest tightness (10)	(GT) Chest pain (6)	(GT) Nasal congestion (5)	(GT) Toothache (4)	(GT) Post-nasal drip (2)	

**Table 2: Most selected data streams (ordered by frequency from top to bottom) of the Multiple Source method at state level.** The number of instances a data stream was selected (values within parentheses) reduced over time, given some locations experienced less outbreak events than others. GT stands for Google trends.

## Discussion

We have presented a set of novel methods that can be deployed in real-time and in prospective mode to anticipate the onset of COVID-19 outbreaks in the United States at the county level. Our proposed methods leverage information from multiple Internet-based data sources, commonly called digital traces, as they are collected when humans navigate the Internet and serve as proxies of human behavior. The early warning system framework presented here extends previous work – conducted retrospectively and at the state level by Kogan et al. (50) – to the county level, a geopolitical spatial resolution where most outbreak mitigation strategies are designed and deployed in the USA. Specifically, our methods were designed to anticipate sharp increases in COVID-19 transmission, as identified by changes in the effective reproduction number ( $R_t$ ), an outbreak indicator preferred by the community of epidemiologists (12, 52–54).

We developed two methods that incorporate single or multiple digital signals, namely (a) a Single Source method, which locally identifies the magnitude and the number of uptrends in the digital signals that precede outbreaks, and (b) a Multiple Source method that dynamically selects a subset of the strongest predictive data streams available at each location historically, and combines them prospectively into a single indicator that quantifies the likelihood of occurrence of an outbreak in the following weeks. Both methods are data-driven techniques that continuously incorporate newly available data as time evolves, making them adaptive and responsive to the frequently changing trends of an emerging disease such as COVID-19.

Both Single and Multiple Source methods successfully anticipated most outbreak events between January 2020 and January 2022 for the 97 US counties in our dataset. To compare our methods with a baseline system, we define a Naive method that triggers an alarm whenever there is an increase in COVID-19 cases. As expected, the Naive method had the highest early warning rates, since there was at least one increase in the COVID-19 case counts at least 6-weeks

before the outbreak onset events. However, the Naive method typically leads to a significantly high number of undesirable false alarms –it produced 612 alarms when only 367 outbreaks were observed. Our intuitive Single Source method alone dropped the number of false alarms significantly while still producing early or at least synchronous warnings on 237 of the 367 outbreak events (Google Trends term “How long does covid last?”). From a decision-making perspective, having fewer false alarms is critical to reducing an unnecessary burden of resources –alarm fatigue–, and workforce (55, 56). Moreover, a system with many false alarms may lead to distrust within the end-user community. Remarkably, our Multiple Source method dramatically decreases the number of false alarms compared to our Single Source method while displaying successful early and synchronous warnings in 69% of observed outbreaks. At the state level, the Naive method also exhibits the highest ability to identify outbreaks at the cost of having more than 200 false alarms. As in the county-level analysis, our methods maintained a high rate of early warnings with a substantial decrease in the number of false alarms. Our Multiple Source method successfully identified 111 (Early/Sync) out of the 202 outbreak events for 50 states, with only 34 false alarms. Tables 4, 5, 6, and 7 in the SI summarize all early percentage rates for the Single and Multiple Source methods at both county and state levels.

At the county level, the Single (for the two performing proxies) and Multiple Source methods mainly activated 1-6 weeks before  $R_t$ . At the state level, most early warnings for the Single and Multiple Source methods preceded the outbreak onset events in 4-6 weeks. This finding can be contrasted with previous work by (50) where a 2-3 week anticipation was found. However, it should be noted that Kogan et al. considered a different target quantity to be anticipated by digital traces, namely when exponential growth in confirmed cases and deaths is observed, not when outbreaks start – in our case defined as when the reproduction number  $R_t$  is higher than 1.

Notably, the performance of our early warning systems at the state level was comparable to

the county level, as shown in Figs 1 and 2. This result is important, given that the signal-to-noise ratio in digital data sources tends to decrease as we *zoom in* to finer spatial resolutions, and thus extracting meaningful signals tends to be more challenging. The spatial-resolution dependency of the signal to noise ration has been documented in multiple studies that have attempted to extend the use of digital streams to monitor disease activity at finer spatial resolutions, and lower population densities (30, 31, 57, 58). Our methods seem to overcome this challenge by showing comparable ability and earliness to identify the onset of outbreaks for county and state levels. Moreover, our methods' predictive performance did not show any dependency on total population or population density across counties, as shown in Fig 7 in the SI.

The predictive performance of our methods varied across counties, indicating the challenge of accurately detecting COVID-19 outbreaks ahead of time on such a fine spatial resolution. Using a k-means algorithm on the normalized disease activity curves over time, we obtained three different COVID-19 activity clusters for the 97 counties analyzed in our validation experiment. By repeating the analysis at the state level, our results showed similar COVID-19 trajectories and geographic regions (North East for early 2020 outbreaks, south for summer, and north for post-summer outbreaks) generated by the clustering algorithm. As presented in Fig 3 and Fig 4, the performance of our methods was consistent throughout each cluster group.

The purely data-driven aspect of our Multiple Source method led to significant differences in the most selected predictive features as time progressed. In the first COVID-19 waves, Google Trends and COVID-19 cases (at both county and state levels) were mainly selected. In later waves, we observed that COVID-19 activity in neighboring counties became a more important predictor. A possible explanation for this alternation of most selected signals might be that Google Searches might have lost their early correlation power as increased awareness of the symptoms COVID-19 was likely in later waves. This preliminary evidence of variability in the chosen signals/features may point to the dynamic nature of how COVID-19 was initially

perceived and investigated by the population, as well as the ever-changing trends in COVID-19 outbreaks.

Our Multiple Source method rarely completely missed an outbreak. Instead, we found that the early warning indicator frequently displayed that something was about to happen even when the indicator did not cross the decision threshold. As mentioned before, we refer to this scenario as a “soft warning” for two reasons. First, a low number of events (for a given location) is not enough to properly calibrate a local predictive system. Second, the changing nature of human behavior and the SARS-CoV-2 virus challenges any prediction system. In these cases, one can always argue that the preferred epidemiological approach (when the effective reproductive number,  $R_t$ , is larger than 1) would eventually identify these sharp increases in COVID-19 activity. In addition, we find that our systems sometimes suggested that an outbreak would occur, but only a slight increase in cases was subsequently observed. We have referred to these instances as “Warning, increased observed” on Figs 1 and 2. Again, these findings should not be interpreted as a failure but a calibration issue that may be mitigated with more observations in a given location. Alternatively, these results raise the hypothesis that our methods might be more accurate on preceding COVID-19 outbreaks with higher incidence, given that  $R_t$  is better inferred at larger case numbers (59). Future studies could address this question at length.

Our present study has multiple limitations. First and foremost, our county-level analysis was conducted in a subset of 97 counties, not in all 3,006. We selected a subset of US counties based on the local health care capacity to conduct clinical trials. We also considered populous counties with more than one million inhabitants, totaling 97 counties. Future studies can explore our Single and Multiple Source methods in a larger subset of or all the 3,006 US counties, which would allow us to explore our methods’ generalisability across all US geographies. From a methodological viewpoint, our Single Source method has shown good predictive power and earliness in anticipating the outbreak onset events. Future studies could refine our analysis by

exploring other nuances of the digital time series, such as uptrend magnitude or downtrends associated with decreased COVID-19 activities. Likewise, the Multiple Source method was designed to identify an outbreak onsets but no other properties, such as magnitude and timing. Further studies could investigate the relationship between those features and the digital signals to build more sophisticated early warning systems. Future efforts could also explore other connections between our results and the probabilistic estimation of  $R_t$  adopted in this study, such as cumulative probabilities lower bounds for the false alarm rates, among others. It is also important to acknowledge that digital traces usually exhibit specific statistical properties, such as lack of first and second-order stationarity, that make results hard to interpret and the application of statistical methods potentially inappropriate (60). From a machine learning perspective, our methods would likely benefit from learning from more outbreaks in a given location (61, 62). These increased datasets will probably improve the robustness and performance of our analysis if the underlying relationship between predictors (Internet-based data streams) and outbreaks maintains temporal coherence.

## **Data and Methods**

In the following sections, we present the data sources that have been used for our study, along with a detailed explanation of our methods. In this work, we collected several data sources from January 2020 to January 2022 for 97 counties that are potential locations for vaccination trials or have a population of at least one million inhabitants.

### **Data sources**

In this section, we present and describe the epidemiological COVID-19 reports, COVID-19 and health-related searches from Google Trends API, UpToDate trends, and Twitter microblogs.



## **Official COVID-19 Reports**

We collected daily COVID-19 case counts from the Johns Hopkins University database (63). The serial interval (time from symptomatic primary infection to symptomatic secondary infection) was obtained from (64). For each US county, we obtained aggregated weekly time series covering the period between January 1, 2020, and January 1, 2022.

## **UpToDate Trends**

UpToDate is a software developed by UpToDate, Inc, a company in the Wolters Kluwer Health division (65). UpToDate is utilized by physicians and health centers as a tool to search for medical resources. Unlike Google Trends, all information provided in the UpToDate database is edited by experts using rigorous standards. This study used state-level COVID-19 related UpToDate searches from January 2020 to March 2021. We note that UpToDate stopped providing data after that period, and hence we could not evaluate the signal performance from April to December 2021.

## **Google Trends**

We utilized the Google Trends Application Programming Interface (API) to obtain daily COVID-19-related search terms. For the Single Source method, we chose the following COVID-19 related terms: “Covid”, Covid19, How Long Does Covid Last, Covid Symptoms and Covid 19 WHO. To account for common COVID-19 symptoms, we also selected Google Trends “Fever” and “Chest Pain”. To account for searches related to vaccination, we also chose the Google Trends terms “After Covid Vaccine”, “Side Effects Of Covid Vaccine”, and “Effects Of Covid Vaccine”. For the Multiple Source method, we increased the Google Trends dataset with more health-related terms to allow for a purely data-driven emergence of most relevant terms. A list of all terms can be found at the supplementary materials Table 11.

### **Twitter API:**

The Twitter data were harvested by an automated crawler connecting to Twitter's APIs in a fully automated fashion. The geo-crawler software collects georeferenced social media posts, i.e., tweets with an explicit geospatial reference. The geo-crawler requests data from two Twitter endpoints: the REST and streaming APIs. The REST API offers several API functionalities to access tweets, including the "search/tweets" endpoint that enables, the collection of tweets from the last seven days in a moving window. This requires a stringently designed collection procedure in order to harvest all provided tweets within the fast-moving time window of the API with a minimal number of requests. In contrast, the streaming API provides a real-time data stream that can be filtered using multiple parameters, including a post's language, location or user IDs.

The geo-crawler software requests tweets that include location information either as a point coordinate from the mobile device used for tweeting (e.g., GPS) or a rectangular outline based on a geocoded place name. The combination of the REST and streaming APIs makes crawling robust against interruptions or backend issues that inevitably lead to data holes. For example, if data from the streaming API cannot be stored in time, the missing data can be retrieved via the partly redundant REST API.

All tweets used for this study are located in the USA. To filter the data for COVID-19-relevant tweets, we used a simple keyword list as shown in Box 3. We opted for keyword-based filtering because of high performance, filtering in near real time, and its simplicity compared to machine-learning based semantic analysis methods. While a machine learning-based semantic clustering method like Guided Latent Dirichlet Allocation (LDA) may generate more comprehensive results (e.g., through identifying co-occurring and unknown terms), controlling the ratio between false positives and false negatives requires extensive experimental work and

expert knowledge, which is typically a strong limitation when dealing with large datasets.

Table 3: Search term list for Twitter.

---

covid, corona, epidemic, flu, influenza, face mask, spread, virus, infection, fever, panic buying, state of emergency, masks, quarantine, sars, 2019-ncov

---

## Apple Mobility

Apple mobility data were generated by counting the number of requests made to Apple Maps for directions in selected locations. Data sent from users' devices to Apple Maps service is associated with random, rotating identifiers, so Apple does not profile users' information. Data availability in a particular location is based on several factors, including minimum thresholds for direction requests per day. More details are available at

<https://www.apple.com/covid19/mobility>.

## Addressing delays in data

Our data streams experience specific availability delays. For example, the most recent values from Google Searches are available up to 36 hours before the current date. In addition, epidemiological reports suffer from backfilling and reporting delays due to post-processing. Thus for Google searches, data reported at time  $t$  was shifted to time  $t + 2$  to address the 36-hour delay. The following table shows the delay (in the number of days) that we imposed on each data source.

Source	Delay (days)
Epidemiological Reports	7
Google	2
UpToDate	1

## Estimating the effective reproductive number $R_t$ and defining outbreak onsets in COVID-19 activity

The effective reproductive number  $R_t$  is defined as the expected number of secondary cases generated by a primary case infected at time  $t$ . It can be used as a near real-time indicator to track trends and changes during an outbreak or to measure the impacts of public health interventions. When  $R_t > 1$ , we can expect epidemic growth, whereas when  $R_t < 1$ , the epidemic decreases. However, estimating  $R_t$  in near real-time can be challenging due to delays in reporting cases and under-ascertainment. While the latter is difficult to correct for general bias in all  $R_t$  estimation methods, we overcome reporting delays by using cases by date of onset. (52, 66). The most popular approach for near real-time estimation of  $R_t$  is the EpiEstim method introduced by Cori et al. (59). This method, while powerful, can suffer from edge effects and unstable inference during periods of low incidence (52). A recent approach from Parag et al. (EpiFilter) (52) circumvents some of these issues by applying Bayesian smoothing theory to improve estimate robustness (or minimize noise), especially in low incidence periods and between outbreaks. As early warning signals are desired in exactly such settings, we use this approach as a ground truth signal for outbreak onset.

In this work, we aimed to anticipate sharp increases in COVID-19 activity, using reported by JHU's confirmatory cases to determine outbreak onset events when the effective reproduction number ( $R_t$ ) was probabilistically higher than 1. To this end, we first defined the concept of **outbreak onset**. In this work, outbreak onsets marked the beginning of an exponential surge for a location's JHU's COVID-19 confirmed cases signal based on the probability  $P(R_t > 1)$ . For details on how this probability is calculated, we refer the reader to the recent work from Parag and Donnelly (67). We labeled a given date as the start of an outbreak onset whenever  $P(R_t > 1)$  crossed the 0.95 threshold for at least two consecutive weeks. An event was considered finished after  $P(R_t > 1) < 0.05$  (consecutive events that happened within at most 1-month

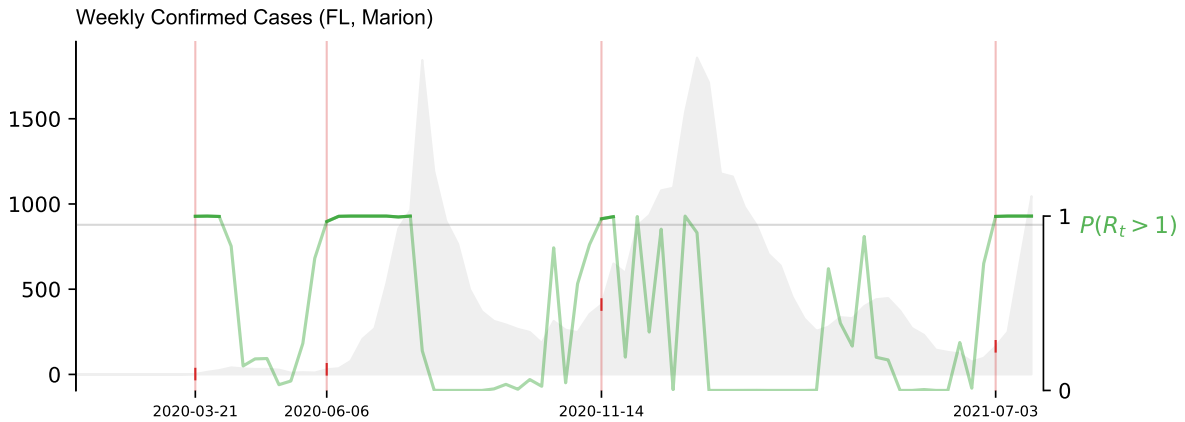


Figure 5: **Defining Outbreak onsets.** The value of  $P(R_t > 1)$  (green line) is calculated for the weekly volume of COVID-19 confirmed cases (gray) in Marion county (FL). A successive increase of COVID-19 confirmed case activity is labeled as an outbreak if  $P(R_t > 1) > 0.95$  for 2 weeks or more. Marked events are enclosed within a rectangle.

gap were considered a single event). Figure 5 exhibits a visual explanation of our outbreak onset definition for the COVID-19 confirmed cases activity of Marion county, Florida. We used this definition to identify the onsets that occurred within each the US locations selected for experimentation (97 counties and 50 states), and tested our ability to anticipate such dates utilizing alternative sources of information.

## Single Source Method

As a way to evaluate the predictive power of individual signals, we developed the Single Source method that explores the volume increase of available digital data to generate early warnings of COVID-19 activity. In Fig 6 (A) and (B), we illustrate the two possible alarm events. Given a 6-week time window spanning both digital and COVID-19 cases data, a *Threshold activation* is defined if the digital signal crosses a given threshold  $\tau$  (Fig 6 A). Fig 6 (B) shows a different kind of alarm, where a number  $\alpha$  of increases happen within the 6-week moving window ( $\alpha = 3$  in the example). In this case, we define an  $\alpha$ -week trend activation. A true positive occurs when an

alarm in the digital signal (either threshold or  $\alpha$ -week trend) precedes the outbreak onset event within the six-week moving window. Fig 6 (C) illustrates other possible outcomes in the Single Source method. We only show threshold activations for simplicity. A false positive occurs when the digital signal activates (either through threshold or  $\alpha$ -week trend) but no outbreak onset event occur. Conversely, a false negative may occur when an event occur but no alarm is triggered by the individual signal. Finally, a true negative takes place when no alarms in the individual signal or outbreak onset events occur within the 6-week moving window.

For the training step, we choose multiple threshold values, which are normalized by the maximum of the digital signal in the training period, resulting in a scale from 0.1 to 0.9. We also select possible values for  $\alpha$  in the  $\alpha$ -week trend activation ranging between 2 and 5 signal uptrends within the 6-week moving window. As the window progresses in time, we compute the number of true positives (TP), false positives (FP), false negatives (FN), and true negatives (TN). With that information, we obtain performance metrics such as accuracy as depicted in Fig 6 (D). From the collection of  $\tau$  and  $\alpha$  maximizing performance metrics (red rectangle in Fig 6 (D)), we choose those minimum parameter values (black star) to promote the earliness of our prediction method. In our simulations, we chose to simultaneously optimize accuracy ( $\frac{TP+TN}{P+N}$ ), precision ( $\frac{TP}{P}$ ) and the negative predictive values ( $\frac{TN}{N}$ ) where  $P = TP + FP$  and  $N = TN + FN$ . By doing this, we arrive at the minimum optimal  $\tau$  and  $\alpha$  maximizing those three quantities at the same time. If there are no such parameter values, we optimize over precision only.

## Multiple Source Method

Here we describe our Multiple Source method. Given that our earlier work had shown the feasibility of implementing digital streams as alternative proxies to track state-level COVID-19 activity (50), we hypothesized that a county-level early warning system could provide a higher

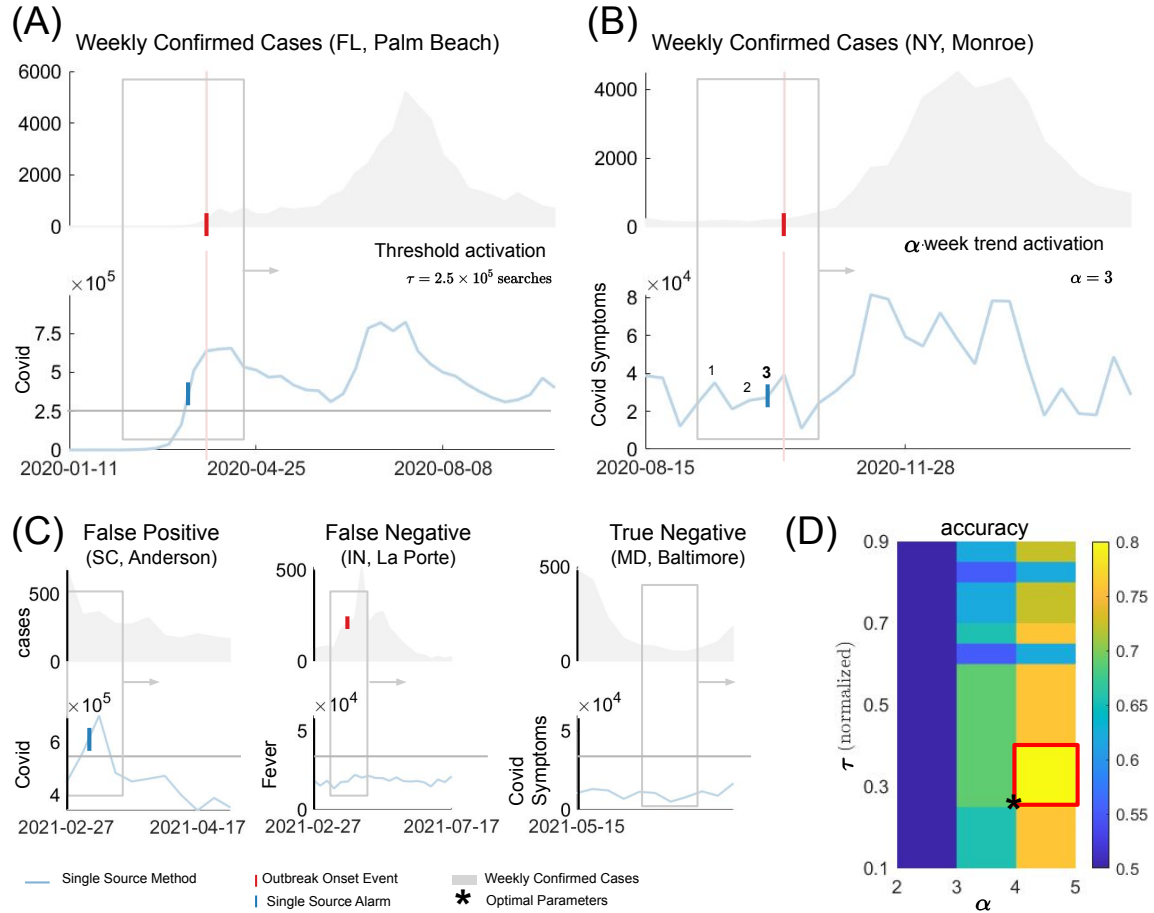


Figure 6: **An Early Warning System for COVID-19 based on single sources (Single Source method).** A moving window spans both predictor (Google trends for the term COVID) and COVID-19 cases. A *Threshold activation* occurs when a predictor signal crosses the value  $\tau$ . In the example,  $\tau = 2.5 \times 10^5$  Google searches for Palm Beach County (FL). The blue tick denotes the week of crossing. The red vertical tick and line denote the week of the outbreak onset event. **(B)** If a number  $\alpha$  of increases happen in the predictor signal, an  $\alpha$ -week trend activation takes place. In the example,  $\alpha = 3$  triggers an alarm for Monroe (NY) county preceding the outbreak onset event. Both **(A)** and **(B)** represent true positive events. **(C)** Definitions of false positive, false negative, and true negative events. **(D)** For the training step, we evaluate the performance of our Single Source method for different thresholds  $\tau$  (normalized by the maximum of the signal on the training period) and  $\alpha$  values for the  $\alpha$ -week trend activation. A colormap with the training accuracy shows the highest rate for  $\tau$  and  $\alpha$ . The example illustrates optimal parameters  $\tau$  and  $\alpha$  as the lowest values such that accuracy is maximized, indicated by a black star in the lower leftmost corner of the red rectangle.

resolution picture of the pandemic at near real-time. In what follows, we define the variables of our early warning system and provide a detailed explanation for each step of our analysis.

## Definitions

To describe our Multiple Source method in detail, in this section we start defining the following variables:

- $\mathbf{y}$ : Target signal to track using our early warning system methodologies. In this work,  $\mathbf{y}$  is given by the time series  $\{P(R_t > 1)\}_{t>0}$ . We define  $y_t$  as the value of  $\mathbf{y}$  at week  $t$ .
- $\mathbf{X} = \{\mathbf{x}_i, i = 1, 2, \dots, N\}$ : The set of all alternative proxies, i.e., official epidemiological reports, Google Search volumes, social network activity, Twitter microblogs, among others. We refer the reader to our data sources section for a detailed description of these datasets. We define  $x_{i,t}$  as the value of  $\mathbf{x}_i$  at week  $t$ .
- $t_e$ : Event onset date and can be used to represent outbreak onset events (denoted by  $t_{e,\mathbf{y}}$ ) generated by the time series  $\{P(R_t > 1)\}_{t>0}$  or proxy events (denoted by  $t_{e,\mathbf{x}_i}$ ) generated by the lambda approach.
- $\mathbf{M} = EWS(\mathbf{y}, \mathbf{X})$ : An early warning system output as a function of all available data from both target and proxies. We define  $M_t$  as the value of  $\mathbf{M}$  at week  $t$ .

## Lambda Approach: capturing increasing activity trends in digital proxies

To define and label proxy events, we utilized a measure of a proxy trend henceforth called  $\lambda$ . Here we emphasize that  $\lambda$  was calculated for our proxy variables, i.e., the Google Trends Signals, Twitter, and other digital traces. However, we derived this measure from the classic SIR epidemic model equations



$$\begin{aligned}\dot{S} &= -\beta SI \\ \dot{I} &= \beta SI - \gamma I\end{aligned}\tag{1}$$

where  $S$  and  $I$  represent the populations of susceptible and infected individuals and  $r = N - S - I$  represents the recovered class in a constant population of size  $N$ . For an inter-outbreak period, where the number of infected individuals  $I$  is very low, the susceptible pool of individuals  $S$  can be assumed as a constant parameter  $S = S^*$ . In this case, the SIR system of equations reduces to

$$\begin{aligned}\dot{S} &= 0 \\ \dot{I} &= (\beta S^* - \gamma)I\end{aligned}\tag{2}$$

and the solution to the equation for the number of infected individuals  $I$  is then an exponential function with the intrinsic growth rate

$$\lambda = \beta S^* - \gamma,\tag{3}$$

which is directly proportional to the size of the susceptibility pool. In the context of epidemiological models,  $\lambda$  can be thought of as an indicator of the susceptible population that is easily interpretable: if  $\lambda > 1$ , then  $I$  increases exponentially. Moreover,  $\lambda$  can be estimated by linear regression, as the coefficient of a 1-lag autoregressive model with no intercept  $I_t = \lambda I_{t-1}$ . In this work, we utilize a 3-week time window to estimate the value of  $\lambda$ .

**Implementing  $\lambda$  in practice:** For each week  $t$ , we calculated the value of  $\lambda_t$  using the most recent data available. Retrospectively, a proxy event was defined as a period where the value  $\lambda_t > 1$  for at least two weeks. If two time periods satisfied such conditions but were only separated at most four weeks apart, they were merged into a single, bigger period.

## Implementing the Multiple Source Method

Our Early Warning system  $M$  was designed to track COVID-19 outbreak events by iteratively identifying proxy signals  $x_i$  that have experienced events preceding a target ( $y$ ) events, and combining them into a single output signal  $M_t$ , where  $0 \leq M_t < 1$  for all  $t > 0$ . This output signal  $M_t$  can be interpreted as an indicator for  $y$  experiencing an outbreak in the near future (up to 6 weeks). Given  $y$  and  $\mathbf{X}$  up to week  $t$  for an specific location, we implement our method as follows:

**Data Preparation:** We begin by identifying all the outbreak events for  $y$  and the proxy events in our dataset  $\mathbf{X}$ . These events are used to establish a performance ranking for each proxy  $x_i$  via the following labeling rules (applied individually to each proxy):

- **True Positive (TP):** If a proxy event  $t_{e,x_i}$  precedes an outbreak onset event  $t_{e,y}$  by at most 6 weeks, we label  $t_{e,x_i}$  as true positive.
- **False Positive (FP):** If a proxy event  $t_{e,x_i}$  occurs but there is no outbreak onset event happening in the next 6 weeks, then we label that proxy's event as a false positive, also referred as false alarm.
- **False Negative (FN):** If an outbreak onset event  $t_{e,y}$  occurs but no proxy event occurs at most 6 weeks retrospectively, then we identify that as a false negative.

The number of TP, FP and FN is then calculated for each proxy  $x_i$ . With the aim of focusing specifically in the detection of outbreak events and avoiding a highly imbalanced dataset, we do not optimize for True Negatives events, since every week where the activity was not an outbreak onset or within the outbreak period (as marked by  $R_t$ ) would be a potential true negative.

**Feature Selection:** A performance ranking is created based on the TP, FP and FN values of each proxy. Given our main objective is to identify outbreak events for  $t_{e,y}$  earlier in time, we

prioritize signals maximizing true positives while minimizing false positives. A subset of six proxies  $\chi = \{\mathbf{x}_1, \mathbf{x}_2, \dots, \mathbf{x}_6\}$  with highest TP and lowest FP is then selected to be used as the input for our early warning system. In the case more than six are fit to be used within our early warning system, those six proxies are then selected randomly.

**Combining Selected Proxies into an Early Warning System:** The value  $M_t$  of our early warning system is given by the expression

$$M_t = 2S(n_{e,t}) - 1$$

where

$$n_{e,t} = \sum_{\mathbf{x}_i \in \chi} g(\mathbf{x}_i, t),$$

and

$$g(\mathbf{x}_i, t) = \begin{cases} 1 & \text{if } t - k \leq t_{e,\mathbf{x}_i} \leq t \\ 0 & \text{otherwise} \end{cases}$$

is the number of proxy events that have occurred in the past  $k = 3$  weeks, and

$$S(x) = \frac{1}{1 + e^{-x}}$$

is the well known sigmoid function. Intuitively, the quantity  $M_t$  changes between 0 and 0.9951 ( $\sim 1$ ) depending on the number of proxies events (from zero to six) within the past  $k$  weeks before the week  $t$ .

**Thresholding:** Although each proxy  $\mathbf{x}_i$  has been selected based on the premise that its events have successfully tracked our target  $y$  during training (and thus, even a low value  $M_t$  may convey some relevant information about an incoming event), there may be some instances when not all proxies in the set  $\chi$  have activated prior to an outbreak onset event. Similarly,

as we compute the value of  $M_t$  every week, there may be some instances when a proxy (for example, Google search activity spiking due to non-COVID related events) triggers an alarm, and thus increasing the value of  $M_t$ . Based on these possibilities, and with the purpose of having a more practical way of interpreting  $M_t$ , we define a decision threshold  $\tau$  which we use to map  $M_t$  into a "yes/no" methodology. If  $M_t > \tau$ , then we interpret it as our early warning system is expecting an outbreak onset event happening in the near future. In practice, we find this threshold by computing the performance of our early warning system as a function of the threshold  $\tau$  (similar to an ROC curve) and selecting the threshold that maximizes a metric of interest (precision, for example).

Given that  $M_t$  is calculated every week using a  $k$ -week moving window, our early warning system events consist in a subset of weeks in which  $M_t > \tau$  (this is to be contrasted to a  $x_i$  event, which consists only of a single week). Based on this behavior, we define a different set of event labels which we use to compute the performance of our early warning system. We label our events in the following way:

- **True Positive (TP):** If  $M_t > \tau$  prior  $t_{e,y}$  within a retrospective window of  $w$  weeks.
- **Strict False Positive (FP):** If  $M_t > \tau$  but no outbreak onset event  $t_{e,y}$  is observed in the following  $w$  weeks.
- **Relaxed False Positive (RFP):** Given a set of  $m$  subsequent weeks where  $M_t > \tau$ , we count all dates as a single misfire (in comparison to a strict misfire, which would  $m$  misfires instead of 1).
- **False Negative (FN):** If  $t_{e,y}$  occurs but  $M_t > \tau$  is not observed retrospectively within a  $w$  week window.

We also define

$$m_1 = \frac{TP}{TP + FP + FN} \quad (4)$$

and

$$m_2 = \frac{TP}{TP + FN + RFP}. \quad (5)$$

Given that the  $M_t$  values are inherently connected overtime (if  $M_t > \tau$  then it may take some weeks to deactivate), optimizing for  $m_1$  usually lead to high threshold values as a way to avoid a high number of strict false positives (i.e. keeping  $M_t > \tau$  a high number of weeks). Although this is desirable in practice (having an system which only activates when it is certain that an event is going to happen, and below the threshold otherwise),  $m_1$  may cause our early warning system to overfit given a) The very low number of events scenario may not convey enough information to find an adequate threshold and b) If  $M_t > 0$  for the first occasion at week  $t$ , then it takes at least  $k$  weeks to change its value. On the other hand, optimizing for  $m_2$  encourages the selection of lower threshold values as it does not penalize  $M_t > \tau$  being true for a long period. Nonetheless,  $m_2$  may go as low as a threshold of  $\tau = 0$  if there are no False Negatives or if the number of Relaxed False Positives is the same below a certain threshold value. We thus opt for optimizing the averaged sum of  $m_1$  and  $m_2$ . Precisely, our optimal threshold  $\tau_{opt}$  is given by

$$\tau_{opt} = \operatorname{argmax}_{\tau \in [0,1]} \left( \frac{m_1 + m_2}{2} \right),$$

where both  $m_1$  and  $m_2$  given by Eqs. 4 and 5 depend on  $\tau$ .

**Out of sample experiment description:** For a given location with outbreak onset events  $\mathbf{E} = \{e_1, e_2, \dots, e_n\}$ , we utilized  $e_1$  as the first event for training, with the aim to predict  $e_2$ . As a next step, we incorporate  $e_2$  into the training dataset, and thus use both  $e_1$  and  $e_2$  to train our early warning system, and predict the following event  $e_3$ . We repeated this procedure until the

last event  $e_n$ . We also defined the out-of-sample period as the time interval between the week when the last outbreak event in the training dataset ended and the week when the out-of-sample outbreak onset occurred.

We counted the number of times when a method triggered an alarm based on the following labels:

- **Early warnings:** When the early warning system triggered an alarm preceding the outbreak onset event with at most six weeks in advance.
- **Synchronous warnings:** When the early warning system triggered an alarm on the same date as the outbreak onset
- **Late Warnings:** Events where the early warning system triggered an alarm up to two weeks later than the outbreak onset event.
- For the Multiple Source method, we considered a **soft warnings** when the output of the early warning system increased at least 70% of the decision threshold and the outbreak onset event was successfully observed six weeks after.
- **Missed outbreaks:** when an outbreak onset event was observed, but no alarm was registered within the observation window.
- In terms of false alarms, we differentiated between two different scenarios:
  1. A **False Alarm with no increase** occurred when the system triggered an alarm, but no event *and* no increase in COVID-19 cases were observed in the following six weeks.
  2. A **False Alarm with increase observed** occurred when the early warning system triggered an alarm and was followed by an increase in COVID-19 cases.

## Acknowledgments

We thank Wolters Kluwer Health's UpToDate team for providing resource-specific data. We also thank Dr. Bill Hanage and the members of the Center for Communicable Disease Dynamics (CCDD) at the Harvard T.H. Chan School of Public Health for insightful comments that improved this work. **Funding:** This project has been funded (in part) by contract 200-2016-91779 with the Centers for Disease Control and Prevention. **Disclaimer:** The findings, conclusions, and views expressed are those of the author(s) and do not necessarily represent the official position of the Centers for Disease Control and Prevention (CDC). Research reported in this publication was also partially supported by the National Institute of General Medical Sciences of the National Institutes of Health under Award Number R01GM130668. The content is solely the responsibility of the authors and does not necessarily represent the official views of the National Institutes of Health. M.S., L.M.S. and L.C. thank the Johnson & Johnson Foundation for providing institutional research funds and Johnson & Johnson Global Public Health for their support **Author contributions:** M.S, L.M.S, and L.C conceptualized the study, interpreted the results and wrote the first draft of the paper; M.S supervised the study. L.M.S and L.C designed and implemented the methodologies, collected and analyzed the data. C.P and K.V.P contributed to the methods section. B.R provided Twitter data. S.M and A.M provided additional subject matter expertise in shaping our methodologies. All authors contributed to and approved the final version of the manuscript. **Competing interests:** The authors declare that they have no competing interests. **Data and materials availability:** All data needed to evaluate the conclusions in the paper are present in the paper and/or the Supplementary Information. Additional data related to this paper may be requested from the authors. Some data sources may require establishing data sharing agreements with the data providers, which have been established with a diverse set of research teams. Code can be made available upon request.

## Supplementary Information

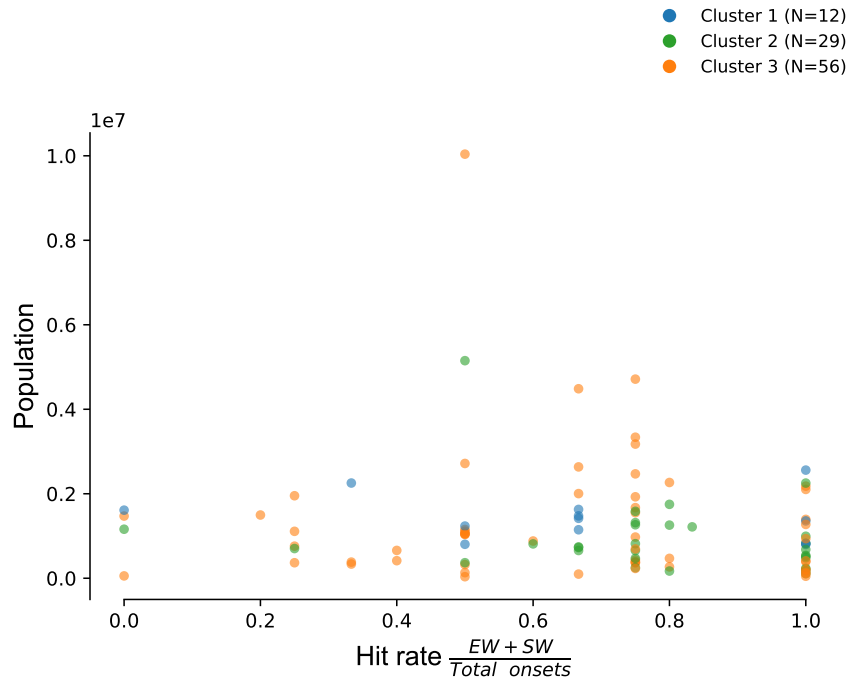


Figure 7: **Performance of the Multiple Source method vs. population sizes** Scatter plot of the relationship between population size and the out-of-sample Hit rate of the Multiple Source method across the 97 counties (color-coded depending on the assigned cluster group from Fig 3)



Model Time	Naive		Single Source ("How long does covid last?")		Single Source ("side effects of vaccine")		Multiple Source		
	Before 2021-12-01	After 2021-12-01	Before 2021-12-01	After 2021-12-01	Before 2021-12-01	After 2021-12-01	Before 2021-12-01	After 2021-12-01	Total
Total Events	305 (100%)	62 (100%)	367 (100%)	62 (100%)	367 (100%)	62 (100%)	305 (100%)	62 (100%)	367 (100%)
Early Warning	305 (100%)	62 (100%)	367 (100%)	35 (56%)	237 (65%)	43 (69%)	175 (57%)	38 (61%)	213 (58%)
Sync Warning	0 (0%)	0 (0%)	0 (0%)	2 (3%)	25 (7%)	3 (5%)	37 (12%)	3 (5%)	40 (11%)
Late Warning	1 (0%)	0 (0%)	0 (0%)	4 (6%)	30 (8%)	1 (2%)	34 (11%)	3 (5%)	37 (10%)
Soft Warning	0 (0%)	0 (0%)	0 (0%)	0 (0%)	0 (0%)	0 (0%)	45 (15%)	16 (26%)	61 (17%)
Missed Outbreaks	0 (0%)	0 (0%)	0 (0%)	21 (34%)	75 (20%)	15 (24%)	14 (5%)	2 (3%)	16 (4%)
Warning, increase observed	224	28	252	17	139	23	148	2	36
False Alarm	502	110	612	47	327	105	374	19	114

Table 4: A Summary of the results at the County-level. Here EWS stands for Early Warning System.

Model Time	Naive		Single Source ("How long does covid last?")		Single Source ("chest pain")		Multiple Source		
	Before 2021-12-01	After 2021-12-01	Before 2021-12-01	After 2021-12-01	Before 2021-12-01	After 2021-12-01	Before 2021-12-01	After 2021-12-01	Total
Total Events	183 (100%)	19 (100%)	202 (100%)	19 (100%)	202 (100%)	19 (100%)	183 (100%)	19 (100%)	202 (100%)
Early Warning	160 (87%)	18 (95%)	178 (88%)	13 (68%)	128 (63%)	12 (63%)	82 (45%)	17 (89%)	99 (49%)
Sync Warning	22 (12%)	1 (5%)	23 (11%)	2 (11%)	13 (6%)	0 (0%)	22 (12%)	0 (0%)	22 (11%)
Late Warning	1 (1%)	0 (0%)	1 (0%)	1 (5%)	18 (9%)	0 (0%)	24 (13%)	0 (0%)	24 (12%)
Soft Warning	0 (0%)	0 (0%)	0 (0%)	0 (0%)	0 (0%)	0 (0%)	39 (21%)	2 (11%)	41 (20%)
Missed Outbreaks	0 (0%)	0 (0%)	0 (0%)	3 (16%)	43 (21%)	7 (37%)	16 (9%)	0 (0%)	16 (8%)
Warning, increase observed	74	8	82	6	63	6	19	1	20
False Alarm	171	39	210	15	119	9	30	4	34

Table 5: A Summary of the results at the state-level. Here EWS stands for Early Warning System.

N = 367	Early Warning	Sync Warning	Late Warning	Missed Outbreaks	Warning, activity increases	False Alarm
gt_howLongDoesCovidLast_rt	237 (65%)	25 (7%)	30 (8%)	74 (20%)	139	327
gt_sideEffectsOfVaccine_rt	227 (62%)	19 (5%)	15 (4%)	105 (29%)	171	479
gt_chestPain_rt	201 (55%)	19 (5%)	38 (10%)	108 (29%)	128	301
gt_covid_19Who	169 (46%)	25 (7%)	20 (5%)	152 (41%)	87	269
JHU_deaths_rt	147 (40%)	16 (4%)	31 (8%)	172 (47%)	93	249
gt_covidSymptoms_rt	145 (40%)	30 (8%)	50 (14%)	141 (38%)	58	122
gt_afterCovidVaccine_rt	141 (38%)	20 (5%)	29 (8%)	176 (48%)	182	463
JHU_cases_rt	135 (37%)	59 (16%)	58 (16%)	114 (31%)	100	204
gt_effectsOfCovidVaccine_rt	107 (29%)	14 (4%)	20 (5%)	225 (61%)	110	374
gt_fever_rt	85 (23%)	24 (7%)	21 (6%)	236 (64%)	40	107
gt_covid_19	79 (22%)	22 (6%)	53 (14%)	212 (58%)	52	127
gt_covid_rt	51 (14%)	19 (5%)	65 (18%)	231 (63%)	10	54
twitter_state_rt	41 (11%)	14 (4%)	56 (15%)	255 (69%)	20	40
up2date_rt_parag	37 (10%)	7 (2%)	24 (7%)	298 (81%)	10	32

**Table 6: County-Level results for the Single Source Method**

N=202	Early Warning	Sync Warning	Late Warning	Missed Outbreaks	Warning, activity increases	False Alarm
gt_howLongDoesCovidLast_rt	128 (63%)	13 (6%)	18 (9%)	42 (21%)	63	119
gt_chestPain_rt	120 (59%)	12 (6%)	12 (6%)	57 (28%)	41	121
gt_covid_19Who	112 (55%)	11 (5%)	19 (9%)	59 (29%)	51	104
gt_sideEffectsOfVaccine_rt	96 (48%)	12 (6%)	18 (9%)	75 (37%)	56	165
gt_covidSymptoms_rt	88 (44%)	8 (4%)	15 (7%)	90 (45%)	28	45
JHU_cases_rt	78 (39%)	22 (11%)	33 (16%)	68 (34%)	29	97
gt_afterCovidVaccine_rt	68 (34%)	8 (4%)	8 (4%)	117 (58%)	67	149
JHU_deaths_rt	65 (32%)	13 (6%)	13 (6%)	110 (54%)	28	72
gt_effectsOfCovidVaccine_rt	63 (31%)	6 (3%)	7 (3%)	125 (62%)	30	90
gt_covid_19	46 (23%)	9 (4%)	30 (15%)	116 (57%)	21	54
gt_fever_rt	45 (22%)	5 (2%)	15 (7%)	136 (67%)	24	42
twitter_state_rt	27 (13%)	8 (4%)	28 (14%)	138 (68%)	10	11
gt_covid_rt	26 (13%)	5 (2%)	21 (10%)	149 (74%)	10	14
up2date_rt_parag	18 (9%)	5 (2%)	14 (7%)	164 (81%)	8	9

**Table 7: State-Level results for the Single Source Method**

Data Source(s) Used	Early Warning	Sync Warning	Late Warning	Soft Warning	Missed Outbreaks	Warning increase observed	False Alarm False Alarm	Non-deployed Non-deployed
Local Epi, Google Searches, Neighbor Data	99 (49%)	22 (11%)	24 (12%)	41 (20%)	16 (8%)	20	34	0 (0%)
Local Epi, Google Searches, Neighbor Data, UpTo...	99 (49%)	22 (11%)	24 (12%)	41 (20%)	16 (8%)	20.0	34.0	0 (0%)
Local Epi, Google Searches, Neighbor Data, Twitter	99 (49%)	22 (11%)	24 (12%)	41 (20%)	16 (8%)	20.0	34.0	0 (0%)
Local Epi, Google Searches, Neighbor Data, Twit...	99 (49%)	22 (11%)	24 (12%)	41 (20%)	16 (8%)	20.0	34.0	0 (0%)
Local Epi, Google Searches, Neighbor Data, Appl...	99 (49%)	21 (10%)	24 (12%)	42 (21%)	16 (8%)	20.0	36.0	0 (0%)
Local Epi, Google Searches, Neighbor Data, Appl...	99 (49%)	21 (10%)	24 (12%)	42 (21%)	16 (8%)	20.0	36.0	0 (0%)
Local Epi, Google Searches, Neighbor Data, Twit...	99 (49%)	21 (10%)	24 (12%)	42 (21%)	16 (8%)	20.0	36.0	0 (0%)
Local Epi, Google Searches, Neighbor Data, Twit...	99 (49%)	21 (10%)	24 (12%)	42 (21%)	16 (8%)	20.0	36.0	0 (0%)
Google Searches, Neighbor Data	97 (48%)	23 (11%)	25 (12%)	41 (20%)	16 (8%)	20.0	37.0	0 (0%)
Google Searches, Neighbor Data, UpToDate	97 (48%)	23 (11%)	25 (12%)	41 (20%)	16 (8%)	20.0	37.0	0 (0%)
Google Searches, Neighbor Data, Twitter	97 (48%)	23 (11%)	25 (12%)	41 (20%)	16 (8%)	20.0	37.0	0 (0%)
Google Searches, Neighbor Data, Twitter, UpToDate	97 (48%)	23 (11%)	25 (12%)	41 (20%)	16 (8%)	20.0	37.0	0 (0%)
Google Searches, Neighbor Data, Apple Mobility	97 (48%)	22 (11%)	25 (12%)	42 (21%)	16 (8%)	20.0	39.0	0 (0%)
Google Searches, Neighbor Data, Apple Mobility,...	97 (48%)	22 (11%)	25 (12%)	42 (21%)	16 (8%)	20.0	39.0	0 (0%)
Google Searches, Neighbor Data, Twitter, Apple ...	97 (48%)	22 (11%)	25 (12%)	42 (21%)	16 (8%)	20.0	39.0	0 (0%)
Google Searches, Neighbor Data, Twitter, Apple ...	97 (48%)	22 (11%)	25 (12%)	42 (21%)	16 (8%)	20.0	39.0	0 (0%)
Google Searches, Apple Mobility	93 (46%)	19 (9%)	23 (11%)	50 (25%)	17 (8%)	20.0	38.0	0 (0%)
Google Searches, Apple Mobility, UpToDate	93 (46%)	19 (9%)	23 (11%)	50 (25%)	17 (8%)	20.0	37.0	0 (0%)
Google Searches,	92 (46%)	20 (10%)	23 (11%)	50 (25%)	17 (8%)	19.0	36.0	0 (0%)
Google Searches, UpToDate	92 (46%)	20 (10%)	23 (11%)	50 (25%)	17 (8%)	19.0	35.0	0 (0%)
Google Searches, Twitter, Apple Mobility	92 (46%)	20 (10%)	24 (12%)	49 (24%)	17 (8%)	20.0	38.0	0 (0%)
Google Searches, Twitter, Apple Mobility, UpToDate	92 (46%)	20 (10%)	24 (12%)	49 (24%)	17 (8%)	20.0	37.0	0 (0%)
Local Epi, Google Searches, Apple Mobility	91 (45%)	23 (11%)	22 (11%)	49 (24%)	17 (8%)	20.0	34.0	0 (0%)
Local Epi, Google Searches, Apple Mobility, UpT...	91 (45%)	23 (11%)	22 (11%)	49 (24%)	17 (8%)	20.0	33.0	0 (0%)
Local Epi, Google Searches, Twitter, Apple Mobi...	91 (45%)	23 (11%)	23 (11%)	48 (24%)	17 (8%)	20.0	34.0	0 (0%)
Local Epi, Google Searches, Twitter, Apple Mobi...	91 (45%)	23 (11%)	23 (11%)	48 (24%)	17 (8%)	20.0	33.0	0 (0%)
Google Searches, Twitter	91 (45%)	21 (10%)	24 (12%)	49 (24%)	17 (8%)	19.0	36.0	0 (0%)
Google Searches, Twitter, UpToDate	91 (45%)	21 (10%)	24 (12%)	49 (24%)	17 (8%)	19.0	35.0	0 (0%)
Local Epi, Google Searches	90 (45%)	24 (12%)	22 (11%)	50 (25%)	16 (8%)	19.0	32.0	0 (0%)
Local Epi, Google Searches, UpToDate	90 (45%)	24 (12%)	22 (11%)	50 (25%)	16 (8%)	19.0	31.0	0 (0%)
Local Epi, Google Searches, Twitter	90 (45%)	24 (12%)	23 (11%)	49 (24%)	16 (8%)	19.0	32.0	0 (0%)
Local Epi, Google Searches, Twitter, UpToDate	90 (45%)	24 (12%)	23 (11%)	49 (24%)	16 (8%)	19.0	31.0	0 (0%)
Local Epi, Twitter, Apple Mobility, UpToDate	86 (43%)	27 (13%)	18 (9%)	44 (22%)	21 (10%)	17.0	60.0	6 (3%)
Local Epi, Apple Mobility	85 (42%)	29 (14%)	8 (4%)	24 (12%)	38 (19%)	18.0	58.0	18 (9%)
Local Epi, Twitter, Apple Mobility	84 (42%)	28 (14%)	17 (8%)	43 (21%)	22 (11%)	17.0	61.0	8 (4%)
Local Epi, Apple Mobility, UpToDate	81 (40%)	27 (13%)	8 (4%)	38 (19%)	36 (18%)	18.0	58.0	12 (6%)
Twitter, Apple Mobility	80 (40%)	17 (8%)	15 (7%)	45 (22%)	32 (16%)	17.0	55.0	13 (6%)
Twitter, Apple Mobility, UpToDate	80 (40%)	17 (8%)	16 (8%)	48 (24%)	30 (15%)	19.0	58.0	11 (5%)
Local Epi, Twitter, UpToDate	79 (39%)	39 (19%)	27 (13%)	3 (1%)	26 (13%)	10.0	20.0	28 (14%)
Neighbor Data, Apple Mobility, UpToDate	76 (38%)	21 (10%)	16 (8%)	59 (29%)	29 (14%)	10.0	27.0	1 (0%)
Local Epi, Neighbor Data, Apple Mobility, UpToDate	76 (38%)	21 (10%)	20 (10%)	57 (28%)	27 (13%)	10.0	24.0	1 (0%)
Neighbor Data, Twitter, Apple Mobility, UpToDate	76 (38%)	20 (10%)	15 (7%)	62 (31%)	28 (14%)	9.0	21.0	1 (0%)
Apple Mobility,	75 (37%)	14 (7%)	5 (2%)	21 (10%)	57 (28%)	16.0	56.0	30 (15%)
Neighbor Data, Twitter, Apple Mobility	74 (37%)	20 (10%)	14 (7%)	63 (31%)	28 (14%)	11.0	22.0	3 (1%)
Neighbor Data, Apple Mobility	74 (37%)	19 (9%)	15 (7%)	60 (30%)	30 (15%)	10.0	25.0	4 (2%)
Local Epi, Neighbor Data, Apple Mobility	73 (36%)	22 (11%)	20 (10%)	57 (28%)	26 (13%)	9.0	23.0	4 (2%)
Local Epi, Neighbor Data, Twitter, Apple Mobili...	73 (36%)	21 (10%)	20 (10%)	62 (31%)	25 (12%)	8.0	20.0	1 (0%)
Apple Mobility, UpToDate	73 (36%)	14 (7%)	7 (3%)	32 (16%)	53 (26%)	18.0	58.0	23 (11%)
Local Epi, Twitter	72 (36%)	40 (20%)	28 (14%)	0 (0%)	23 (11%)	8.0	22.0	39 (19%)
Local Epi, Neighbor Data, Twitter, Apple Mobility	70 (35%)	23 (11%)	20 (10%)	60 (30%)	26 (13%)	9.0	21.0	3 (1%)
Twitter, UpToDate	67 (33%)	18 (9%)	37 (18%)	0 (0%)	36 (18%)	9.0	21.0	44 (22%)
Neighbor Data, Twitter, UpToDate	62 (31%)	23 (11%)	17 (8%)	55 (27%)	38 (19%)	6.0	14.0	7 (3%)
Neighbor Data, UpToDate	59 (29%)	25 (12%)	19 (9%)	52 (26%)	40 (20%)	7.0	15.0	7 (3%)
Local Epi, Neighbor Data, Twitter, UpToDate	59 (29%)	23 (11%)	22 (11%)	59 (29%)	32 (16%)	5.0	13.0	7 (3%)
Local Epi, Neighbor Data, UpToDate	58 (29%)	25 (12%)	23 (11%)	55 (27%)	34 (17%)	7.0	13.0	7 (3%)
Neighbor Data, Twitter	56 (28%)	27 (13%)	16 (8%)	54 (27%)	39 (19%)	6.0	13.0	10 (5%)
Twitter,	56 (28%)	17 (8%)	39 (19%)	0 (0%)	32 (16%)	7.0	19.0	58 (29%)
Neighbor Data,	55 (27%)	23 (11%)	17 (8%)	53 (26%)	43 (21%)	6.0	13.0	11 (5%)
Local Epi, Neighbor Data	53 (26%)	24 (12%)	22 (11%)	56 (28%)	36 (18%)	6.0	11.0	11 (5%)
Local Epi, Neighbor Data, Twitter	51 (25%)	28 (14%)	22 (11%)	57 (28%)	34 (17%)	5.0	11.0	10 (5%)
Local Epi, UpToDate	37 (18%)	48 (24%)	13 (6%)	0 (0%)	43 (21%)	8.0	9.0	61 (30%)
Local Epi,	23 (11%)	43 (21%)	10 (5%)	0 (0%)	21 (10%)	4.0	6.0	105 (52%)
UpToDate,	17 (8%)	6 (3%)	6 (3%)	0 (0%)	49 (24%)	5.0	3.0	124 (61%)

**Table 8: State-level performance of the Multiple Source method for different data sources used for the training step.** An additional column, 'Non-deployed,' indicates the number of outbreak events where our Multiple Source method did not find a reasonable set of proxies to fit a model. Thus, an early warning system was not deployed to forecast the out-of-sample period.

Data Source(s) Used	Early Warning	Sync Warning	Late Warning	Soft Warning	Missed Outbreaks	Warning increase observed	False Alarm False Alarm	Non-deployed Non-deployed
Local Epi, Google Searches	224 (61%)	27 (7%)	36 (10%)	64 (17%)	16 (4%)	43	117	0 (0%)
Local Epi, Google Searches, UpToDate	224 (61%)	27 (7%)	36 (10%)	64 (17%)	16 (4%)	43.0	117.0	0 (0%)
Local Epi, Google Searches, Apple Mobility	224 (61%)	27 (7%)	36 (10%)	64 (17%)	16 (4%)	43.0	117.0	0 (0%)
Local Epi, Google Searches, Apple Mobility, UpT...	224 (61%)	27 (7%)	36 (10%)	64 (17%)	16 (4%)	43.0	117.0	0 (0%)
Local Epi, Google Searches, Twitter	224 (61%)	27 (7%)	36 (10%)	64 (17%)	16 (4%)	43.0	117.0	0 (0%)
Local Epi, Google Searches, Twitter, UpToDate	224 (61%)	27 (7%)	36 (10%)	64 (17%)	16 (4%)	43.0	117.0	0 (0%)
Local Epi, Google Searches, Twitter, Apple Mobi...	224 (61%)	27 (7%)	36 (10%)	64 (17%)	16 (4%)	43.0	117.0	0 (0%)
Local Epi, Google Searches, Twitter, Apple Mobi...	224 (61%)	27 (7%)	36 (10%)	64 (17%)	16 (4%)	43.0	117.0	0 (0%)
Google Searches,	220 (60%)	23 (6%)	32 (9%)	78 (21%)	14 (4%)	42.0	114.0	0 (0%)
Google Searches, UpToDate	220 (60%)	23 (6%)	32 (9%)	78 (21%)	14 (4%)	42.0	114.0	0 (0%)
Google Searches, Apple Mobility	220 (60%)	23 (6%)	32 (9%)	78 (21%)	14 (4%)	42.0	114.0	0 (0%)
Google Searches, Apple Mobility, UpToDate	220 (60%)	23 (6%)	32 (9%)	78 (21%)	14 (4%)	42.0	114.0	0 (0%)
Google Searches, Twitter	220 (60%)	23 (6%)	32 (9%)	78 (21%)	14 (4%)	42.0	114.0	0 (0%)
Google Searches, Twitter, UpToDate	220 (60%)	23 (6%)	32 (9%)	78 (21%)	14 (4%)	42.0	114.0	0 (0%)
Google Searches, Twitter, Apple Mobility	220 (60%)	23 (6%)	32 (9%)	78 (21%)	14 (4%)	42.0	114.0	0 (0%)
Google Searches, Twitter, Apple Mobility, UpToDate	220 (60%)	23 (6%)	32 (9%)	78 (21%)	14 (4%)	42.0	114.0	0 (0%)
Google Searches, Neighbor Data	216 (59%)	31 (8%)	35 (10%)	71 (19%)	14 (4%)	35.0	110.0	0 (0%)
Google Searches, Neighbor Data, UpToDate	216 (59%)	31 (8%)	35 (10%)	71 (19%)	14 (4%)	35.0	110.0	0 (0%)
Google Searches, Neighbor Data, Apple Mobility	216 (59%)	31 (8%)	35 (10%)	71 (19%)	14 (4%)	35.0	110.0	0 (0%)
Google Searches, Neighbor Data, Apple Mobility,...	216 (59%)	31 (8%)	35 (10%)	71 (19%)	14 (4%)	35.0	110.0	0 (0%)
Google Searches, Neighbor Data, Twitter	216 (59%)	31 (8%)	35 (10%)	71 (19%)	14 (4%)	35.0	110.0	0 (0%)
Google Searches, Neighbor Data, Twitter, UpToDate	216 (59%)	31 (8%)	35 (10%)	71 (19%)	14 (4%)	35.0	110.0	0 (0%)
Google Searches, Neighbor Data, Twitter, Apple ...	216 (59%)	31 (8%)	35 (10%)	71 (19%)	14 (4%)	35.0	110.0	0 (0%)
Google Searches, Neighbor Data, Twitter, Apple ...	216 (59%)	31 (8%)	35 (10%)	71 (19%)	14 (4%)	35.0	110.0	0 (0%)
Local Epi, Google Searches, Neighbor Data	213 (58%)	40 (11%)	37 (10%)	61 (17%)	16 (4%)	36.0	114.0	0 (0%)
Local Epi, Google Searches, Neighbor Data, UpTo...	213 (58%)	40 (11%)	37 (10%)	61 (17%)	16 (4%)	36.0	114.0	0 (0%)
Local Epi, Google Searches, Neighbor Data, Appl...	213 (58%)	40 (11%)	37 (10%)	61 (17%)	16 (4%)	36.0	114.0	0 (0%)
Local Epi, Google Searches, Neighbor Data, Appl...	213 (58%)	40 (11%)	37 (10%)	61 (17%)	16 (4%)	36.0	114.0	0 (0%)
Local Epi, Google Searches, Neighbor Data, Twitter	213 (58%)	40 (11%)	37 (10%)	61 (17%)	16 (4%)	36.0	114.0	0 (0%)
Local Epi, Google Searches, Neighbor Data, Twit...	213 (58%)	40 (11%)	37 (10%)	61 (17%)	16 (4%)	36.0	114.0	0 (0%)
Local Epi, Google Searches, Neighbor Data, Twit...	213 (58%)	40 (11%)	37 (10%)	61 (17%)	16 (4%)	36.0	114.0	0 (0%)
Local Epi, Google Searches, Neighbor Data, Twit...	213 (58%)	40 (11%)	37 (10%)	61 (17%)	16 (4%)	36.0	114.0	0 (0%)
Local Epi, Google Searches, Neighbor Data, Twit...	213 (58%)	40 (11%)	37 (10%)	61 (17%)	16 (4%)	36.0	114.0	0 (0%)
Local Epi, Neighbor Data, Twitter, UpToDate	135 (37%)	59 (16%)	41 (11%)	65 (18%)	37 (10%)	29.0	60.0	30 (8%)
Local Epi, Neighbor Data, Twitter	133 (36%)	60 (16%)	42 (11%)	65 (18%)	35 (10%)	28.0	60.0	32 (9%)
Local Epi, Neighbor Data, UpToDate	131 (36%)	57 (16%)	41 (11%)	66 (18%)	41 (11%)	27.0	58.0	31 (8%)
Local Epi, Twitter, Apple Mobility, UpToDate	130 (35%)	40 (11%)	16 (4%)	37 (10%)	82 (22%)	17.0	50.0	62 (17%)
Local Epi, Neighbor Data, Twitter, Apple Mobili...	129 (35%)	60 (16%)	33 (9%)	83 (23%)	48 (13%)	29.0	61.0	14 (4%)
Neighbor Data, Twitter, UpToDate	128 (35%)	53 (14%)	37 (10%)	70 (19%)	39 (11%)	27.0	60.0	40 (11%)
Local Epi, Neighbor Data	127 (35%)	58 (16%)	40 (11%)	63 (17%)	34 (9%)	27.0	56.0	45 (12%)
Local Epi, Neighbor Data, Twitter, Apple Mobility	126 (34%)	59 (16%)	34 (9%)	87 (24%)	46 (13%)	28.0	62.0	15 (4%)
Neighbor Data, Twitter	126 (34%)	55 (15%)	38 (10%)	69 (19%)	36 (10%)	26.0	61.0	43 (12%)
Local Epi, Neighbor Data, Apple Mobility, UpToDate	125 (34%)	57 (16%)	33 (9%)	87 (24%)	50 (14%)	27.0	60.0	15 (4%)
Local Epi, Twitter, UpToDate	125 (34%)	51 (14%)	23 (6%)	3 (1%)	49 (13%)	16.0	40.0	116 (32%)
Local Epi, Twitter, Apple Mobility	125 (34%)	41 (11%)	19 (5%)	33 (9%)	84 (23%)	22.0	61.0	65 (18%)
Neighbor Data, UpToDate	124 (34%)	52 (14%)	37 (10%)	70 (19%)	43 (12%)	25.0	58.0	41 (11%)
Neighbor Data, Twitter, Apple Mobility, UpToDate	123 (34%)	53 (14%)	29 (8%)	88 (24%)	54 (15%)	30.0	61.0	20 (5%)
Local Epi, Twitter	122 (33%)	51 (14%)	22 (6%)	1 (0%)	44 (12%)	19.0	50.0	127 (35%)
Local Epi, Neighbor Data, Apple Mobility	121 (33%)	58 (16%)	33 (9%)	82 (22%)	53 (14%)	27.0	58.0	20 (5%)
Neighbor Data, Twitter, Apple Mobility	121 (33%)	53 (14%)	30 (8%)	90 (25%)	51 (14%)	29.0	63.0	22 (6%)
Neighbor Data,	120 (33%)	53 (14%)	36 (10%)	67 (18%)	35 (10%)	25.0	57.0	56 (15%)
Neighbor Data, Apple Mobility, UpToDate	120 (33%)	51 (14%)	29 (8%)	90 (25%)	56 (15%)	28.0	60.0	21 (6%)
Neighbor Data, Apple Mobility	116 (32%)	52 (14%)	29 (8%)	85 (23%)	58 (16%)	28.0	59.0	27 (7%)
Local Epi, Apple Mobility, UpToDate	92 (25%)	44 (12%)	21 (6%)	37 (10%)	93 (25%)	17.0	44.0	80 (22%)
Local Epi, UpToDate	85 (23%)	56 (15%)	26 (7%)	1 (0%)	62 (17%)	14.0	33.0	137 (37%)
Twitter, Apple Mobility, UpToDate	84 (23%)	9 (2%)	2 (1%)	21 (6%)	105 (29%)	14.0	36.0	146 (40%)
Local Epi, Apple Mobility	82 (22%)	46 (13%)	21 (6%)	29 (8%)	91 (25%)	16.0	46.0	98 (27%)
Twitter, Apple Mobility	80 (22%)	7 (2%)	5 (1%)	19 (5%)	104 (28%)	14.0	36.0	152 (41%)
Local Epi,	75 (20%)	54 (15%)	24 (7%)	0 (0%)	42 (11%)	11.0	32.0	172 (47%)
Twitter, UpToDate	69 (19%)	6 (2%)	7 (2%)	0 (0%)	27 (7%)	11.0	19.0	258 (70%)
Twitter,	62 (17%)	6 (2%)	8 (2%)	0 (0%)	10 (3%)	10.0	15.0	281 (77%)
Apple Mobility, UpToDate	27 (7%)	3 (1%)	1 (0%)	24 (7%)	125 (34%)	7.0	20.0	187 (51%)
Apple Mobility,	20 (5%)	3 (1%)	1 (0%)	15 (4%)	106 (29%)	6.0	21.0	222 (60%)
UpToDate,	9 (2%)	2 (1%)	4 (1%)	0 (0%)	49 (13%)	2.0	2.0	303 (83%)

**Table 9: County-level performance of the Multiple Source with different data sources used for the training step.** An additional column, 'Non-deployed,' indicates the number of outbreak events where our Multiple Source method did not find a reasonable set of proxies to fit a model. Thus, an early warning system was not deployed to forecast the out-of-sample period.

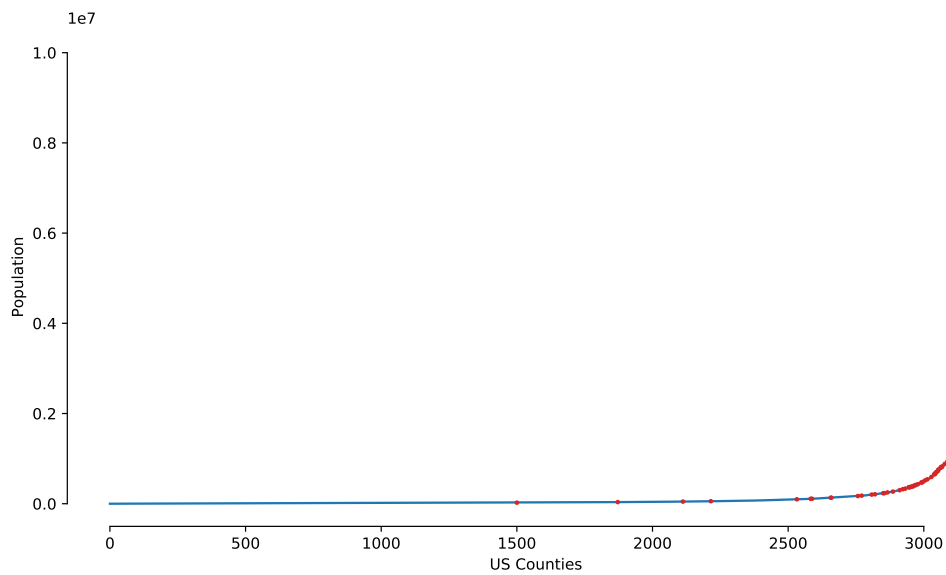


Figure 8: **Population sizes for every county within the United States.** Our selected counties are marked with red dots.



Figure 9: Graphical representation of the reproductive number,  $R_t$ , along with the weekly confirmed COVID-19 cases (gray-filled curve in the top), and three representative early warning methods (Naive, Single and Multiple Source) at county level.



Figure 10: Graphical representation of the reproductive number,  $R_t$ , along with the weekly confirmed COVID-19 cases (gray-filled curve in the top), and three representative early warning methods (Naive, Single and Multiple Source) at county level.



Figure 11: Graphical representation of the reproductive number,  $R_t$ , along with the weekly confirmed COVID-19 cases (gray-filled curve in the top), and three representative early warning methods (Naive, Single and Multiple Source) at county level.





Figure 12: Graphical representation of the reproductive number,  $R_t$ , along with the weekly confirmed COVID-19 cases (gray-filled curve in the top), and three representative early warning methods (Naive, Single and Multiple Source) at county level.

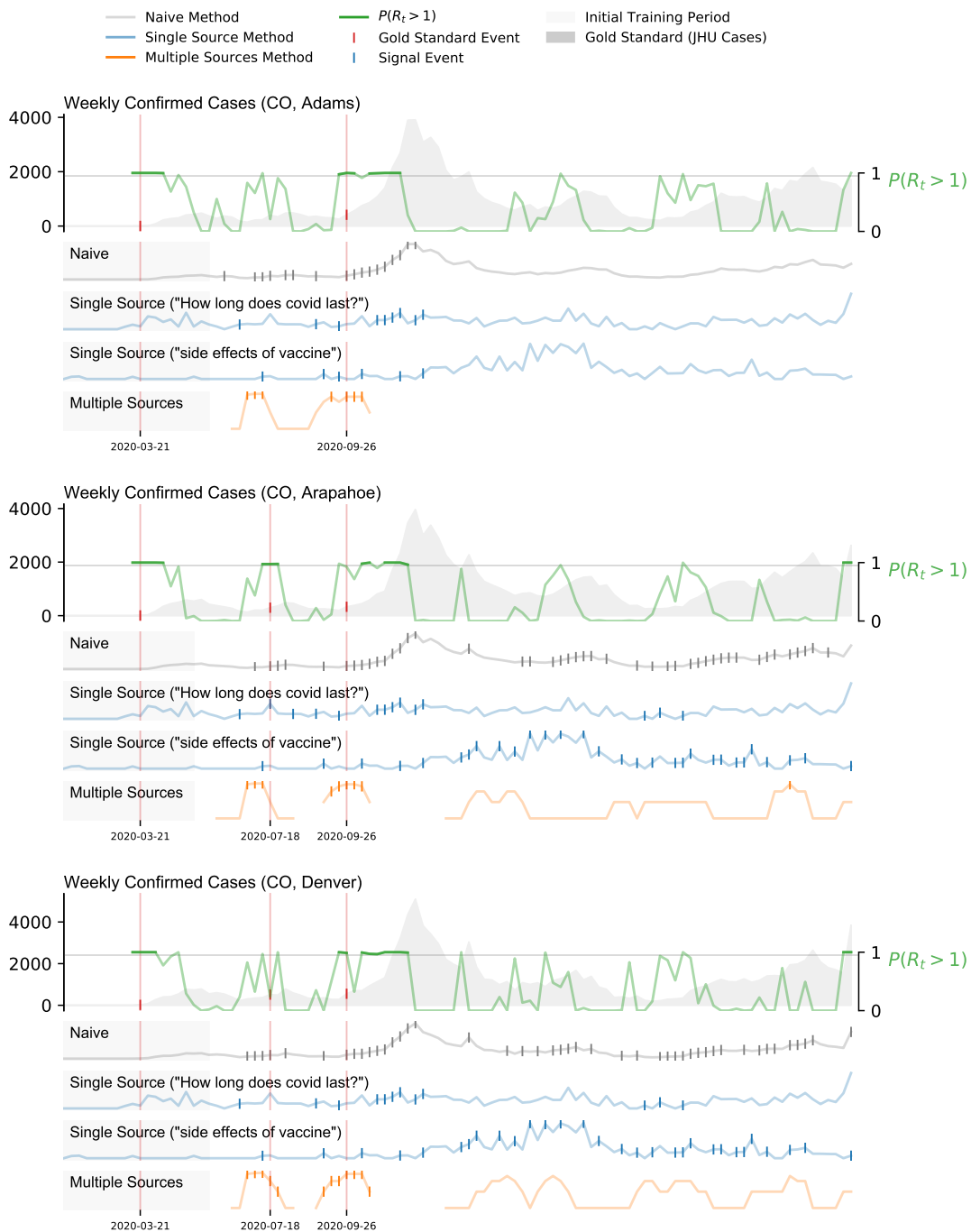


Figure 13: Graphical representation of the reproductive number,  $R_t$ , along with the weekly confirmed COVID-19 cases (gray-filled curve in the top), and three representative early warning methods (Naive, Single and Multiple Source) at county level.



Figure 14: Graphical representation of the reproductive number,  $R_t$ , along with the weekly confirmed COVID-19 cases (gray-filled curve in the top), and three representative early warning methods (Naive, Single and Multiple Source) at county level.



Figure 15: Graphical representation of the reproductive number,  $R_t$ , along with the weekly confirmed COVID-19 cases (gray-filled curve in the top), and three representative early warning methods (Naive, Single and Multiple Source) at county level.



Figure 16: Graphical representation of the probability of resurgence  $P(R_t > 1)$ , along with the weekly confirmed COVID-19 cases (gray-filled curve in the top), and three representative early warning methods (Naive, Single and Multiple Source) at county level.



Figure 17: Graphical representation of the reproductive number,  $R_t$ , along with the weekly confirmed COVID-19 cases (gray-filled curve in the top), and three representative early warning methods (Naive, Single and Multiple Source) at county level.



Figure 18: Graphical representation of the reproductive number,  $R_t$ , along with the weekly confirmed COVID-19 cases (gray-filled curve in the top), and three representative early warning methods (Naive, Single and Multiple Source) at county level.



Figure 19: Graphical representation of the reproductive number,  $R_t$ , along with the weekly confirmed COVID-19 cases (gray-filled curve in the top), and three representative early warning methods (Naive, Single and Multiple Source) at county level.





Figure 20: Graphical representation of the reproductive number,  $R_t$ , along with the weekly confirmed COVID-19 cases (gray-filled curve in the top), and three representative early warning methods (Naive, Single and Multiple Source) at county level.

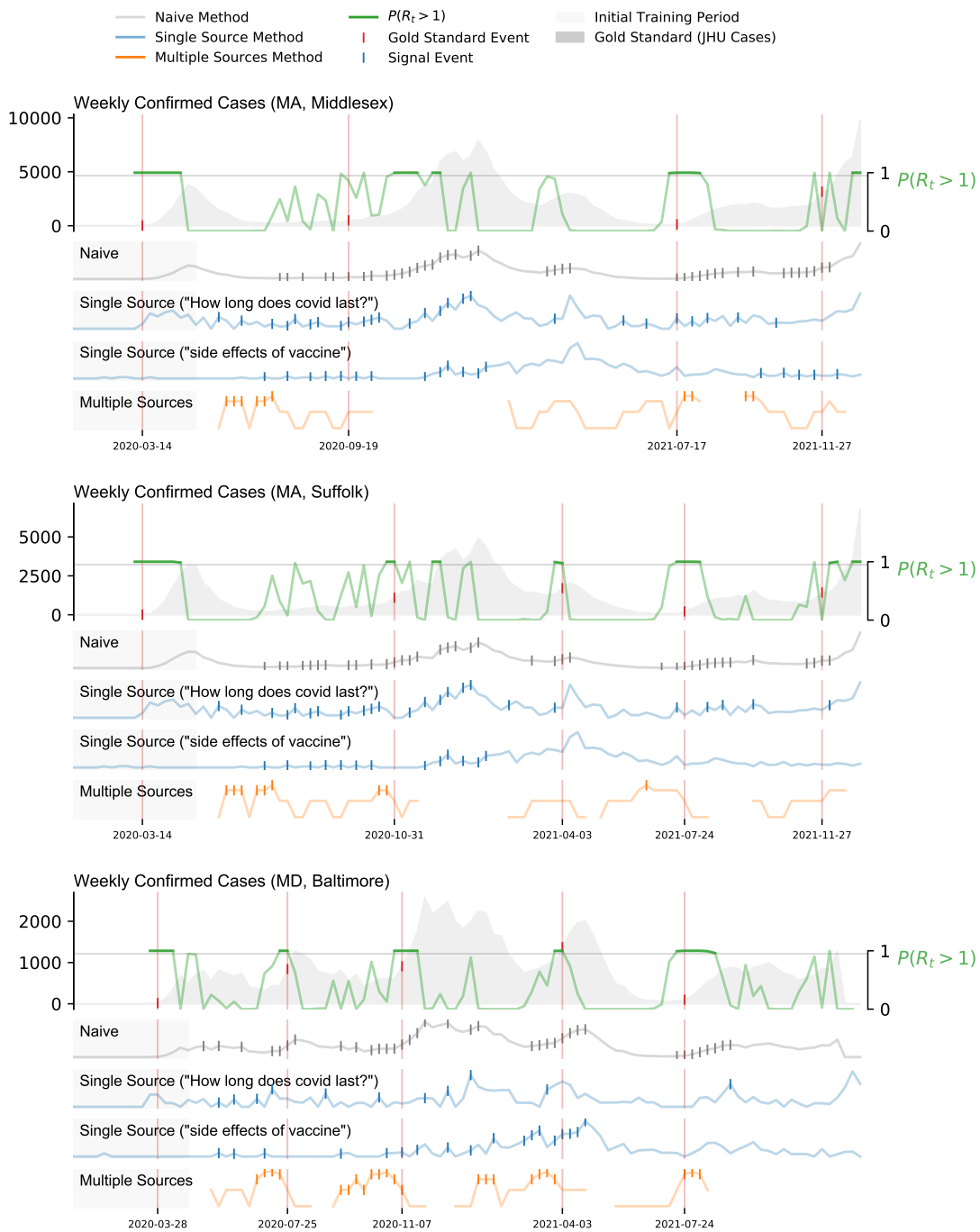


Figure 21: Graphical representation of the reproductive number,  $R_t$ , along with the weekly confirmed COVID-19 cases (gray-filled curve in the top), and three representative early warning methods (Naive, Single and Multiple Source) at county level.

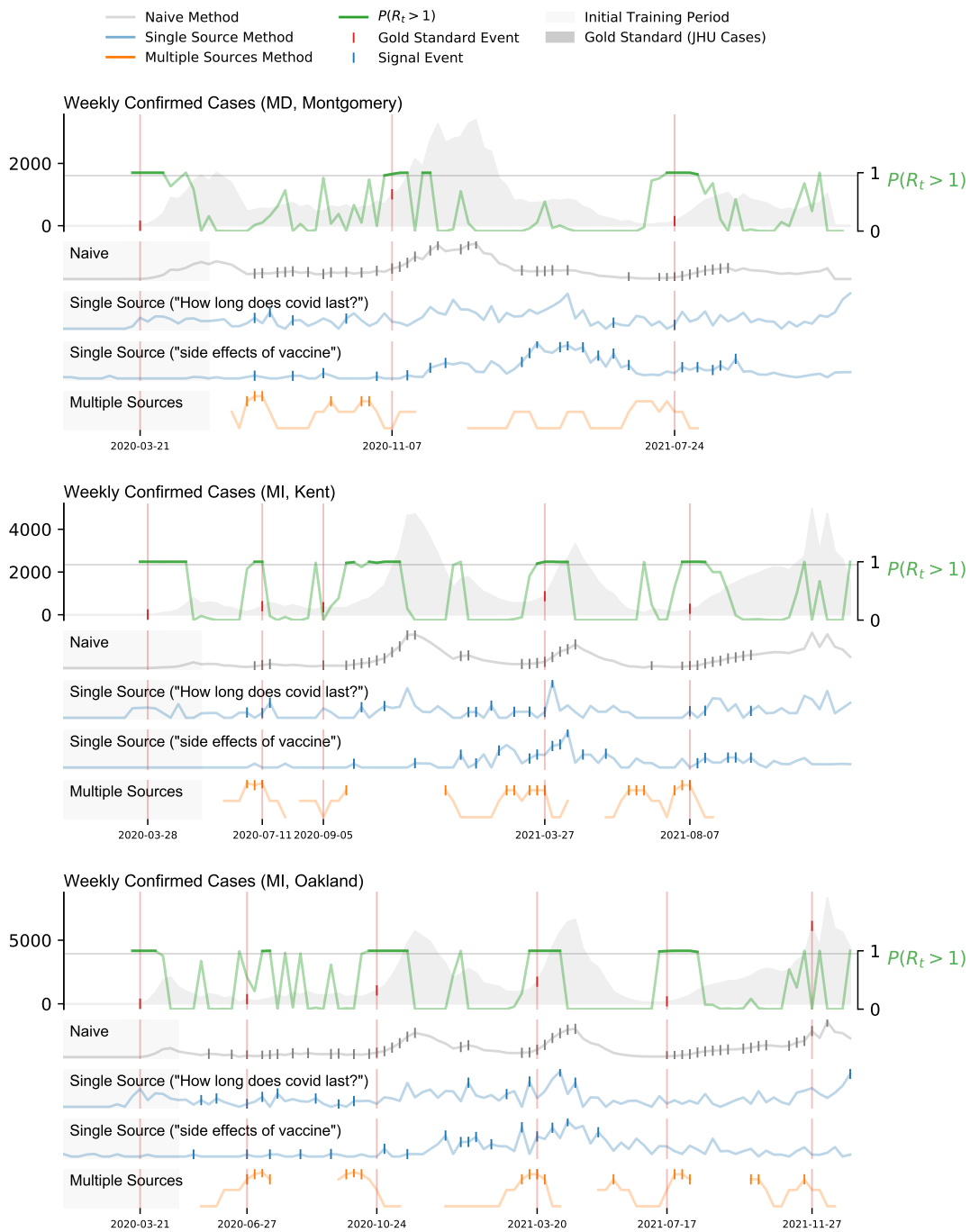


Figure 22: Graphical representation of the reproductive number,  $R_t$ , along with the weekly confirmed COVID-19 cases (gray-filled curve in the top), and three representative early warning methods (Naive, Single and Multiple Source) at county level.



Figure 23: Graphical representation of the reproductive number,  $R_t$ , along with the weekly confirmed COVID-19 cases (gray-filled curve in the top), and three representative early warning methods (Naive, Single and Multiple Source) at county level.



Figure 24: Graphical representation of the reproductive number,  $R_t$ , along with the weekly confirmed COVID-19 cases (gray-filled curve in the top), and three representative early warning methods (Naive, Single and Multiple Source) at county level.



Figure 25: Graphical representation of the reproductive number,  $R_t$ , along with the weekly confirmed COVID-19 cases (gray-filled curve in the top), and three representative early warning methods (Naive, Single and Multiple Source) at county level.



Figure 26: Graphical representation of the reproductive number,  $R_t$ , along with the weekly confirmed COVID-19 cases (gray-filled curve in the top), and three representative early warning methods (Naive, Single and Multiple Source) at county level.

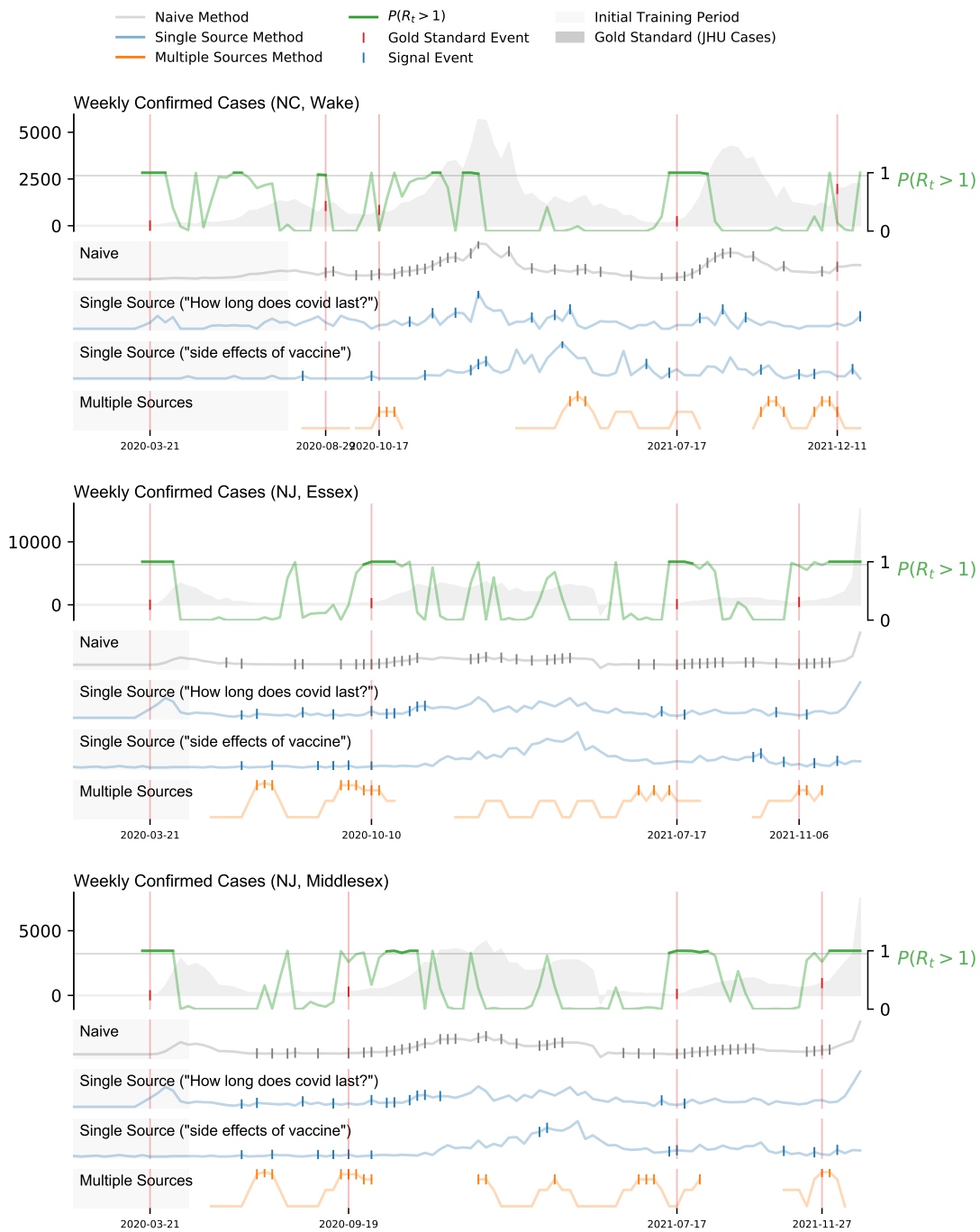


Figure 27: Graphical representation of the reproductive number,  $R_t$ , along with the weekly confirmed COVID-19 cases (gray-filled curve in the top), and three representative early warning methods (Naive, Single and Multiple Source) at county level.





Figure 28: Graphical representation of the reproductive number,  $R_t$ , along with the weekly confirmed COVID-19 cases (gray-filled curve in the top), and three representative early warning methods (Naive, Single and Multiple Source) at county level.



Figure 29: Graphical representation of the reproductive number,  $R_t$ , along with the weekly confirmed COVID-19 cases (gray-filled curve in the top), and three representative early warning methods (Naive, Single and Multiple Source) at county level.

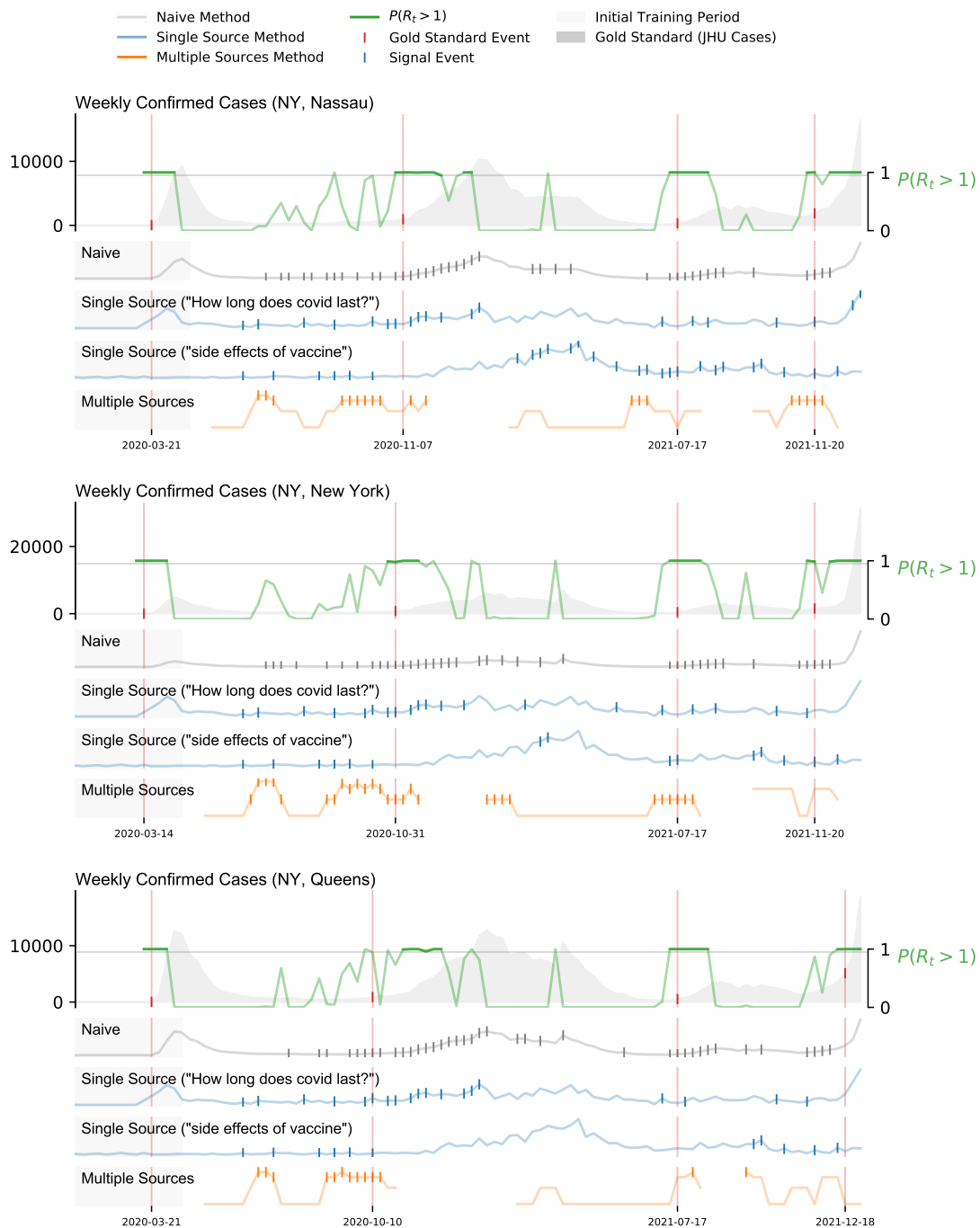


Figure 30: Graphical representation of the reproductive number,  $R_t$ , along with the weekly confirmed COVID-19 cases (gray-filled curve in the top), and three representative early warning methods (Naive, Single and Multiple Source) at county level.

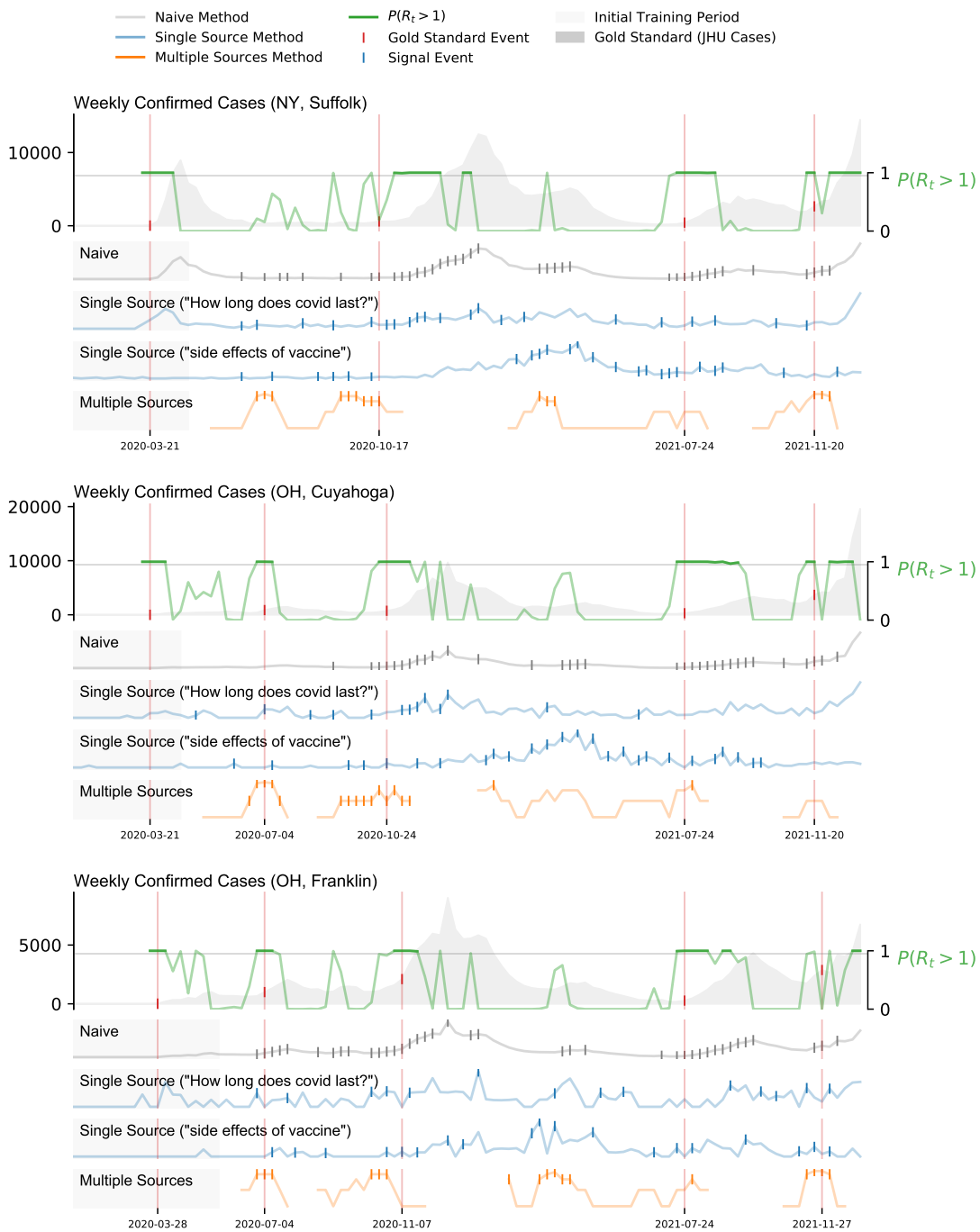


Figure 31: Graphical representation of the reproductive number,  $R_t$ , along with the weekly confirmed COVID-19 cases (gray-filled curve in the top), and three representative early warning methods (Naive, Single and Multiple Source) at county level.



Figure 32: Graphical representation of the reproductive number,  $R_t$ , along with the weekly confirmed COVID-19 cases (gray-filled curve in the top), and three representative early warning methods (Naive, Single and Multiple Source) at county level.



Figure 33: Graphical representation of the reproductive number,  $R_t$ , along with the weekly confirmed COVID-19 cases (gray-filled curve in the top), and three representative early warning methods (Naive, Single and Multiple Source) at county level.



Figure 34: Graphical representation of the reproductive number,  $R_t$ , along with the weekly confirmed COVID-19 cases (gray-filled curve in the top), and three representative early warning methods (Naive, Single and Multiple Source) at county level.



Figure 35: Graphical representation of the reproductive number,  $R_t$ , along with the weekly confirmed COVID-19 cases (gray-filled curve in the top), and three representative early warning methods (Naive, Single and Multiple Source) at county level.





Figure 36: Graphical representation of the reproductive number,  $R_t$ , along with the weekly confirmed COVID-19 cases (gray-filled curve in the top), and three representative early warning methods (Naive, Single and Multiple Source) at county level.

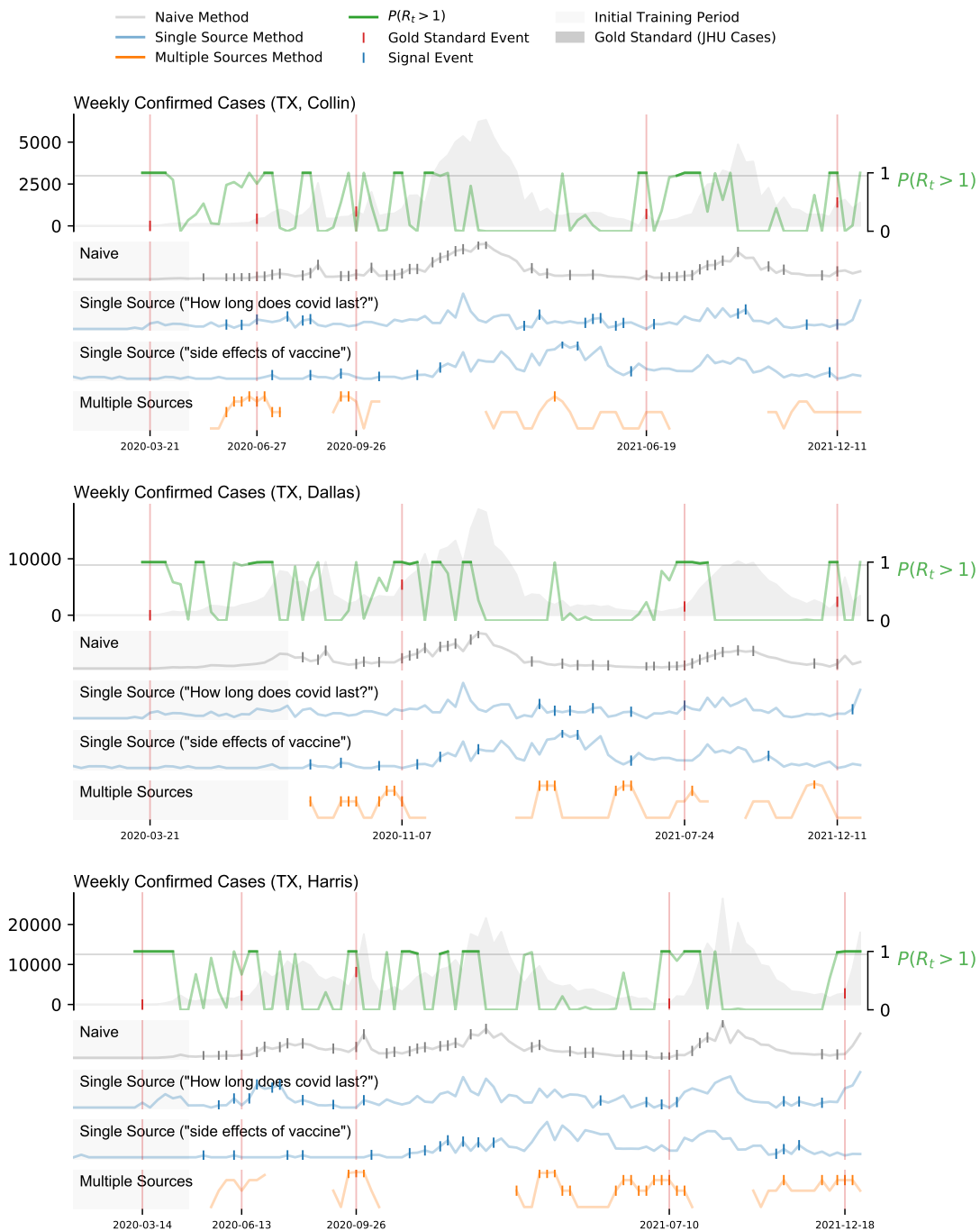


Figure 37: Graphical representation of the reproductive number,  $R_t$ , along with the weekly confirmed COVID-19 cases (gray-filled curve in the top), and three representative early warning methods (Naive, Single and Multiple Source) at county level.



Figure 38: Graphical representation of the reproductive number,  $R_t$ , along with the weekly confirmed COVID-19 cases (gray-filled curve in the top), and three representative early warning methods (Naive, Single and Multiple Source) at county level.



Figure 39: Graphical representation of the reproductive number,  $R_t$ , along with the weekly confirmed COVID-19 cases (gray-filled curve in the top), and three representative early warning methods (Naive, Single and Multiple Source) at county level.

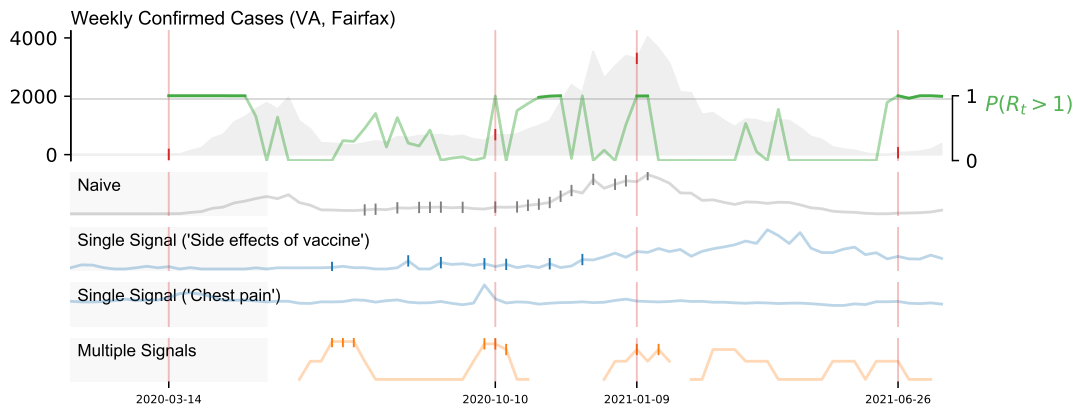
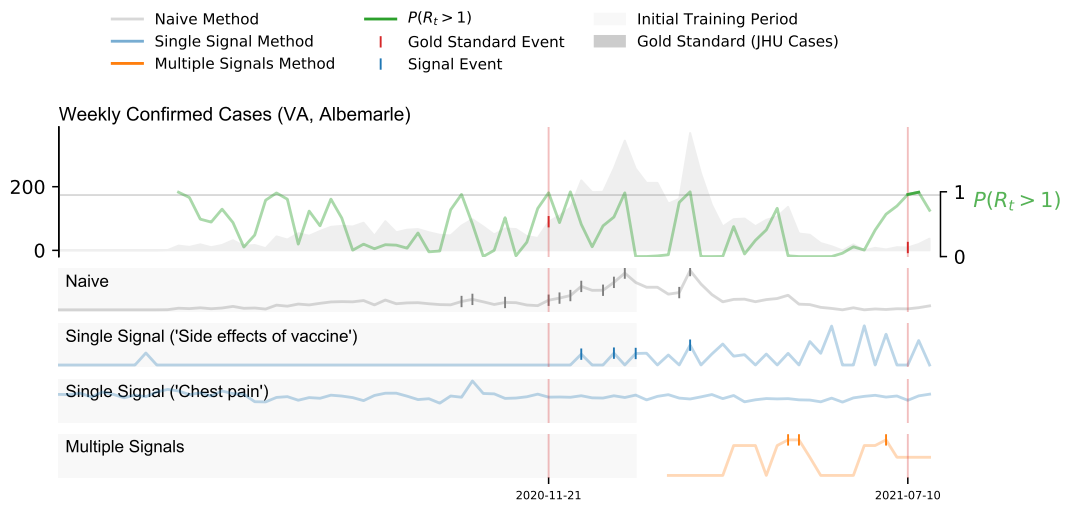


Figure 40: Graphical representation of the reproductive number,  $R_t$ , along with the weekly confirmed COVID-19 (gray-filled curve in the top), and three representative early warning methods (Naive, Single and Multiple Source) at county level.

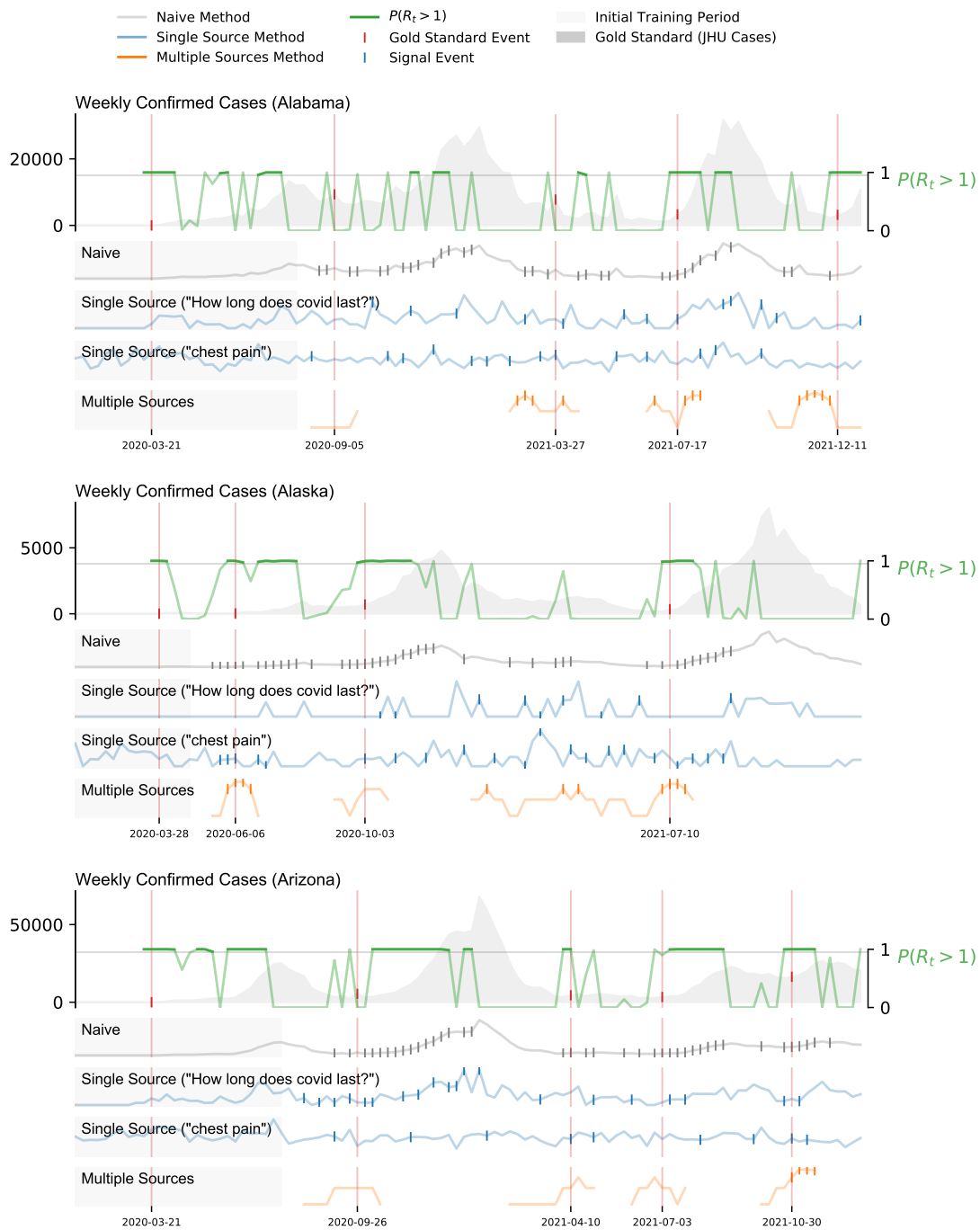


Figure 41: Graphical representation of the reproductive number,  $R_t$ , along with the weekly confirmed COVID-19 cases (gray-filled curve in the top), and three representative early warning methods (Naive, Single and Multiple Source) at county level.

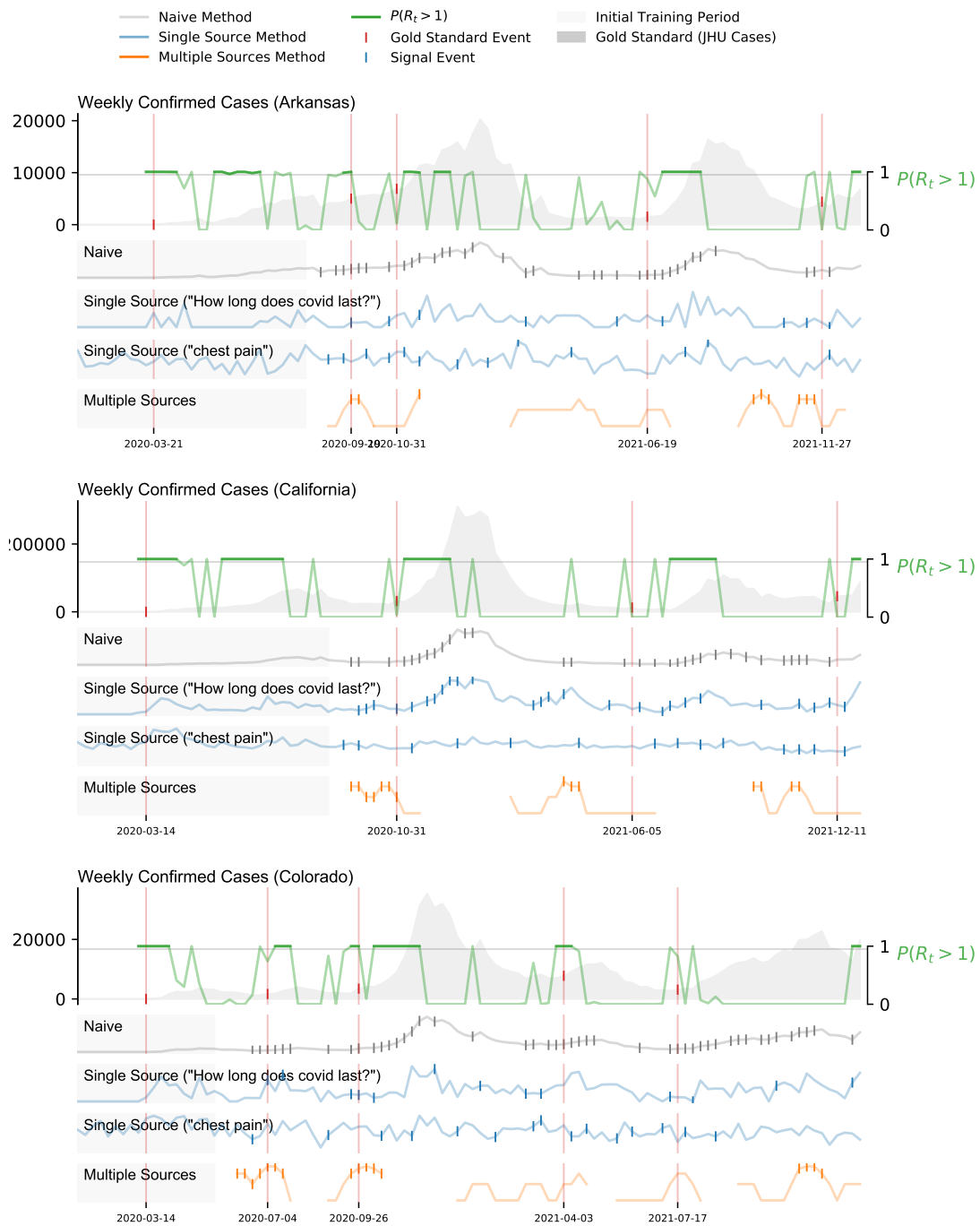


Figure 42: Graphical representation of the reproductive number,  $R_t$ , along with the weekly confirmed COVID-19 cases (gray-filled curve in the top), and three representative early warning methods (Naive, Single and Multiple Source) at county level.

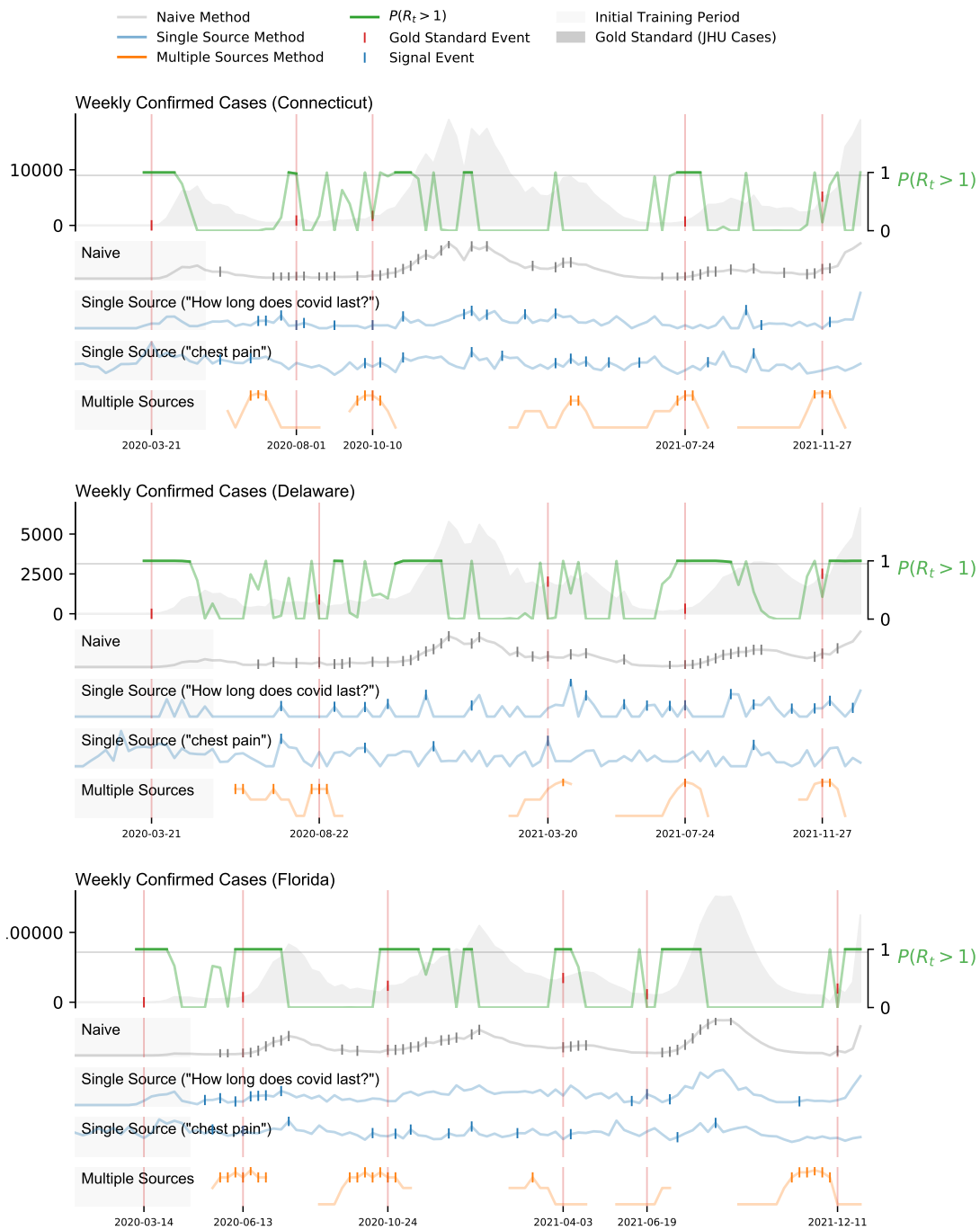


Figure 43: Graphical representation of the reproductive number,  $R_t$ , along with the weekly confirmed COVID-19 cases (gray-filled curve in the top), and three representative early warning methods (Naive, Single and Multiple Source) at county level.



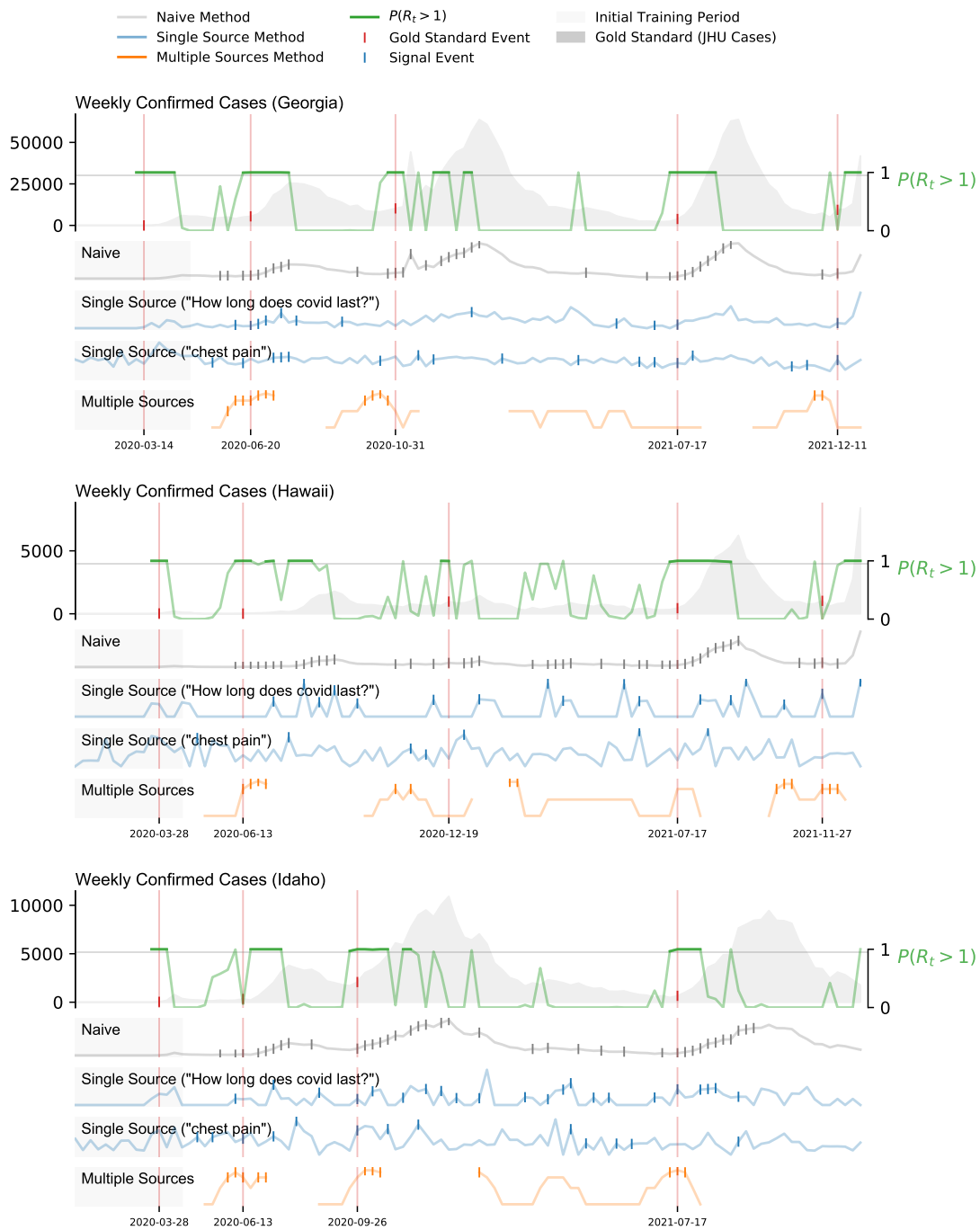


Figure 44: Graphical representation of the reproductive number,  $R_t$ , along with the weekly confirmed COVID-19 cases (gray-filled curve in the top), and three representative early warning methods (Naive, Single and Multiple Source) at county level.

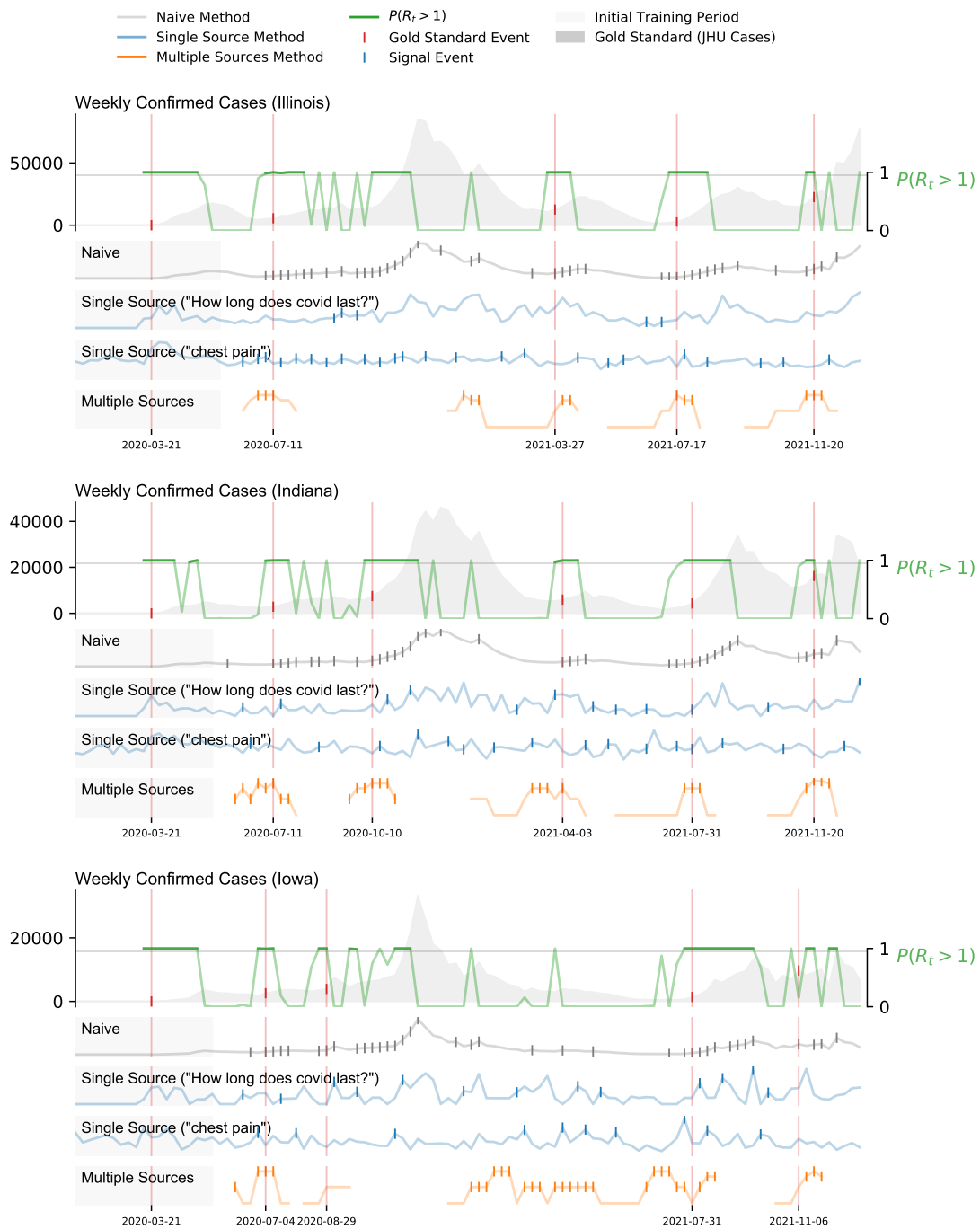


Figure 45: Graphical representation of the reproductive number,  $R_t$ , along with the weekly confirmed COVID-19 cases (gray-filled curve in the top), and three representative early warning methods (Naive, Single and Multiple Source) at county level.

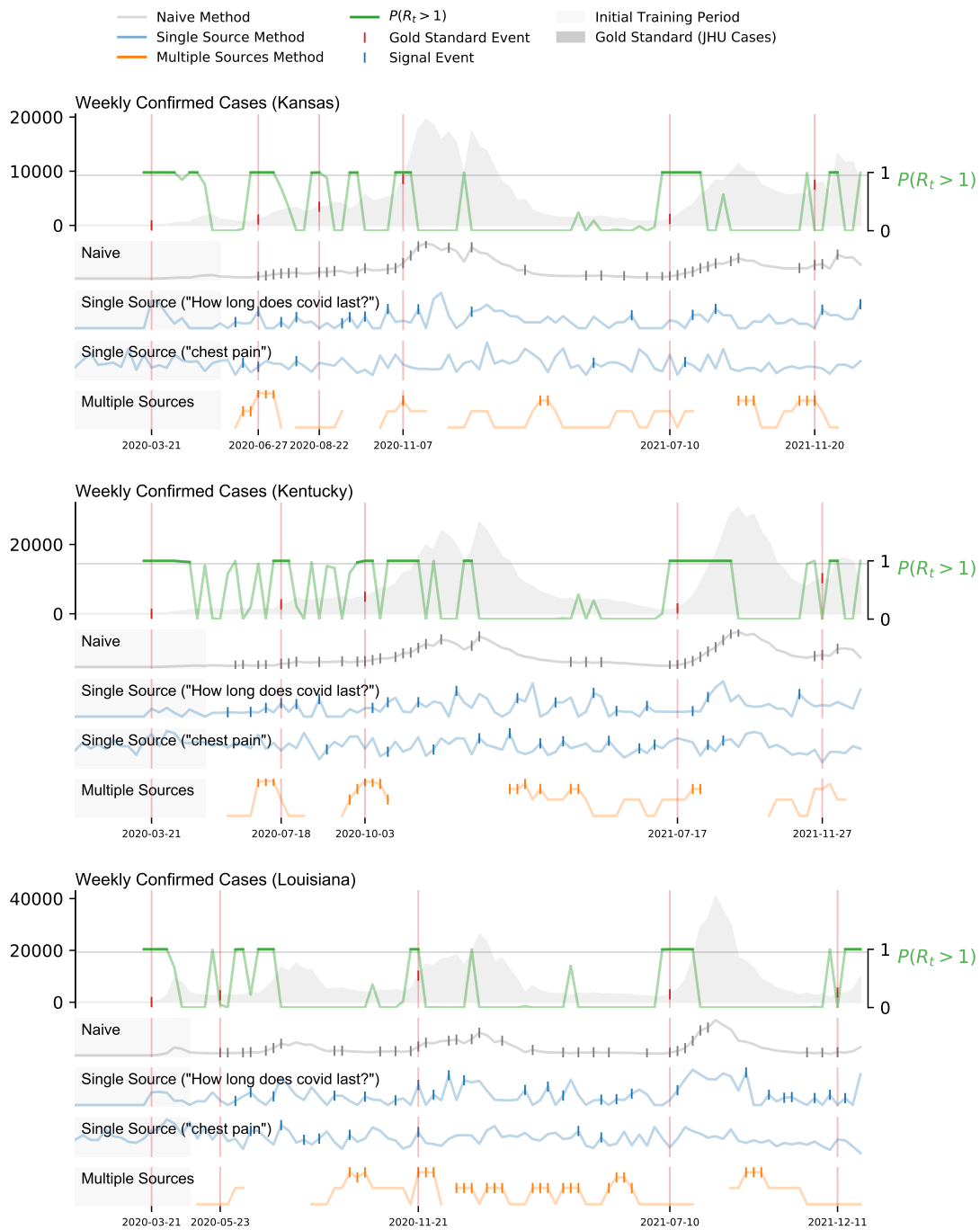


Figure 46: Graphical representation of the reproductive number,  $R_t$ , along with the weekly confirmed COVID-19 cases (gray-filled curve in the top), and three representative early warning methods (Naive, Single and Multiple Source) at county level.



Figure 47: Graphical representation of the reproductive number,  $R_t$ , along with the weekly confirmed COVID-19 cases (gray-filled curve in the top), and three representative early warning methods (Naive, Single and Multiple Source) at county level.

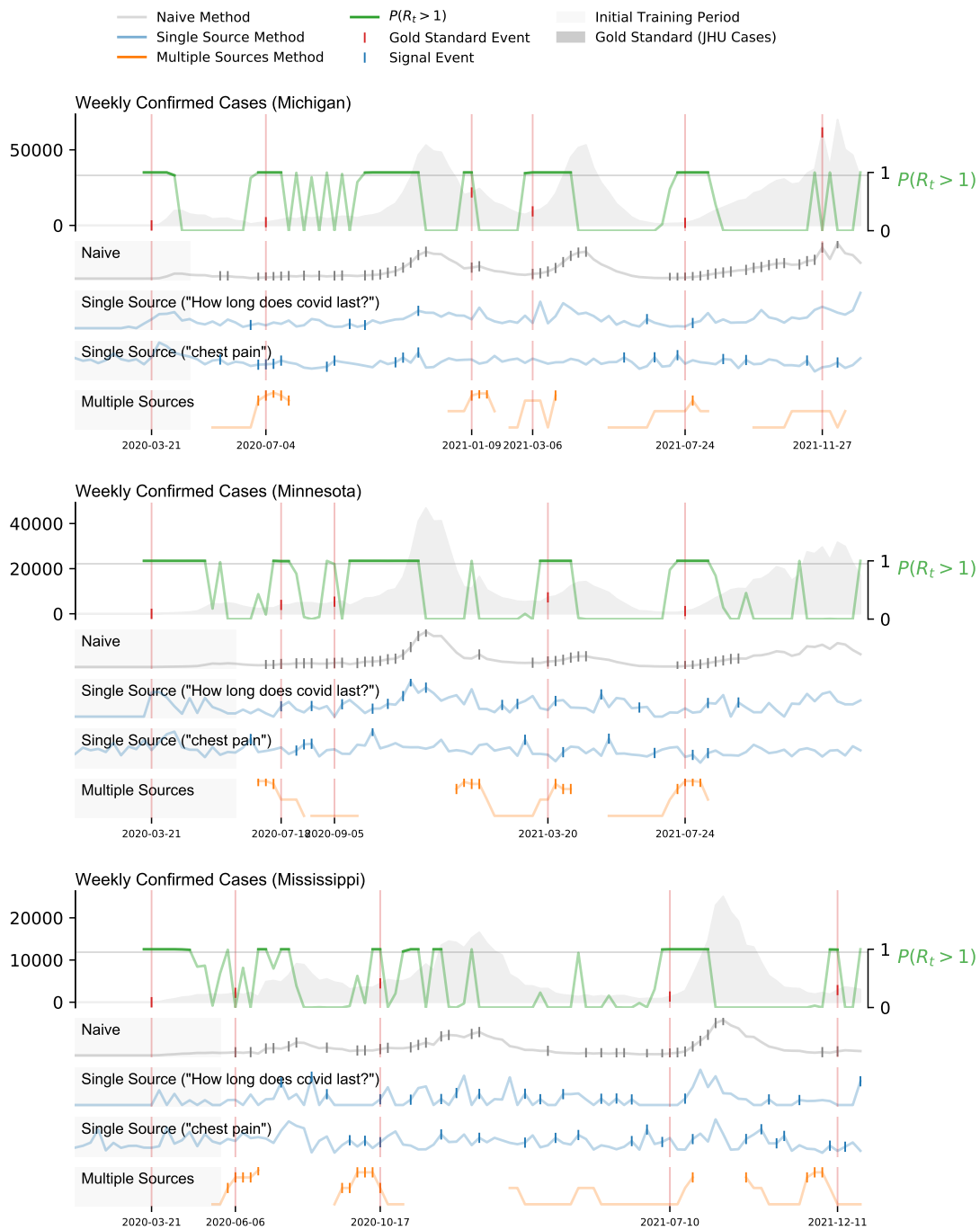


Figure 48: Graphical representation of the reproductive number,  $R_t$ , along with the weekly confirmed COVID-19 cases (gray-filled curve in the top), and three representative early warning methods (Naive, Single and Multiple Source) at county level.

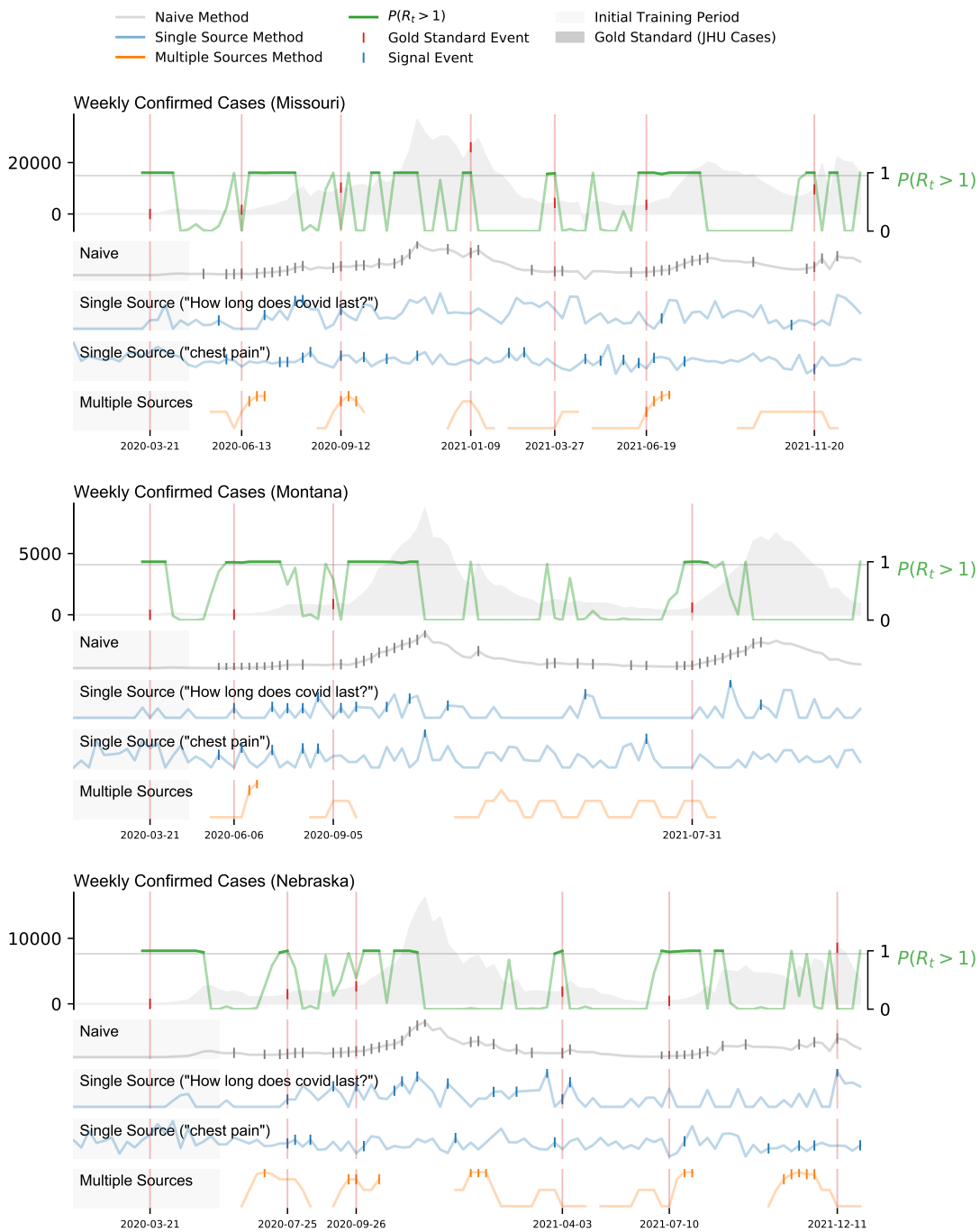


Figure 49: Graphical representation of the reproductive number,  $R_t$ , along with the weekly confirmed COVID-19 cases (gray-filled curve in the top), and three representative early warning methods (Naive, Single and Multiple Source) at county level.

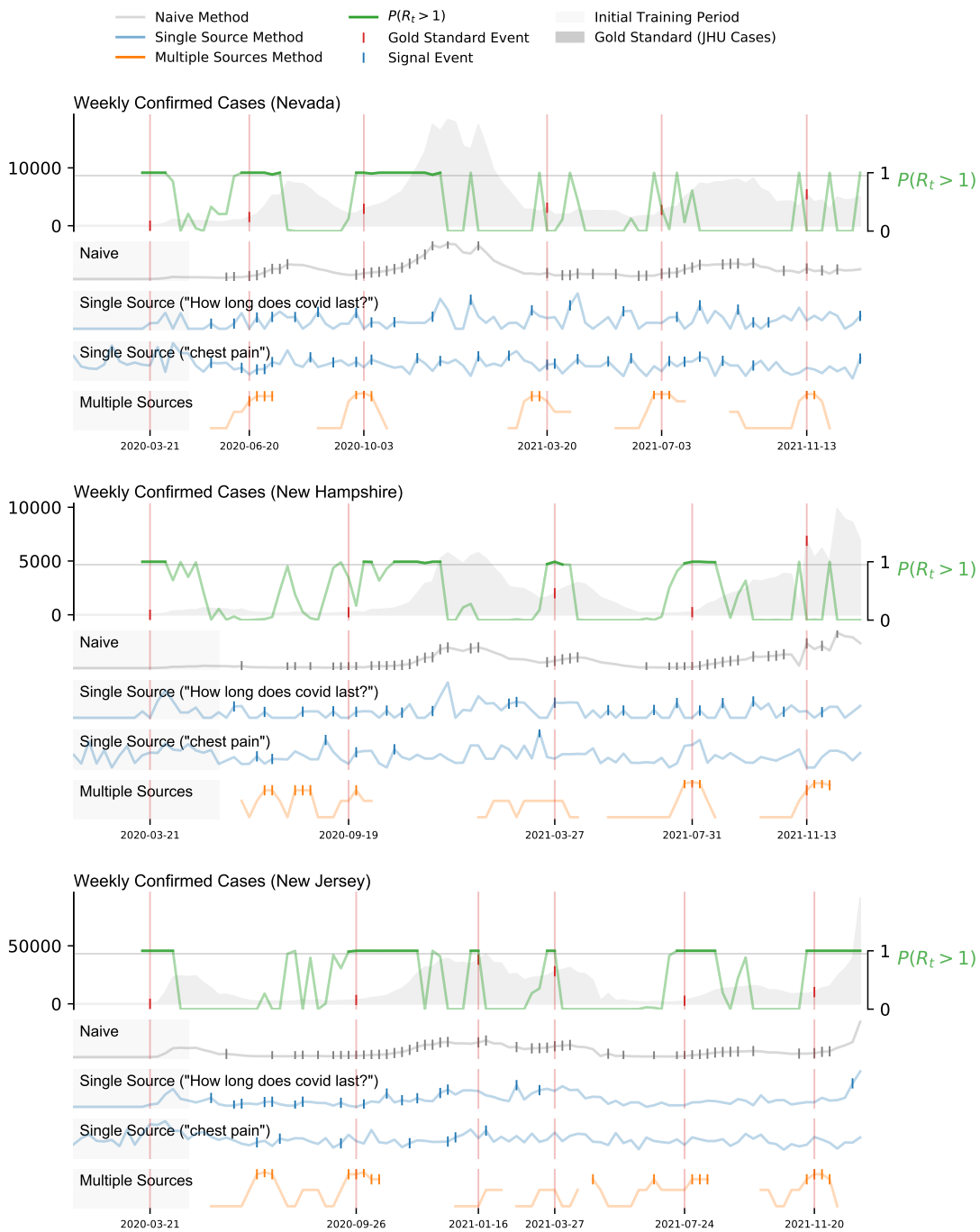


Figure 50: Graphical representation of the reproductive number,  $R_t$ , along with the weekly confirmed COVID-19 cases (gray-filled curve in the top), and three representative early warning methods (Naive, Single and Multiple Source) at county level.



Figure 51: Graphical representation of the reproductive number,  $R_t$ , along with the weekly confirmed COVID-19 cases (gray-filled curve in the top), and three representative early warning methods (Naive, Single and Multiple Source) at county level.



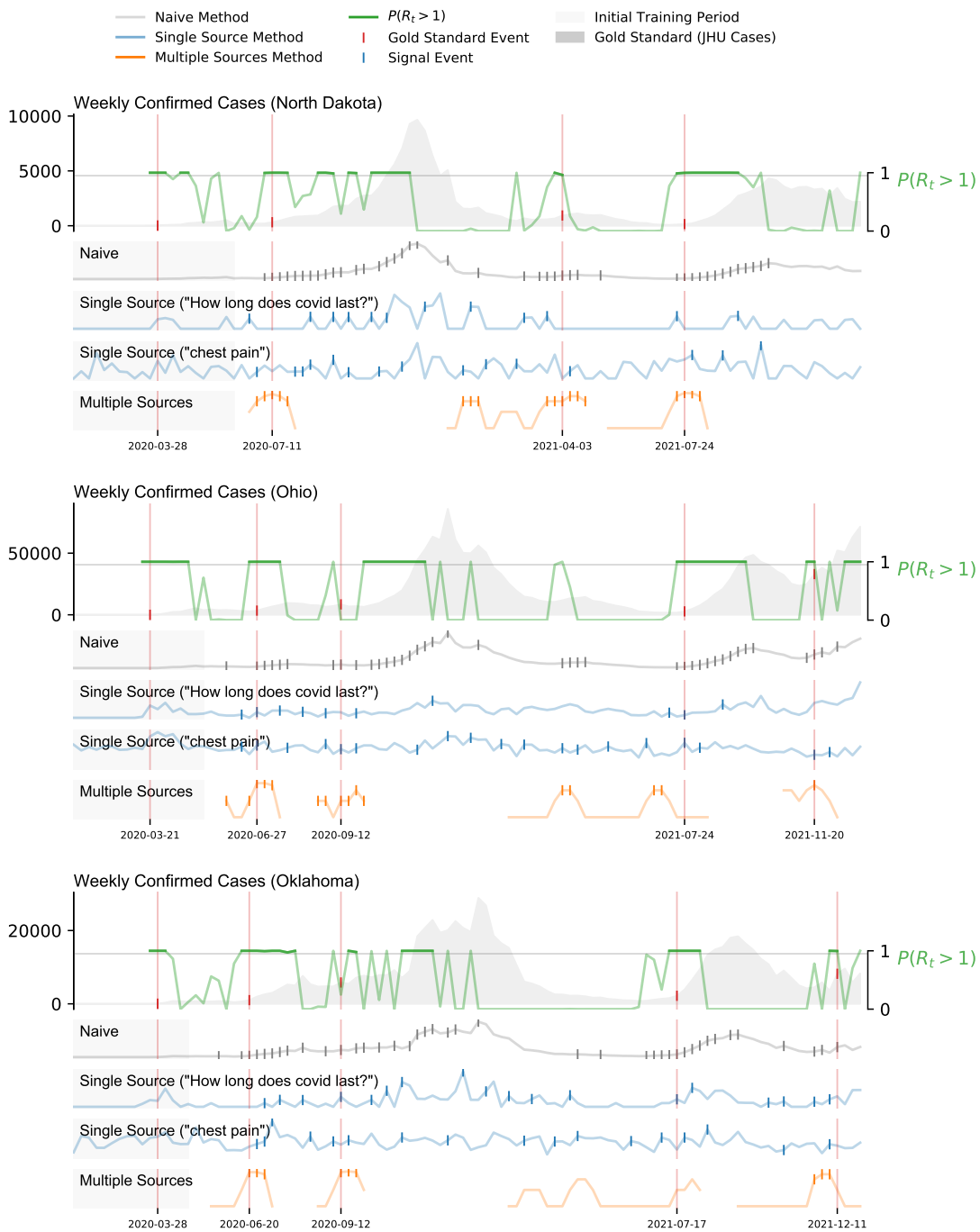


Figure 52: Graphical representation of the reproductive number,  $R_t$ , along with the weekly confirmed COVID-19 cases (gray-filled curve in the top), and three representative early warning methods (Naive, Single and Multiple Source) at county level.

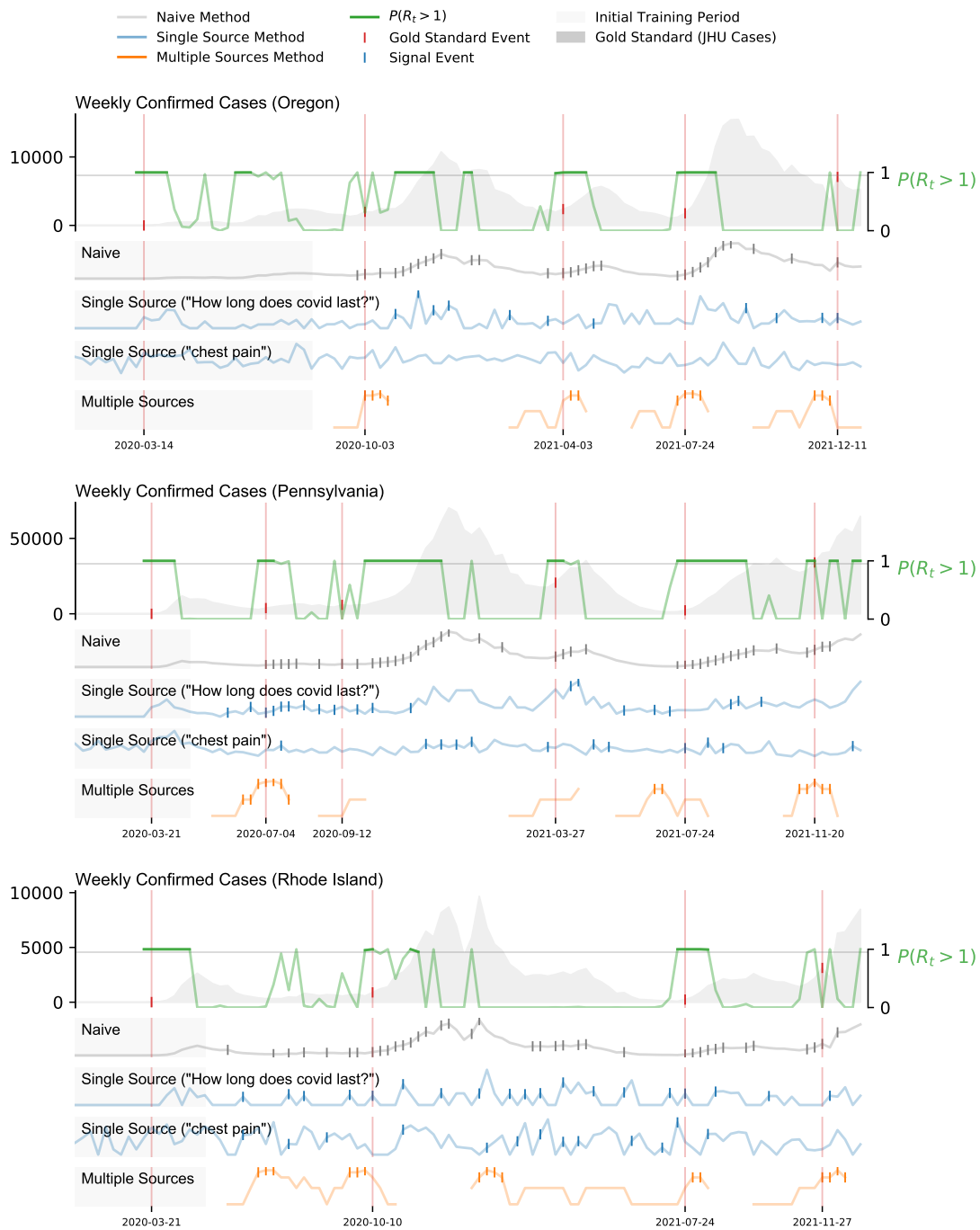


Figure 53: Graphical representation of the reproductive number,  $R_t$ , along with the weekly confirmed COVID-19 cases (gray-filled curve in the top), and three representative early warning methods (Naive, Single and Multiple Source) at county level.

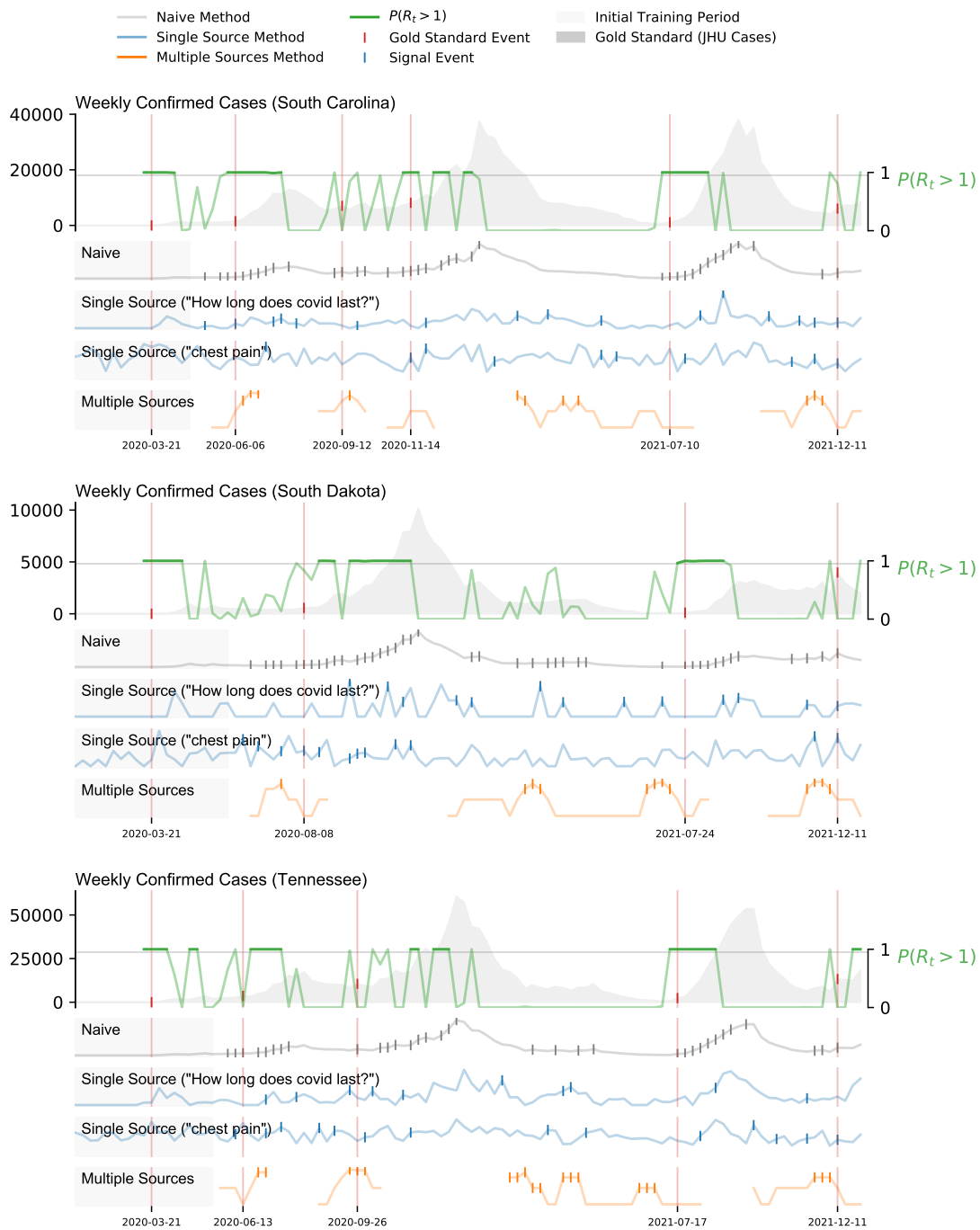


Figure 54: Graphical representation of the reproductive number,  $R_t$ , along with the weekly confirmed COVID-19 cases (gray-filled curve in the top), and three representative early warning methods (Naive, Single and Multiple Source) at county level.

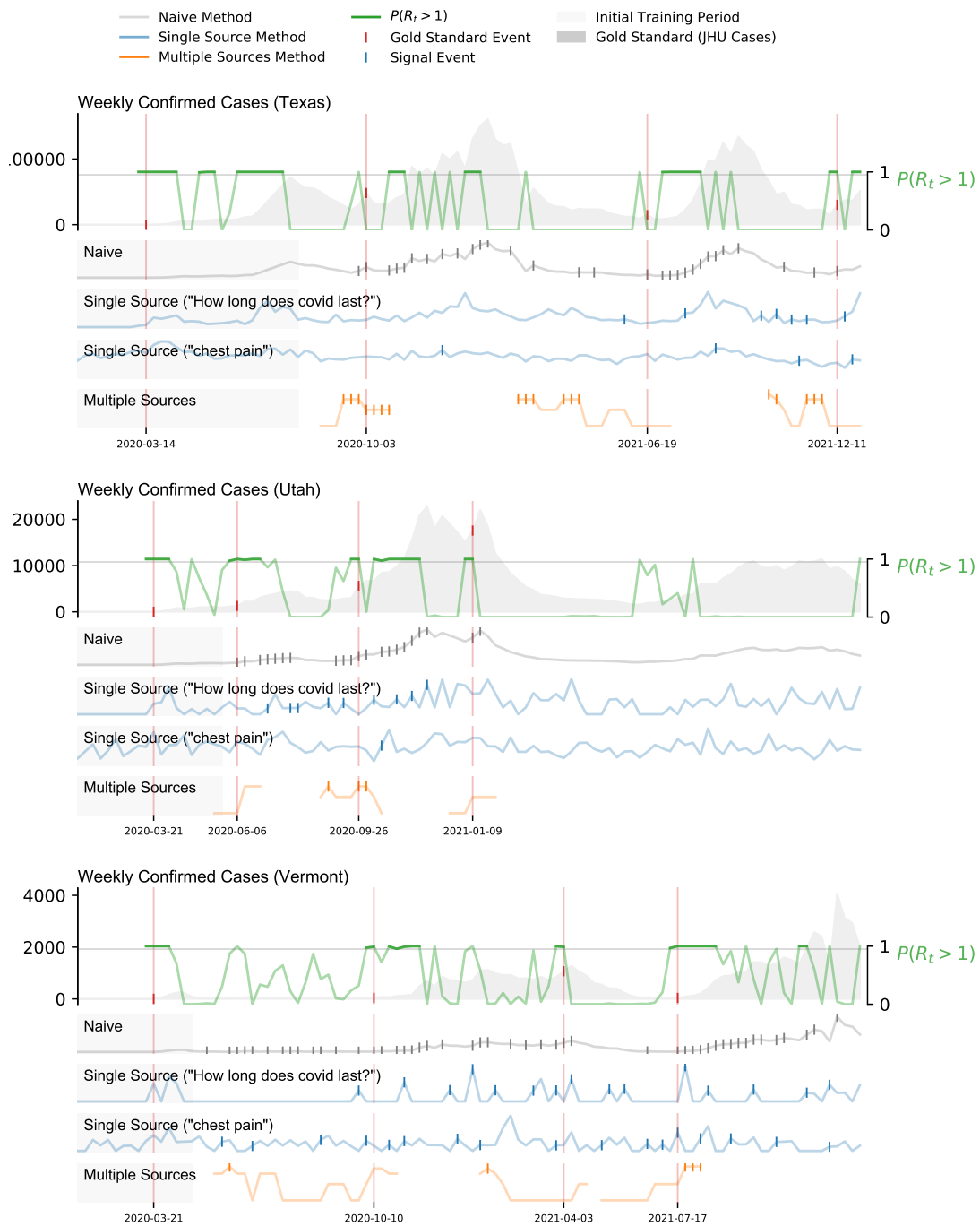


Figure 55: Graphical representation of the reproductive number,  $R_t$ , along with the weekly confirmed COVID-19 cases (gray-filled curve in the top), and three representative early warning methods (Naive, Single and Multiple Source) at county level.

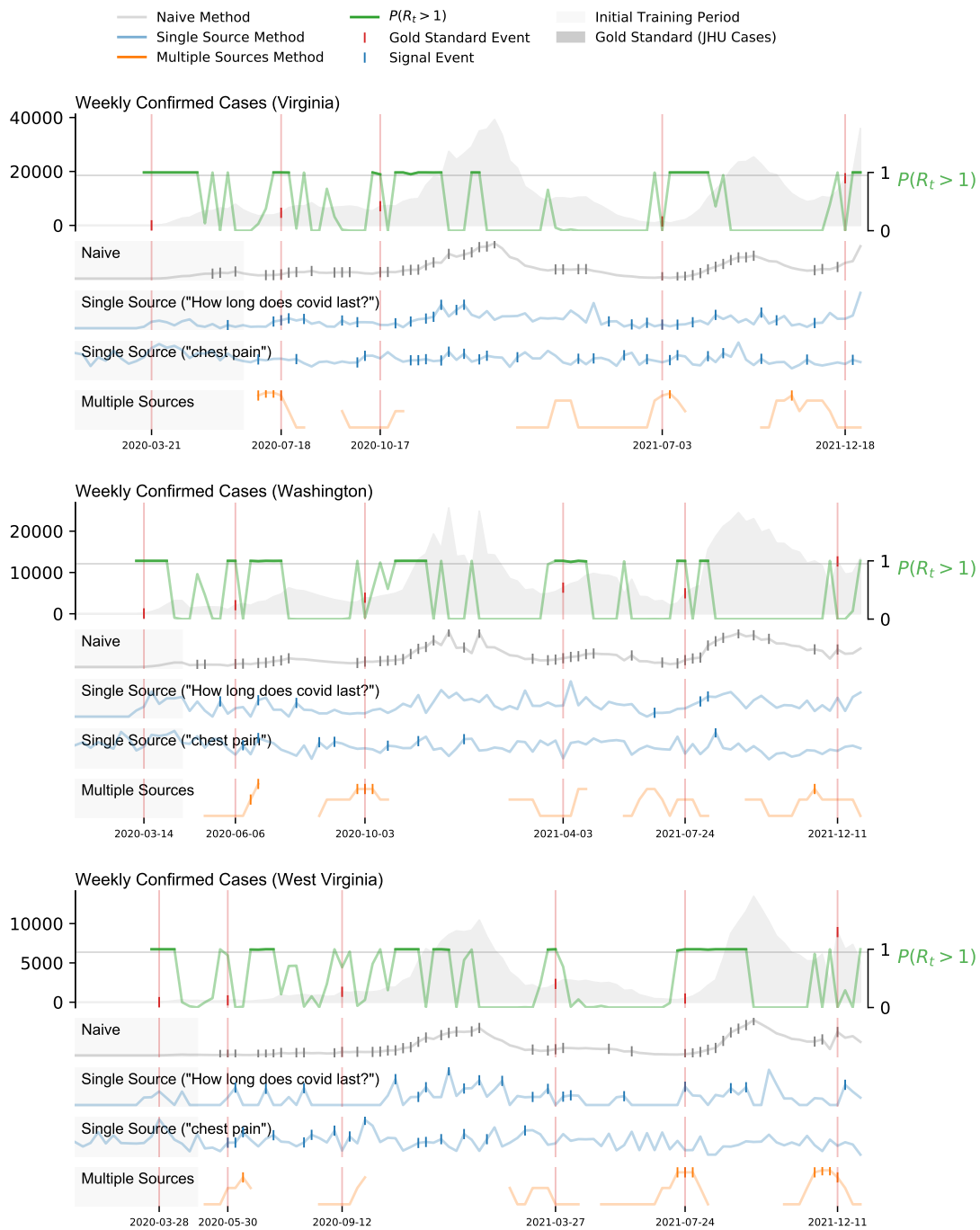


Figure 56: Graphical representation of the reproductive number,  $R_t$ , along with the weekly confirmed COVID-19 cases (gray-filled curve in the top), and three representative early warning methods (Naive, Single and Multiple Source) at county level.

	Early Warning	Sync Warning	Late Warning	Missed Outbreaks	False Alarm, Increase	False Alarm, No Increase
(GT) Side effects of vaccine	176 (67%)	5 (2%)	12 (5%)	71 (27%)	16	450
(GT) Chest pain	170 (64%)	20 (8%)	14 (5%)	60 (23%)	8	273
(GT) How long does covid last?	168 (64%)	14 (5%)	21 (8%)	61 (23%)	6	365
(GT) covid 19 who	150 (57%)	12 (5%)	29 (11%)	73 (28%)	11	353
(GT), covid symptoms	126 (48%)	11 (4%)	40 (15%)	87 (33%)	3	249
(GT) fever	115 (44%)	14 (5%)	26 (10%)	109 (41%)	10	265
(GT) after covid vaccine	112 (42%)	10 (4%)	20 (8%)	122 (46%)	23	473
COVID-19 Confirmed Deaths (county level)	99 (38%)	8 (3%)	16 (6%)	141 (53%)	3	222
(GT) covid 19	93 (35%)	10 (4%)	27 (10%)	134 (51%)	9	258
COVID-19 Confirmed Cases (state level)	91 (34%)	25 (9%)	49 (19%)	99 (38%)	5	214
COVID-19 Confirmed Cases (county level)	84 (32%)	27 (10%)	40 (15%)	113 (43%)	5	200
(GT) Effects of covid vaccine	78 (30%)	4 (2%)	7 (3%)	175 (66%)	11	281
(GT) UpToDate	78 (30%)	16 (6%)	20 (8%)	150 (57%)	0	99
(GT) covid	72 (27%)	16 (6%)	51 (19%)	125 (47%)	9	254
COVID-19 Confirmed Deaths (state level)	71 (27%)	10 (4%)	12 (5%)	171 (65%)	4	158
Twitter	56 (21%)	10 (4%)	17 (6%)	181 (69%)	1	72

Table 10: Performance of selected terms for the Single Source method, at county level (N=263)

Abdominal obesity	Abdominal pain	Acne	Actinic keratosis	Acute bronchitis	Adrenal crisis
Ageusia	Alcoholism	Allergic conjunctivitis	Allergy	Amblyopia	Anemia
Amenorrhea	Amnesia	Anal fissure	Anaphylaxis	Anxiety	Arthritis
Angina pectoris	Angioedema	Angular cheilitis	Anosmia	Astigmatism	Autoimmune disease
Aphasia	Aphonia	Aplasia	Arthralgia	Astigmatism	Beau's lines
Ascites	Asperger syndrome	Atheroma	Asthma	Autoimmune disease	Bleeding on probing
Ataxia	Atheroma	Attention deficit hyperactivity disorder	Auditory hallucination	Beau's lines	Blushing
Avoidant personality disorder	Back pain	Bacterial vaginosis	Balance disorder	Bleeding on probing	Bradycardia
Bell's palsy	Biliary colic	Binge eating	Bleeding	Blushing	Bruise
Blepharospasm	Bloating	Blood in stool	Blurred vision	Bleeding on probing	Bruise
Boil	Bone fracture	Bone tumor	Bowel obstruction	Blushing	Bruise
Braxton Hicks contractions	Breakthrough bleeding	Breast pain	Bronchitis	Bleeding on probing	Bruise
Bruxism	Bunion	Burn	Burning Chest Pain	Bleeding on probing	Bruise
Candidiasis	Canker sore	Cardiac arrest	Carpal tunnel syndrome	Bleeding on probing	Bruise
Cataract	Chancere	Cheilitis	Chest pain	Bleeding on probing	Bruise
Chorea	Chronic pain	Cirrhosis	Cleft lip and cleft palate	Bleeding on probing	Bruise
Cluster headache	Colitis	Coma	Common cold	Bleeding on probing	Bruise
Compulsive hoarding	Confusion	Congenital heart defect	Conjunctivitis	Bleeding on probing	Bruise
Convulsion	Cough	Crackles	Cramp	Bleeding on probing	Bruise
Croup	Cyanosis	Dandruff	Delayed onset muscle soreness	Bleeding on probing	Bruise
Dentin hypersensitivity	Depersonalization	Depression	Dermatitis	Bleeding on probing	Bruise
Developmental disability	Diabetes	Diabetic ketoacidosis	Diarrhea	Bleeding on probing	Bruise
Dry eye syndrome	Dysautonomia	Dysgeusia	Dysmenorrhea	Bleeding on probing	Bruise
Dysphagia	Dysphoria	Dystonia	Dysuria	Bleeding on probing	Bruise
Eczema	Edema	Encephalitis	Encephalopathy	Bleeding on probing	Bruise
Epilepsy	Epiphora	Erectile dysfunction	Erythema	Bleeding on probing	Bruise
Esophagitis	Excessive daytime sleepiness	Eye pain	Eye strain	Bleeding on probing	Bruise
Facial swelling	Fasciculation	Fatigue	Fatty liver disease	Bleeding on probing	Bruise
Fever	Fibrillation	Fibrocystic breast changes	Fibromyalgia	Bleeding on probing	Bruise
Floater	Focal seizure	Folate deficiency	Food craving	Bleeding on probing	Bruise
Frequent urination	Gastroesophageal reflux disease	Gastroparesis	Generalized anxiety disorder	Bleeding on probing	Bruise
Genital wart	Gingival recession	Gingivitis	Globus pharyngis	Bleeding on probing	Bruise
Gout	Grandiosity	Granuloma	Guilt	Bleeding on probing	Bruise
Halitosis	Hay fever	Headache	Heart arrhythmia	Bleeding on probing	Bruise
Heartburn	Hematochezia	Hematoma	Hematuria	Bleeding on probing	Bruise
Hemoptysis	Hemorrhoids	Hepatic encephalopathy	Hepatitis	Bleeding on probing	Bruise
Hiccup	Hip pain	Hives	Hot flash	Bleeding on probing	Bruise
Hypercalcaemia	Hypercapnia	Hypercholesterolemia	Hyperemesis gravidarum	Bleeding on probing	Bruise
Hyperkalemia	Hyperlipidemia	Hypermobility	Hyperpigmentation	Bleeding on probing	Bruise
Hypertension	Hyperthermia	Hypertthyroidism	Hypertriglyceridemia	Bleeding on probing	Bruise
Hyperventilation	Hypocalcaemia	Hypochondriasis	Hypoglycemia	Bleeding on probing	Bruise
Hypokalemia	Hypomania	Hyponatremia	Hypotension	Bleeding on probing	Bruise
Hypoxemia	Hypoxia	Impetigo	Implantation bleeding	Bleeding on probing	Bruise
Indigestion	Infection	Inflammation	Inflammatory bowel disease	Bleeding on probing	Bruise
Insomnia	Insulin resistance	Intermenstrual bleeding	Intracranial pressure	Bleeding on probing	Bruise
Irregular menstruation	Itch	Jaundice	Kidney failure	Bleeding on probing	Bruise
Knee Pain	Kyphosis	Lactose intolerance	Laryngitis	Bleeding on probing	Bruise
Lesion	Leukorrhea	Lightheadedness	Low back pain	Bleeding on probing	Bruise
Lymphedema	Major depressive disorder	Malabsorption	Male infertility	Bleeding on probing	Bruise
Melasma	Melena	Meningitis	Menorrhagia	Bleeding on probing	Bruise
Migraine	Milium	Mitral insufficiency	Mood disorder	Bleeding on probing	Bruise
Morning sickness	Motion sickness	Mouth ulcer	Muscle atrophy	Bleeding on probing	Bruise
Myalgia	Mydriasis	Myocardial infarction	Myoclonus	Bleeding on probing	Bruise
Nasal polyp	Nausea	Neck mass	Neck pain	Bleeding on probing	Bruise
Nerve injury	Neuralgia	Neutropenia	Night sweats	Bleeding on probing	Bruise
Nocturnal enuresis	Nodule	Nosebleed	Nystagmus	Bleeding on probing	Bruise
Onychorrhexis	Oral candidiasis	Orthostatic hypotension	Osteopenia	Bleeding on probing	Bruise
Osteoporosis	Otitis	Otitis externa	Otitis media	Bleeding on probing	Bruise
Palpitations	Panic attack	Papule	Paranoia	Bleeding on probing	Bruise
Pelvic inflammatory disease	Pericarditis	Periosteal disease	Periorbital puffiness	Bleeding on probing	Bruise
Perspiration	Petechia	Phlegm	Photodermatitis	Bleeding on probing	Bruise
Photopsia	Pleural effusion	Pleurisy	Pneumonia	Bleeding on probing	Bruise
Polycythemia	Polydipsia	Polyneuropathy	Polyuria	Bleeding on probing	Bruise
Post-nasal drip	Postural orthostatic tachycardia syndrome	Prediabetes	Proteinuria	Bleeding on probing	Bruise
Psychosis	Ptosis	Pulmonary edema	Pulmonary hypertension	Bleeding on probing	Bruise
Pus	Pyelonephritis	Radiculopathy	Rectal pain	Bleeding on probing	Bruise
Red eye	Renal colic	Restless legs syndrome	Rheum	Bleeding on probing	Bruise
Rhinorrhea	Rosacea	Round ligament pain	Rumination	Bleeding on probing	Bruise
Sciatica	Scoliosis	Seborrheic dermatitis	Self-harm	Bleeding on probing	Bruise
Sexual dysfunction	Shallow breathing	Sharp pain	Shivering	Bleeding on probing	Bruise
Shyness	Sinusitis	Skin condition	Skin rash	Bleeding on probing	Bruise
Skin ulcer	Sleep apnea	Sleep deprivation	Sleep disorder	Bleeding on probing	Bruise
Sore throat	Spasticity	Splenomegaly	Sputum	Bleeding on probing	Bruise
Strabismus	Stretch marks	Stridor	Stroke	Bleeding on probing	Bruise
Subdural hematoma	Suicidal ideation	Swelling	Swollen feet	Bleeding on probing	Bruise
Syncope	Tachycardia	Tachypnea	Telangiectasia	Bleeding on probing	Bruise
Testicular pain	Throat irritation	Thrombocytopenia	Thyroid nodule	Bleeding on probing	Bruise
Tinnitus	Tonsillitis	Toothache	Tremor	Bleeding on probing	Bruise
Tumor	Type 2 diabetes	Unconsciousness	Underweight	Bleeding on probing	Bruise
Urethritis	Urinary incontinence	Urinary tract infection	Urinary urgency	Bleeding on probing	Bruise
Vaginal bleeding	Vaginal discharge	Vaginitis	Varicose veins	Bleeding on probing	Bruise
Ventricular fibrillation	Ventricular tachycardia	Vertigo	Viral pneumonia	Bleeding on probing	Bruise
Vomiting	Wart	Water retention	Weakness	Bleeding on probing	Bruise
Wheeze	Xeroderma	Xerostomia	Yawn	Bleeding on probing	Bruise
anosmia	chest pain	chest tightness	covid	Bleeding on probing	Bruise
covid symptoms	covid-19	how long does covid last	effects of covid vaccine	Bleeding on probing	Bruise
feeling tired	fever	loss taste	hyperhidrosis	Bleeding on probing	Bruise
loss of smell	loss smell		nose bleed	Bleeding on probing	Bruise

Table 11: Google Search term list used in the Multiple Source method

## References and Notes

1. Marc Lipsitch and Mauricio Santillana. Enhancing situational awareness to prevent infectious disease outbreaks from becoming catastrophic. *Global Catastrophic Biological Risks*, pages 59–74, 2019.
2. Worldometer. <https://www.worldometers.info/coronavirus>, 2021. Accessed: 2023-03-06.
3. Yair Goldberg, Micha Mandel, Yinon M Bar-On, Omri Bodenheimer, Laurence Freedman, Eric J Haas, Ron Milo, Sharon Alroy-Preis, Nachman Ash, and Amit Huppert. Waning immunity after the bnt162b2 vaccine in israel. *New England Journal of Medicine*, 385(24):e85, 2021.
4. Stephen M Kissler, Christine Tedijanto, Edward Goldstein, Yonatan H Grad, and Marc Lipsitch. Projecting the transmission dynamics of sars-cov-2 through the postpandemic period. *Science*, 368(6493):860–868, 2020.
5. Mohammadali Dashtbali and Mehdi Mirzaie. A compartmental model that predicts the effect of social distancing and vaccination on controlling covid-19. *Scientific Reports*, 11(1):1–11, 2021.
6. Bruno Buonomo and Rossella Della Marca. Effects of information-induced behavioural changes during the covid-19 lockdowns: the case of italy. *Royal Society open science*, 7(10):201635, 2020.
7. The covid tracking project. <https://covidtracking.com/analysis-updates/three-covid-19-data-problems>, 2021. Accessed: 2021-12-09.



8. Justin Kaashoek and Mauricio Santillana. Covid-19 positive cases, evidence on the time evolution of the epidemic or an indicator of local testing capabilities? a case study in the united states. *A Case Study in the United States (April 10, 2020)*, 2020.
9. Thibaut Jombart, Stéphane Ghazzi, Dirk Schumacher, Timothy J Taylor, Quentin J Leclerc, Mark Jit, Stefan Flasche, Felix Greaves, Tom Ward, Rosalind M Eggo, et al. Real-time monitoring of covid-19 dynamics using automated trend fitting and anomaly detection. *Philosophical Transactions of the Royal Society B*, 376(1829):20200266, 2021.
10. Emilio Gutierrez, Adrian Rubli, and Tiago Tavares. Delays in death reports and their implications for tracking the evolution of covid-19. *Available at SSRN 3645304*, 2020.
11. Fred S Lu, Andre T Nguyen, Nicholas B Link, Mathieu Molina, Jessica T Davis, Matteo Chinazzi, Xinyue Xiong, Alessandro Vespignani, Marc Lipsitch, and Mauricio Santillana. Estimating the cumulative incidence of covid-19 in the united states using influenza surveillance, virologic testing, and mortality data: Four complementary approaches. *PLOS Computational Biology*, 17(6):e1008994, 2021.
12. Pablo Martinez de Salazar, Fred Lu, James A Hay, Diana Gomez-Barroso, Pablo Fernandez-Navarro, Elena Vanessa Martinez, Jenaro Astray-Mochales, Rocio Amillategui, Ana Garcia-Fulgueiras, Maria Dolores Chirlaque, et al. Near real-time surveillance of the sars-cov-2 epidemic with incomplete data. *medRxiv*, 2021.
13. IHME COVID-19 forecasting team. Modeling covid-19 scenarios for the united states. *Nature medicine*, 2020.
14. Mélodie Monod, Alexandra Blenkinsop, Xiaoyue Xi, Daniel Hebert, Sivan Bershan, Simon Tietze, Marc Baguelin, Valerie C Bradley, Yu Chen, Helen Coupland, et al. Age groups that

- sustain resurging covid-19 epidemics in the united states. *Science*, 371(6536):eabe8372, 2021.
15. Fabio Della Rossa, Davide Salzano, Anna Di Meglio, Francesco De Lellis, Marco Coraggio, Carmela Calabrese, Agostino Guarino, Ricardo Cardona-Rivera, Pietro De Lellis, Davide Liuzza, et al. A network model of italy shows that intermittent regional strategies can alleviate the covid-19 epidemic. *Nature communications*, 11(1):1–9, 2020.
  16. Alessandro Vespignani, Huaiyu Tian, Christopher Dye, James O Lloyd-Smith, Rosalind M Eggo, Munik Shrestha, Samuel V Scarpino, Bernardo Gutierrez, Moritz UG Kraemer, Joseph Wu, et al. Modelling covid-19. *Nature Reviews Physics*, 2(6):279–281, 2020.
  17. Shengjie Lai, Nick W Ruktanonchai, Liangcai Zhou, Olivia Prosper, Wei Luo, Jessica R Floyd, Amy Wesolowski, Mauricio Santillana, Chi Zhang, Xiangjun Du, et al. Effect of non-pharmaceutical interventions to contain covid-19 in china. *nature*, 585(7825):410–413, 2020.
  18. Jessica T Davis, Matteo Chinazzi, Nicola Perra, Kunpeng Mu, Ana Pastore y Piontti, Marco Ajelli, Natalie E Dean, Corrado Gioannini, Maria Litvinova, Stefano Merler, et al. Cryptic transmission of sars-cov-2 and the first covid-19 wave. *Nature*, 600(7887):127–132, 2021.
  19. Serina Chang, Emma Pierson, Pang Wei Koh, Jaline Gerardin, Beth Redbird, David Grusky, and Jure Leskovec. Mobility network models of covid-19 explain inequities and inform reopening. *Nature*, 589(7840):82–87, 2021.
  20. . u.s. cdc, forecasts of total covid-19 deaths. <https://www.cdc.gov/coronavirus/2019-ncov/science/forecasting/forecasting-us.html>, 2021. Accessed: 2021-12-10.

21. Rachel E Baker, Wenchang Yang, Gabriel A Vecchi, C Jessica E Metcalf, and Bryan T Grenfell. Assessing the influence of climate on wintertime sars-cov-2 outbreaks. *Nature communications*, 12(1):1–7, 2021.
22. Seth Flaxman, Swapnil Mishra, Axel Gandy, H Juliette T Unwin, Thomas A Mellan, Helen Coupland, Charles Whittaker, Harrison Zhu, Tresnia Berah, Jeffrey W Eaton, et al. Estimating the effects of non-pharmaceutical interventions on covid-19 in europe. *Nature*, 584(7820):257–261, 2020.
23. Evan L Ray, Nutchawan Wattanachit, Jarad Niemi, Abdul Hannan Kanji, Katie House, Estee Y Cramer, Johannes Bracher, Andrew Zheng, Teresa K Yamana, Xinyue Xiong, et al. Ensemble forecasts of coronavirus disease 2019 (covid-19) in the us. *MedRXiv*, 2020.
24. Shihao Yang, Mauricio Santillana, and Samuel C Kou. Accurate estimation of influenza epidemics using google search data via argo. *Proceedings of the National Academy of Sciences*, 112(47):14473–14478, 2015.
25. Sarah F McGough, John S Brownstein, Jared B Hawkins, and Mauricio Santillana. Forecasting zika incidence in the 2016 latin america outbreak combining traditional disease surveillance with search, social media, and news report data. *PLoS neglected tropical diseases*, 11(1):e0005295, 2017.
26. Mauricio Santillana, André T Nguyen, Mark Dredze, Michael J Paul, Elaine O Nsoesie, and John S Brownstein. Combining search, social media, and traditional data sources to improve influenza surveillance. *PLoS computational biology*, 11(10):e1004513, 2015.
27. Andrea Freyer Dugas, Mehdi Jalalpour, Yulia Gel, Scott Levin, Fred Torcaso, Takeru Igusa, and Richard E Rothman. Influenza forecasting with google flu trends. *PloS one*, 8(2):e56176, 2013.

28. Kathy Lee, Ankit Agrawal, and Alok Choudhary. Forecasting influenza levels using real-time social media streams. In *2017 IEEE International Conference on Healthcare Informatics (ICHI)*, pages 409–414. IEEE, 2017.
29. Emily L Aiken, Sarah F McGough, Maimuna S Majumder, Gal Wachtel, Andre T Nguyen, Cecile Viboud, and Mauricio Santillana. Real-time estimation of disease activity in emerging outbreaks using internet search information. *PLoS computational biology*, 16(8):e1008117, 2020.
30. Fred Sun Lu, Suqin Hou, Kristin Baltrusaitis, Manan Shah, Jure Leskovec, Jared Hawkins, John Brownstein, Giuseppe Conidi, Julia Gunn, Josh Gray, et al. Accurate influenza monitoring and forecasting using novel internet data streams: a case study in the boston metropolis. *JMIR public health and surveillance*, 4(1):e4, 2018.
31. Fred S Lu, Mohammad W Hattab, Cesar Leonardo Clemente, Matthew Biggerstaff, and Mauricio Santillana. Improved state-level influenza nowcasting in the united states leveraging internet-based data and network approaches. *Nature communications*, 10(1):1–10, 2019.
32. Qingyu Yuan, Elaine O Nsoesie, Benfu Lv, Geng Peng, Rumi Chunara, and John S Brownstein. Monitoring influenza epidemics in china with search query from baidu. *PloS one*, 8(5):e64323, 2013.
33. Rebecca Tave Gluskin, Michael A Johansson, Mauricio Santillana, and John S Brownstein. Evaluation of internet-based dengue query data: Google dengue trends. *PLoS neglected tropical diseases*, 8(2):e2713, 2014.

34. Benjamin M Althouse, Yih Yng Ng, and Derek AT Cummings. Prediction of dengue incidence using search query surveillance. *PLoS neglected tropical diseases*, 5(8):e1258, 2011.
35. Jeremy Ginsberg, Matthew H Mohebbi, Rajan S Patel, Lynnette Brammer, Mark S Smolinski, and Larry Brilliant. Detecting influenza epidemics using search engine query data. *Nature*, 457(7232):1012–1014, 2009.
36. Ruchit Nagar, Qingyu Yuan, Clark C Freifeld, Mauricio Santillana, Aaron Nojima, Rumi Chunara, and John S Brownstein. A case study of the new york city 2012-2013 influenza season with daily geocoded twitter data from temporal and spatiotemporal perspectives. *Journal of medical Internet research*, 16(10):e236, 2014.
37. Eiji Aramaki, Sachiko Maskawa, and Mizuki Morita. Twitter catches the flu: detecting influenza epidemics using twitter. In *Proceedings of the 2011 Conference on empirical methods in natural language processing*, pages 1568–1576, 2011.
38. Michael J Paul, Mark Dredze, and David Broniatowski. Twitter improves influenza forecasting. *PLoS currents*, 6, 2014.
39. Shihao Yang, Mauricio Santillana, John S Brownstein, Josh Gray, Stewart Richardson, and SC Kou. Using electronic health records and internet search information for accurate influenza forecasting. *BMC infectious diseases*, 17(1):1–9, 2017.
40. Prashant Rangarajan, Sandeep K Mody, and Madhav Marathe. Forecasting dengue and influenza incidences using a sparse representation of google trends, electronic health records, and time series data. *PLoS computational biology*, 15(11):e1007518, 2019.

41. Mauricio Santillana, Andre T Nguyen, Tamara Louie, Anna Zink, Josh Gray, Iyue Sung, and John S Brownstein. Cloud-based electronic health records for real-time, region-specific influenza surveillance. *Scientific reports*, 6(1):1–8, 2016.
42. Mauricio Santillana, D Wendong Zhang, Benjamin M Althouse, and John W Ayers. What can digital disease detection learn from (an external revision to) google flu trends? *American journal of preventive medicine*, 47(3):341–347, 2014.
43. David Lazer, Ryan Kennedy, Gary King, and Alessandro Vespignani. The parable of google flu: traps in big data analysis. *Science*, 343(6176):1203–1205, 2014.
44. Vasileios Lampos, Maimuna S Majumder, Elad Yom-Tov, Michael Edelstein, Simon Moura, Yohhei Hamada, Molebogeng X Rangaka, Rachel A McKendry, and Ingemar J Cox. Tracking covid-19 using online search. *NPJ digital medicine*, 4(1):1–11, 2021.
45. Dianbo Liu, Leonardo Clemente, Canelle Poirier, Xiyu Ding, Matteo Chinazzi, Jessica Davis, Alessandro Vespignani, Mauricio Santillana, et al. Real-time forecasting of the covid-19 outbreak in chinese provinces: machine learning approach using novel digital data and estimates from mechanistic models. *Journal of medical Internet research*, 22(8):e20285, 2020.
46. Tina Lu and Ben Y Reis. Internet search patterns reveal clinical course of covid-19 disease progression and pandemic spread across 32 countries. *NPJ digital medicine*, 4(1):1–9, 2021.
47. Ana I Bento, Thuy Nguyen, Coady Wing, Felipe Lozano-Rojas, Yong-Yeol Ahn, and Kosali Simon. Evidence from internet search data shows information-seeking responses to news of local covid-19 cases. *Proceedings of the National Academy of Sciences*, 117(21):11220–11222, 2020.

48. Marcel Salathe, Linus Bengtsson, Todd J Bodnar, Devon D Brewer, John S Brownstein, Caroline Buckee, Ellsworth M Campbell, Ciro Cattuto, Shashank Khandelwal, Patricia L Mabry, et al. Digital epidemiology. 2012.
49. Mauricio Santillana. Perspectives on the future of internet search engines and biosurveillance systems. *Clinical Infectious Diseases*, page ciw660, 2016.
50. Nicole E Kogan, Leonardo Clemente, Parker Liautaud, Justin Kaashoek, Nicholas B Link, Andre T Nguyen, Fred S Lu, Peter Huybers, Bernd Resch, Clemens Havas, et al. An early warning approach to monitor covid-19 activity with multiple digital traces in near real time. *Science Advances*, 7(10):eabd6989, 2021.
51. Kris V Parag and Christl A Donnelly. Using information theory to optimise epidemic models for real-time prediction and estimation. *PLoS computational biology*, 16(7):e1007990, 2020.
52. Kris V. Parag. Improved estimation of time-varying reproduction numbers at low case incidence and between epidemic waves. *PLOS Computational Biology*, (9):1–23, 2021. Publisher: Public Library of Science.
53. H Juliette T Unwin, Swapnil Mishra, Valerie C Bradley, Axel Gandy, Thomas A Mellan, Helen Coupland, Jonathan Ish-Horowicz, Michaela AC Vollmer, Charles Whittaker, Sarah L Filippi, et al. State-level tracking of covid-19 in the united states. *Nature communications*, 11(1):1–9, 2020.
54. Benjamin J Cowling, Max SY Lau, Lai-Ming Ho, Shuk-Kwan Chuang, Thomas Tsang, Shao-Haei Liu, Pak-Yin Leung, Su-Vui Lo, and Eric HY Lau. The effective reproduction number of pandemic influenza: prospective estimation. *Epidemiology (Cambridge, Mass.)*, 21(6):842, 2010.

55. Andrew B Lawson and Ken Kleinman. *Spatial and syndromic surveillance for public health*. John Wiley & Sons, 2005.
56. Elena Surkova, Vladyslav Nikolayevskyy, and Francis Drobniowski. False-positive covid-19 results: hidden problems and costs. *The Lancet Respiratory Medicine*, 8(12):1167–1168, 2020.
57. Kristin Baltrusaitis, John S Brownstein, Samuel V Scarpino, Eric Bakota, Adam W Crawley, Giuseppe Conidi, Julia Gunn, Josh Gray, Anna Zink, and Mauricio Santillana. Comparison of crowd-sourced, electronic health records based, and traditional health-care based influenza-tracking systems at multiple spatial resolutions in the united states of america. *BMC infectious diseases*, 18(1):1–8, 2018.
58. Emily L Aiken, Andre T Nguyen, Cecile Viboud, and Mauricio Santillana. Toward the use of neural networks for influenza prediction at multiple spatial resolutions. *Science Advances*, 7(25):eabb1237, 2021.
59. Anne Cori, Neil M. Ferguson, Christophe Fraser, and Simon Cauchemez. A new framework and software to estimate time-varying reproduction numbers during epidemics. *American Journal of Epidemiology*, (9):1505–1512, 2013.
60. Alessandro Rovetta. Reliability of google trends: Analysis of the limits and potential of web infoveillance during covid-19 pandemic and for future research. *Frontiers in research metrics and analytics*, 6:28, 2021.
61. Sina F Ardabili, Amir Mosavi, Pedram Ghamisi, Filip Ferdinand, Annamaria R Varkonyi-Koczy, Uwe Reuter, Timon Rabczuk, and Peter M Atkinson. Covid-19 outbreak prediction with machine learning. *Algorithms*, 13(10):249, 2020.



62. Youssoufa Mohamadou, Aminou Halidou, and Pascal Tiam Kapen. A review of mathematical modeling, artificial intelligence and datasets used in the study, prediction and management of covid-19. *Applied Intelligence*, 50(11):3913–3925, 2020.
63. Ensheng Dong, Hongru Du, and Lauren Gardner. An interactive web-based dashboard to track covid-19 in real time. *The Lancet infectious diseases*, 20(5):533–534, 2020.
64. Neil M Ferguson, Daniel Laydon, Gemma Nedjati-Gilani, Natsuko Imai, Kylie Ainslie, Marc Baguelin, Sangeeta Bhatia, Adhiratha Boonyasiri, Zulma Cucunubá, Gina Cuomo-Dannenburg, et al. Impact of non-pharmaceutical interventions (npis) to reduce covid-19 mortality and healthcare demand. 2020.
65. Donald W Marion and John F Dashe. Pacing the diaphragm: Patient selection, evaluation, implantation, and complications. *UpToDate, Waltham, MA.[Accessed 4 January 2018]*, 2015.
66. Katelyn M. Gostic, Lauren McGough, Edward B. Baskerville, Sam Abbott, Keya Joshi, Christine Tedijanto, Rebecca Kahn, Rene Niehus, James A. Hay, Pablo M. De Salazar, Joel Hellewell, Sophie Meakin, James D. Munday, Nikos I. Bosse, Katharine Sherratt, Robin N. Thompson, Laura F. White, Jana S. Huisman, Jérémie Scire, Sebastian Bonhoeffer, Tanja Stadler, Jacco Wallinga, Sebastian Funk, Marc Lipsitch, and Sarah Cobey. Practical considerations for measuring the effective reproductive number,  $r_t$ . *PLOS Computational Biology*, (12):1–21, 2020. Publisher: Public Library of Science.
67. Kris V Parag and Christl A Donnelly. Fundamental limits on inferring epidemic resurgence in real time. *medRxiv*, 2021.